THE
PHYSICAL REVIEW
A Journal of Experimental and Theoretical Physics Established by E. L. Nichols in 1893
VOL. 57, NO. 7 APRIL 1, 1940 SECOND SERIES

On the Interpretation of Neutron Measurements in Cosmic Radiation

H. A. BETHE, *Cornell University, Ithaca, New York*
S. A. KORFF, *Bartol Research Foundation, Philadelphia, Pennsylvania*
AND
G. PLACZEK, *Cornell University, Ithaca, New York*
(Received November 23, 1939)

The measurements of cosmic-ray neutrons are essentially determined by the energy distribution of neutrons in the atmosphere. The various factors influencing this distribution are investigated (§ 1). It is found that diffusion equilibrium exists in the atmosphere except for about one meter of water at the top and one meter above ground (§ 2). It is probable that the energy distribution below 100 kev can be represented by the simple Eq. (2, 3); it does not contain an appreciable number of thermal neutrons. The calculation of the number of neutrons originally produced from the present experimental data is uncertain because of capture of fast neutrons (§ 1). As an example of the influence of the ground, the neutron distribution is calculated in the air above a water surface (§ 3). Measurements in the water may be most suitable for a quantitative determination of the neutron intensity.

The various experimental arrangements are discussed in § 4, 5. A $1/v$-detector such as a BF_3 counter measures essentially the density of neutrons if care is taken to minimize the effect of recoil nuclei by using a high bias (§ 4). The evaluation of experiments using hydrogenic material to slow down the neutrons is discussed in § 5. From these two types of experiments, provisional results for the neutron production are obtained which are in agreement with each other. From the altitude distribution of neutron intensity it can be concluded that the production of neutrons of very long range is not very important (§ 7). The role of neutrons for the energy budget of cosmic radiation is discussed (§ 8).

I. THE NEUTRON INTENSITY IN COSMIC RAYS

MEASUREMENTS of the neutron intensity in cosmic radiation were made by several authors[1–16] using various experimental techniques and working at different altitudes. In order to interpret these experiments, we must know the energy distribution of the neutrons in the atmosphere and the relative sensitivity of the detectors for neutrons of various energies. In the following we shall determine the energy distribution arising from the diffusion in the atmosphere (§1). We shall further show that a neutron diffuses only

[1] L. H. Rumbaugh and G. L. Locher, Phys. Rev. **44**, 855 (1936).
[2] E. Schopper, Naturwiss **25**, 557 (1937).
[3] E. Schopper and L. Schopper, Physik. Zeits. **40**, 22 (1939).
[4] W. Heitler, C. F. Powell and G. E. F. Fertel, Nature **144**, 283 (1939).
[5] G. L. Locher, Phys. Rev. **44**, 774 (1933).
[6] G. L. Locher, Phys. Rev. **45**, 296 (1934).
[7] G. L. Locher, Phys. Rev. **50**, 394 (1936).
[8] G. L. Locher, J. Frank. Inst. **224**, 555 (1937).
[9] D. K. Froman and J. C. Stearns, Phys. Rev. **54**, 969 (1938).
[10] E. Fünfer, Naturwiss. **25**, 235 (1937).
[11] E. Fünfer, Zeits. f. Physik **111**, 351 (1938).
[12] C. G. and D. D. Montgomery, Phys. Rev. **56**, 10 (1939).
[13] S. A. Korff, Phys. Rev. **56**, 210 (1939).
[14] S. A. Korff and W. E. Danforth, Phys. Rev. **55**, 980 (1939).
[15] S. A. Korff, Rev. Mod. Phys. **11**, 211 (1939).
[16] H. v. Halban, M. Magat and L. Kowarski, Comptes rendus **208**, 572 (1939).

over a limited part[17] of the atmosphere. From this it follows that the energy distribution is very nearly the same at different altitudes, with the exception of the regions near the top and bottom of the atmosphere. This makes it possible to interpret the measured dependence of the intensity on altitude as giving the altitude distribution of the production of neutrons of moderate energy (cf. footnote 17 and §7).

§ 1. Energy distribution of neutrons in the atmosphere

The energy distribution is determined by the diffusion of the neutrons in the atmosphere. In treating this process, we shall restrict ourselves to those phenomena for which the theory is reasonably certain, i.e., to neutron energies for which the concept of the compound nucleus is applicable; we shall assume that this is the case up to about 30 Mev. Up to this energy, the interaction between particle and nuclei will certainly be at least as great as the kinetic energy of the particle, and under these conditions the result of a collision does not depend appreciably on the nature of the forces. For higher energies, the analytical form of the interaction will be essential, and since we do not know it we cannot make predictions about collisions of very fast neutrons.[18]

We shall therefore assume that a certain number of neutrons below 30 Mev is produced at a given point in the atmosphere. We shall leave it open whether these neutrons are directly produced by other particles or whether they arise from the slowing down of faster neutrons. In any case the neutrons must be produced in the atmosphere because, according to present ideas about β-disintegration, the neutron has a finite lifetime of about one hour. Some more information about the production process can be obtained from the analysis of the experiments, cf. §7.

Neutrons below about 30 Mev can be treated with the Bohr method of the compound nucleus.[19] In colliding with nuclei, neutrons may disappear due to n, p or n, α reactions, etc., or their number may increase due to $n, 2n$ or similar reactions, or we may have simple inelastic scattering. In any case, if a neutron comes out from the reaction, its energy will only be of the order of the nuclear temperature, i.e., much smaller than the energy of the incident neutron.

This process of energy loss due to excitation of nuclei can take place if the energy of the incident neutron is greater than the lowest excited level of the nuclei present in air. The lowest excited level in O^{16} is almost certainly[20] at 6 Mev. In nitrogen, an excitation level[21] of 4 Mev has been found but there is not yet sufficient experimental evidence to show or exclude the existence of lower levels. We shall assume in the following that 4 Mev is the lowest excited level.

One or two inelastic collisions are in general sufficient to reduce the energy of a neutron below that of the first excitation level of nitrogen. The cross section for neutrons in the energy range considered, is of the order of the geometrical cross section of the nucleus, i.e., about 0.5×10^{-24} cm^2 for nitrogen and oxygen. This is equivalent to a mean free path of about[22] 50 g/cm^2.

Below the first excited state of N^{14} which we tentatively assume at 4 Mev, there will be no more inelastic collisions. Any further slowing down must therefore be due to elastic collisions with N^{14} and O^{16} nuclei. Since these nuclei are quite light, elastic collisions will be quite effective in reducing the energy of the neutrons. The amount of the average energy loss per collision depends to some extent on the angular distribution of the elastically scattered neutrons which is not known. If we assume it to be spherically symmetrical in the center of mass system the average energy loss will be $2/M$ times the initial energy of the neutron where M is the atomic weight of the nucleus. Seven collisions with nitrogen are as effective as one with hydrogen, reducing the average neutron energy to $1/e$ of its initial value.

[17] This may not be correct for extremely fast neutrons (cf. §1) but it can be shown from the experimental altitude dependence that the neutrons for which it is incorrect are not very important (§7).

[18] Earlier theories of Heisenberg (Naturwiss. **25**, 749 (1937)) and Williams (Nature **142**, 431 (1938)) were based on special assumptions about the nuclear forces which can no longer be regarded as well founded.

[19] N. Bohr, Nature **137**, 344 (1936). N. Bohr and F. Kalckar, Kgl. Danske Vid. Selsk. Medd. **14**, 10 (1939).

[20] W. A. Fowler and C. C. Lauritsen, Phys. Rev. **56**, 840, 841 (1939).

[21] M. S. Livingston and H. A. Bethe, Rev. Mod. Phys. **9**, 245 (1937).

[22] We measure mean free paths in g/cm^2 rather than in physical dimensions. One g/cm^2 is the same as one cm water equivalent, the unit customary in cosmic-ray investigations.

TABLE I. *Cross sections of nitrogen and oxygen (in 10^{-24} cm²).*

PROCESS	D+D NEUTRONS σ	REF.	PHOTO-NEUTRONS σ	REF.	THERMAL NEUTRONS σ	REF.
N^{14}, elastic scattering	1.4	23	1.6	25	10.7	26, 27, 28
O^{16}, elastic scattering	1.2	23	1.8	25	4.2	26, 27
$N^{14}+n=C^{14}+H^1$	0.04	24	—	—	1.3	29
$N^{14}+n=B^{11}+He^4$	0.16	24	0		0	

The elastic collisions would slow all the neutrons down to thermal energies if no capture processes occurred. In reality such processes do occur and are quite frequent both at high energies (of the order of millions of volts) and very low energies (of the order of volts). The fraction of neutrons of initial energy E_1 which get down to energy E_2 without being captured is given by[30]

$$\exp\left(-\tfrac{1}{2}M\int_{E_2}^{E_1}\frac{\sigma_c}{\sigma_s}\frac{dE}{E}\right), \qquad (1)$$

where σ_c is the capture cross section, σ_s the scattering cross section and σ_c/σ_s is to be taken as a function of energy. In deriving this formula, it has been assumed that the angular distribution of the scattered neutrons is spherically symmetrical. For σ_c and σ_s we must insert the average values for nitrogen and oxygen, taking account of the concentrations.

Cross sections have been measured for neutrons of 2.6 Mev obtained from the D−D reaction, for photoneutrons arising from the photoelectric disintegration of beryllium with RaC γ-rays (neutron energy about 150 kev), and for thermal neutrons. The results are given in Table I, in units of 10^{-24} cm² which we shall use throughout in this paper.

Considering first the elastic cross section of N^{14}, we notice a large increase between 150 kev and thermal energies. At what energy this change occurs is unknown; the fact that it occurs indicates the presence of resonance levels. For a nucleus as light as nitrogen it would be unreasonable to assume a resonance level of less than, say, 10 kev width; therefore we shall take as extreme assumptions for the energy at which the cross section changes, $E_S=10$ and $E_S=150$ kev, respectively. For the average elastic cross section of an "air" nucleus we have then about $1.3_5\times10^{-24}$ for energies greater than E_S, and 9.4×10^{-24} cm² for smaller energies. This corresponds to a mean free path of the neutrons of 18 and 2.6 cm water equivalent, respectively.

The process $N^{14}(n,\alpha)B^{11}$ is impossible for low energy neutrons, being endothermic by about 0.3 Mev. Above the threshold of 0.3 Mev the cross section will increase with increasing neutron energy because the α-particles will have a greater chance to escape through the Coulomb potential barrier. Taking for the radius of the compound nucleus N^{15}, $R=1.5\times10^{-13}A^{\frac{1}{3}}=3.7\times10^{-13}$ cm, and taking account of the recoil and of the reaction energy of −0.3 Mev, we find that neutrons of 4.2 Mev will produce α-particles which go over the top of the barrier. Therefore a considerable increase of the cross section for the n, α process may be expected when the energy increases to 4 Mev; on the other hand, the n, α process will be of negligible importance below 2 Mev neutron energy.

The process $N^{14}(n,p)C^{14}$ is exothermic by about 0.7 Mev; the height of the barrier (with the same nuclear radius as above) is 2.2 Mev. Thus the small cross section at 2.6 Mev suggests that the process is intrinsically improbable. The thermal cross section of 1.3 is relatively even smaller; namely if we would assume that the capture cross section σ_H is proportional to the penetrability P_H for the proton, divided by the velocity v of the neutron, extrapolation from the measured cross section at 2.6 Mev would give about 15 times more for the cross section at thermal energy. This shows again that resonances must play an important role, and that it is therefore difficult to make any definite statements about the cross

[23] W. H. Zinn, S. Seely and V. W. Cohen, Phys. Rev. **56**, 260 (1939).
[24] E. Baldinger and P. Huber, Nature **143**, 844 (1939).
[25] E. Fedorow and N. Perfiliewna, Sow. Phys. **11**, 660 (1939).
[26] J. R. Dunning and H. Carroll, Phys. Rev. **54**, 541 (1938).
[27] M. Goldhaber and G. H. Briggs, Proc. Roy. Soc. **A162**, 127 (1937).
[28] Dunning and Carroll measured directly the total cross section $\sigma=12.0$ from which we have to subtract the capture cross section $\sigma_c=1.3$ (cf. reference 24). Goldhaber and Briggs have made a direct measurement of the elastic cross section and obtain 8.2. The experimental error given by Dunning and Carroll being smaller, we have used their value. All measurements may be influenced by interference effects between the neutrons scattered from different nuclei in the molecule or crystal.
[29] O. R. Frisch, H. v. Halban, J. Koch, Kgl. Danske Vid. Selsk. Medd. **15**, 10 (1938); Nature **140**, 895 (1937).
[30] G. Placzek, Phys. Rev., to appear shortly.

section. Nevertheless it is quite possible that the resonances above the $1/v$-region do not appreciably reduce the number of neutrons because of the small intrinsic probability of the reaction. Below 10 kev we can, for a nucleus as light as nitrogen, assume that the capture cross section is proportional to $1/v$ and calculate it from the measured value at thermal energy. If we assume that the cross section for the n, α and n, p processes are determined mostly by the penetrability of the potential barrier, we should find that about 70 percent of all neutrons of 3 Mev initial energy, and about 40 percent of all 4-Mev neutrons are slowed down to the region of validity of the $1/v$-law (below 10 kev). The underlying assumptions and therefore these figures are of course very uncertain but it seems likely that the capture will not reduce the number of neutrons by orders of magnitude. The reduction will be less if the first excited state of nitrogen is lower, but will be greater if there is strong resonance capture.

From this discussion we see that not enough experimental data are available above the $1/v$-region. Since the more accurate experiments consist in the determination of the number of relatively slow neutrons in cosmic radiation (cf. §4, 5), we shall in the following refer only to those neutrons which escape capture at high energies, i.e., capture above the $1/v$-region.

We denote by q the number of neutrons produced per gram and sec. which escape capture at high energies, and by v_1 the smallest velocity at which high energy capture takes place. The energy $E_1=\frac{1}{2}mv_1^2$ may be as low as 10 kev but possibly as high as 2 Mev. Then the number of neutrons per cm³ having a velocity between v and $v+dv$ (for $v<v_1$) is given with sufficient accuracy by[30]

$$N(v)dv = Mq\,l(v)\frac{dv}{v^2} \times \exp\left\{-M\int_v^{v_1}\frac{\sigma_c(v')}{\sigma_s(v')}\frac{dv'}{v'}\right\}. \quad (2)$$

According to our assumption about v_1, the exponential will only become important when σ_c obeys the $1/v$ law, so that it may be written

$$\exp\left\{-M\frac{\sigma_{\text{eth}}}{\sigma_s}\left(\frac{kT}{E}\right)^{\frac{1}{2}}\right\}, \quad (3)$$

where σ_{eth} is the capture cross section at energy kT. The observed values are (cf. Table I)

$$\sigma_s = 9.4 \text{ per "air atom"};$$
$$\sigma_{\text{eth}} = 1.04 \text{ per "air atom."} \quad (4)$$

With $M=14$, the exponent in (3) becomes unity for

$$E_{\text{capt}} \sim 2.4kT, \quad (4a)$$

i.e., the neutrons will on the average be slowed down to $2.4kT$ before being captured.

This shows that no thermal equilibrium will be established among the neutrons in the atmosphere because the capture probability is too large. The value of the limiting energy is probably not exactly $2.4kT$ because at neutron energies below $\frac{1}{3}$ volt $=13kT$ the chemical binding in the nitrogen molecule and the velocity of the nitrogen molecules will be important[30] and will reduce the slowing effect of the collisions. This will also modify the velocity distribution (2) at the lowest energies.

Another modification is introduced by the presence of water vapor. If the partial pressure of water vapor is p_W and the total pressure is p_0, the average energy loss of a neutron will be increased in the ratio

$$1+14p_W/p_0.$$

If we admit an increase by 20 percent, p_W must be less than 11 mm at ground and correspondingly less at higher elevations. For saturation, this means that the temperature should be less than 14° at sea level or 8° at 3 meters of water elevation. Usually the humidity is far from saturation, and therefore the water vapor will be unimportant even near ground except on hot humid days.

§ 2. Spatial distribution of the neutrons

Thus far we have calculated the energy distribution with the tacit assumption that the nitrogen in the atmosphere is sufficient to slow the neutrons down to below one volt. We shall now verify this assumption by calculating the mean square distance from the point of origin of the neutrons to the point of absorption.

As we pointed out above (§1), only one or two collisions, and a path of about 50 cm water equivalent, will be needed to reduce the energy

of the neutron to below 4 Mev, this value being again taken for the position of the first excited level of N^{14}.

When the slowing down is done by elastic collisions, i.e., below the first excited level of N^{14}, the mean square distance traveled is

$$(r^2)_{Av}=M_{eff}\int_{E_2}^{E_1} l^2(E)\frac{dE}{E}, \tag{5}$$

where E_1 is the initial, E_2 the final energy, l the mean free path as a function of the neutron energy and $M_{eff}=15.6$ (cf. reference 30). In (5) we have again assumed that the scattering is isotropic; if the scattered neutrons go preferentially forward, $(r^2)_{Av}$ will be larger. From the measurements (cf. §1) we have $l\approx 18$ cm water equivalent for $E>E_S$ and $l\approx 2.6$ cm water for $E<E_S$ where the critical energy E_S is unknown but probably lies between 10 and 150 kev. Taking $E_2=2.4kT=0.06$ ev (cf. 4a) we find $[(r^2)_{Av}]^{\frac{1}{2}}$ in cm of water equivalent (see Table II).

The spatial distribution of neutrons produced at height x_0 after the slowing down process will be

$$N(x)dx=\pi^{-\frac{1}{2}}L^{-1}\exp\left[-(x-x_0)^2/L^2\right], \tag{5a}$$

where

$$L=((r^2)_{Av}/3)^{\frac{1}{2}} \tag{5b}$$

is between 72 and 103 cm. For neutrons below 30 Mev initial energy, these figures will be raised by only 10–15 cm when the path above 4 Mev is included. For such neutrons, the results are probably correct within 50 percent.

This calculation shows that the neutrons measured at a given point in the atmosphere have in general originated close to that point. Therefore a measurement of the neutron intensity as a function of altitude is significant for the production of neutrons at various altitudes, provided the production is approximately constant over a distance of one meter of water. That this is so is shown by the fact that the detected neutron intensity changes only by a factor of two per meter of water (cf. §6). Therefore it is legitimate to use Eqs. (2) to (4a) for an approximate determination of the number of neutrons produced as a function of altitude. In these statements neutrons of high energy (>30 Mev) have been excluded. Some evidence on these very fast neutrons can be obtained from the effects observed near the top of the atmosphere (cf. §6).

TABLE II. *Root mean square distance of diffusion in air* $[(r^2)_{Av}]^{\frac{1}{2}}$, *in cm of water equivalent.*

	E_1=2 MEV	E_1=4 MEV
E_S=150 kev	124	135
E_S= 10 kev	169	178

The approximate proportionality between measured intensity and neutron production is no longer true within a distance of the order L from the upper and the lower boundary of the atmosphere. The effects at the top of the atmosphere are easier to discuss in principle but more difficult to evaluate quantitatively.

If $q(x_0)$ is the number of neutrons produced per gram and sec. at a depth x_0 below the top of the atmosphere, then at a depth x the number per cm^3 of neutrons of velocity between v and $v+dv$ is[31]

$$N(v,x)dv=Ml(v)\frac{dv}{v^2}(2\pi)^{-\frac{1}{2}}L^{-1}(v)\cdot\int\left\{\exp\left(-\frac{(x-x_0)^2}{2L^2(v)}\right)-\exp\left(-\frac{(x+x_0+2l/\sqrt{3})^2}{2L^2(v)}\right)\right\}q(x_0)dx_0. \tag{6}$$

This formula can be obtained from (2) by using standard procedures of diffusion theory. $L(v)$ can be calculated from (5), (5b) and is about 1 meter of water (cf. Table II) for small v.

The actual distribution in depth will depend on the production probability q as a function of x_0. However, irrespective of the altitude dependence of the neutron production, the neutron density must *decrease* with increasing altitude within a distance L from the top of the atmosphere. For if we assume that all neutrons are produced at the very top of the atmosphere, the neutron density will be

$$N(v,x)\sim x\exp\left(-x^2/2L^2\right) \tag{6a}$$

and will thus have a maximum at $x=L$. If the production is at a depth between 0 and L, the maximum of the density will shift only slightly to

[31] H. A. Bethe, Phys. Rev., to appear shortly.

greater depth. Since we know from experiment that the neutron density increases with elevation at the lower altitudes we must expect that a maximum will be reached at a depth greater than $L \approx 1$ meter water below the top of the atmosphere.

The position of the maximum as determined from experiments permits some conclusions on the properties of the neutrons originally produced. (Cf. §7.)

§ 3. Effects near the surface of the earth

Near the surface of the earth, the energy and altitude distribution of the neutrons will again be modified. This modification will depend on the chemical composition of the earth at the point in question. Therefore measurements made at ground are very difficult to interpret and do not give the neutron intensity in the free atmosphere. If one wants to measure this intensity, the essential point is not to go to high altitudes but away from the earth's surface. A distance of at least 1 meter of water from ground is required which necessitates the use of airplanes or balloons. It should be investigated in each case whether the amount of material of the airplane or balloon is ineffective in changing the energy distribution of the neutrons coming from the atmosphere.

In order to show how large the effects of the earth can be we shall investigate a case which is simple enough for mathematical treatment, namely that of an extended water surface. In this case, both water and air will participate in the diffusion process. The theoretical treatment shows that the production of neutrons in water is unimportant for the effects observable near the surface. The most important effects will be due to neutrons which are produced in air and diffuse into the water while they have energies between 4 Mev and 0.06 ev. These neutrons will then not be subject to capture by nitrogen nuclei near E_{capt} (cf. Eq. (4b)) but will continue to be slowed down to thermal energies. Some of the thermal neutrons will then emerge back into the air so that the air near a water surface contains a considerable amount of thermal neutrons, in contrast to the free atmosphere.

If we neglect the production of neutrons in water, the number of neutrons of velocity v in the water per cm³ is approximately

$$N_W(v,x)dv = \frac{Mq_A l_A}{1+\kappa}\frac{dv}{v^2}\left\{1-\Phi\left(\frac{x}{L_W}\right)\right\}, \quad (7)$$

where x is the depth below the water surface in cm, the subscript A refers to air and W to water, l is an average of the mean free path in g/cm² for neutrons between 1 ev and 4 Mev, q the number of neutrons escaping high energy capture per gram and sec., $3L^2$ the mean square distance traveled by a neutron from ~4 Mev energy to velocity v, Φ the error function, and

$$\kappa \approx (3M/2)^{\frac{1}{2}}, \quad (7a)$$

where $M=14.4$ is the atomic weight of an average air atom. From (7a), $\kappa=4.6$; a more accurate calculation (including the effect of oxygen in the water) gives $\kappa=4.1$. L_W is about 20 cm; therefore at more than ~20 cm below the surface, only neutrons produced in the water itself will be found (cf. Eq. (10a)).

In air, the number of neutrons of energy $>E_{\text{capt}}$ becomes

$$N_A(v,x)dv = \frac{Mq_A l_A}{1+\kappa}\frac{dv}{v^2}\left\{1+\kappa\Phi\left(\frac{x}{L_A}\right)\right\}, \quad (8)$$

where x is the height above the water surface. The density of neutrons of $E>E_{\text{capt}}$ in air directly above the water is thus reduced by a factor $1+\kappa \approx 5$ as compared with the free atmosphere. This reduction is of course due to the diffusion of neutrons into the water. It will make itself felt up to heights of the order of L_A, i.e., about 1 meter of water above ground. The density in water exactly at the surface is the same as in air.

The density of *thermal* neutrons immediately above the water surface is

$$N_{thA}(x=0) = N_{\text{fast}}(x=\infty)\frac{l_{W_s} Z^{\frac{1}{2}}}{2l_{Wf}(1+\kappa)} \times\left(\frac{\pi E_{\text{capt}}}{4kT}\right)^{\frac{1}{2}}, \quad (9)$$

where $N_{\text{fast}}(x=\infty)$ is the total density of neutrons above E_{capt}, as given by (4a); l_{W_s} and l_{Wf} are the mean free paths for thermal and 1-ev neutrons in water ($l_{Wf}/l_{W_s} \approx 2.8$), $Z \approx 200$ is the

average number of collisions of a neutron in water before capture, and $(4/\pi)kT$ is an average energy for thermal neutrons. Evaluation of (9) gives

$$N_{thA}(0)=0.88N_{fast}(\infty). \quad (9a)$$

Remembering that the density of fast neutrons is reduced to 20 percent of $N_{fast}(\infty)$ near the surface of the water, we find that the total intensity is about the same near water as in the free atmosphere (which, of course, is accidental); but more than 80 percent of the neutrons are thermal as against only about 15 percent in the free atmosphere. The number of thermal neutrons decreases very rapidly with the distance from the water surface because of absorption in air; at a distance of about 10 cm water equivalent (~100 meters of air), the ratio of thermal to fast neutrons will be practically the same as in the free atmosphere, and therefore the total density of neutrons (fast+slow) will be only about one-fifth of that in the free atmosphere.

Inside the water, we have for the density of thermal neutrons

$$N_{thW}(x=0)\approx N_{thA}Z^{\frac{1}{2}}\approx 12N_{fast}(\infty), \quad (10)$$

if we measure at a depth large compared with the diffusion length $L_{Ws}=l_{Ws}(Z/3)^{\frac{1}{2}}\approx 2.5$ cm but small compared with $L_W\approx 20$ cm. In the surface layer, the number of thermal neutrons is smaller because of diffusion into the air; at greater depths, it is again smaller because neutrons produced in air cannot penetrate there. The number of neutrons per cc at great depth is

$$N_W(x=\infty)=q_W\tau_W\rho_W \quad (10a)$$

$$=N_{air}(x=\infty)\frac{q_W}{q_A}\frac{\tau_W}{\tau_A}\frac{\rho_W}{\rho_A}$$

$$=2.4\frac{q_W}{q_A}N_{air}(\infty), \quad (10b)$$

where q_W is the number of neutrons produced per gram of water and second, τ is the lifetime of the neutron in the respective medium, and ρ the density. If we assumed that production as well as multiplication and absorption of neutrons were the same in oxygen and nitrogen, the neutron density in water below 20 centimeters would be about twice the density in the free atmosphere; actually, it seems likely that the absorption is greater in nitrogen which would shift the ratio more in favor of the water.

We have investigated the case of water mainly in order to demonstrate the great influence of the earth on the neutron distribution in air. In addition, however, we have shown that measurements in water would be valuable in themselves. Measurements directly below the water surface (~5 cm) would be rather accurate because of the high density of neutrons in the water (cf. 10) and because it can be most easily ascertained that actually neutrons are counted, by taking the difference of the counts with and without cadmium.

Measurements at greater depths (>30 cm) would be free from the effects of neutron absorption in air (10a) and would therefore furnish a more reliable measurement of the number of neutrons produced. The absorption of neutrons above thermal energies in water can be expected to be very slight, firstly because the neutrons are slowed down very rapidly by collisions with hydrogen, and secondly because the reaction $O^{16}(n,\alpha)C^{13}$ which is the only one giving rise to appreciable capture, is endothermic with 2.2 Mev and will therefore not become important below about 5 Mev neutron energy. It is particularly fortunate that the diffusion of neutrons in water goes only over about 20 cm, i.e., a distance over which the intensity of the cosmic radiation, and therefore the neutron production, do not change very much. A comparison of the number of neutrons in water below 30 cm, and at a point of the same elevation in the free atmosphere, would permit an estimate of the fraction of fast neutrons captured in air.

Experiments in water near its surface (~5 cm depth) must be made at least one kilometer from shore because part of the diffusion is through air. Experiments at greater depth (>30 cm) do not require this precaution. In salt water, a correction must be made for the capture of neutrons by chlorine.

II. Experiments

§ 4. Thin, unshielded 1/v detector

Let us assume a detector of sensitivity varying as $1/v$ between neutron energies of 0 and 10 kev

and not responding to neutrons of energy higher than 10 kev. This detector will measure the total number, per cm³, of neutrons ($\int N(v)dv$) in this energy region. This number is $q\tau_A\rho_A$ where q is the number produced per gram and second (cf. §4), ρ_A is the density of air, and τ_A the lifetime of a neutron in air.

The activation (number of counts per second) n of the detector is

$$n=q\frac{\tau_A}{\tau_D}\frac{\rho_A}{\rho_D}m_D=q\frac{l_A}{l_D}m_D=q\frac{\sigma_D}{\sigma_A}\frac{\mu_A}{\mu_D}m_D \qquad (11)$$

(τ_D lifetime of neutrons in the detector, m_D mass of the detector, ρ density, μ molecular weight, l mean free paths for capture in g/cm² in air and detector, respectively, σ capture cross section per molecule). If the detector is a gas,

$$m_D=\mu_D V_D p_{0D}/(2.24\times10^4)$$

(V_D volume of the detector, p_{0D} pressure in atmospheres of the detector gas at 0°), and hence

$$q=(n/V_D)(\sigma_A/\sigma_D)(780/p_{0D}). \qquad (12)$$

The question arises now how a detector of the required properties can be realized. We will discuss how far it can be approximated by an ionization chamber lined with thin boron, or a BF_3 chamber. The following points must be considered. First, the extension of the $1/v$ region in boron is not known. Second, also neutrons of more than 10 kev will produce boron disintegrations and will be counted. Third, neutrons and other particles of the cosmic radiation may produce recoils in the gas of the chamber, which may also influence the count, unless special precautions are taken. Fourth and finally, also slow electrons, produced as secondaries of the soft component of the cosmic radiation may produce effects.

1. The $1/v$-law in boron will certainly hold up to about 10 kev because the levels of the compound nucleus will be fairly wide as for any light element. For the energy distribution (3) this is quite sufficient provided no large maxima of the capture cross section in boron occur at higher energies. The occurrence of maxima which play any role in comparison with the cross section at low energies is much less likely than in nitrogen mainly because the low energy cross section of B^{10} is about 2000 times larger.

2. The capture cross section of B^{10} for high energy neutrons has not been measured but it can certainly not be larger than the geometrical cross section of the nucleus, i.e., about 10^{-24} cm². If the cross section had this value whenever it is greater than the value following from the $1/v$-law, and if there were no capture of neutrons below 4 Mev in air, the contribution of the capture of high energy neutrons in boron would be less than one percent of the slow neutron effect. The capture in air will tend to increase the relative effect of fast neutrons but even under unfavorable assumptions it will be unimportant.

3. Fast neutrons of energy E will produce recoil nuclei of atomic weight M_r with an average energy of $(2/M_r)E$ and a maximum energy of $(4/M_r)E$. In a proportional counter, the recoil nuclei will only be counted when they lose more than a certain minimum energy E_r in the counter. As long as the range of the recoil nuclei is smaller than the dimensions of the counter, they will be counted if their energy is greater than E_r which corresponds on the average to a neutron energy greater than $\frac{1}{2}M_rE_r$. If the boron is used in the form of BF_3 gas, the ratio of the number of recoils to the number of disintegration alphas is approximately[32]

$$n_r/n=\int_{v_r}^{\infty}N(v)\sigma_r(v)dv\Big/\int_0^{\infty}N(v)\sigma_c(v)dv, \qquad (13)$$

where v_r is the velocity of a neutron of energy $\frac{1}{2}M_rE_r$, $N(v)dv$ the number of neutrons in the velocity interval dv, $\sigma_r(v)$ the elastic cross section and $\sigma_c(v)$ the capture cross section of one BF_3 molecule for neutrons of velocity v. Integration gives

$$\frac{n_r}{n}=\frac{q_N}{q}\frac{l_f}{l_s}\frac{\sigma_{rN}}{\sigma_c(E_{\text{capt}})}\frac{1}{2}\log\frac{2E_i}{M_rE_r}, \qquad (14)$$

where l_f and l_s are the mean free paths of fast and slow neutrons in air ($l_f=18$ cm, $l_s=2.6$ cm), $\sigma_c(E_{\text{capt}})$ is the capture cross section of boron at

[32] In (13), the effect from the walls of the counter have been neglected. They will in general give a small contribution because the range of the recoil nuclei is small. An exception may occur if the material of the walls is of low atomic weight (e.g., boron) and the gas very heavy. In such a case it would be necessary to know the range-energy relation for the atoms in the wall.

the energy E_{capt} given in (4a), E_i is an energy of the order of the first excited level of N^{14}, σ_{rAv} is an average of the recoil cross section σ_r over the energy region from M_rE_r to E_i, and q_{Av} is an average over the same region of the expression (cf. 3)

$$q(v)=q\exp\left\{M\int_{v_1}^{v}\frac{\sigma_c}{\sigma_s}\frac{dv'}{v'}\right\}. \qquad (14a)$$

The factor q_{Av}/q takes account of the capture of fast neutrons. In the experiments of one of us[13,14] the value of E_r was certainly more than 40 kev and probably of the order of 100 kev (cf. below). We take $E_i=4$ Mev, $M_r=16$ as an average between B and F. The scattering cross section σ_r varies from 23 at 0.15 Mev [25] to 8 at 2.6 Mev.[23,33] Since $M_rE_r\approx 800$ kev, the average σ_r may be about 10 to 12. Then

$$\frac{n_r}{n}\approx 0.2\frac{q_{Av}}{q}. \qquad (14b)$$

With reasonable assumptions about the capture of fast neutrons in air, n_r/n will be somewhat smaller than unity. It must be remembered, however, that our assumptions about the constants are very crude.

In any case, the recoils will constitute an appreciable fraction of the total counts, and the exact ratio of recoils to disintegrations cannot be calculated at present. Experimental information on this question can be obtained in two ways. One possibility is the use of a counter sensitive only to recoils (see §6) but in this case there will remain a considerable uncertainty in the ratio of the recoil cross sections as a function of energy between the substance used in the recoil counter and BF_3. The second possibility is to change the value of E_r in the BF_3 counter experiments. Raising of E_r will exclude the weaker recoils but a limit is set by the consideration that E_r must not be greater than the energy lost by a disintegration α-particle in the counter. It would be most advantageous to choose the dimensions of the counter equal to or larger than the range of the α-particles. If this is done, E_r can be raised to about 2 Mev which will exclude all recoils from neutrons below 4 Mev and will leave only the recoils from the rare faster neutrons. Investigation of the count as a function of E_r will give a direct measure of n_r/n which is much more accurate than the crude theoretical estimate in Eq. (14b). It may turn out that such experiments would indicate that a moderate value of $E_r(\approx\frac{1}{2}$ Mev) is sufficient to make the effect of recoils unimportant.

Recoils from particles other than neutrons can be shown to be unimportant. In the first place there will be recoils due to protons produced in the same processes as the neutrons. For the same rate of production, the current of protons per cm^2 and sec. is smaller in the ratio of the ranges (total distance traveled), i.e., about 1 in 10^3. It can easily be seen that the electrostatic interaction of the protons with the nuclei of the gas is unimportant for the production of fast recoils; the nuclear interaction is the same as for neutrons; therefore the number of recoils produced by protons will be negligible.

Secondly, there may be primary fast protons in cosmic radiation. If we assume ten percent of the incident radiation to be protons, we should have 1 proton per cm^2 and min. With a cross section of 10^{-24} cm^2 for boron as well as fluorine, the number of recoils in a BF_3 chamber of $\frac{1}{10}$ atmosphere pressure would be 10^{-5} per cm^3 and min., as compared with an observed number of counts of 0.1 per cm^3 and min. at a depth of 1 meter of water. The same conclusion will also hold for recoils produced by mesons, the meson intensity at its maximum being about 10 per cm^2 and min.[34]

Recoils produced by electrons are also unimportant. It is true that the number of shower electrons is about 1000 per cm^2 and min. at a depth of one meter water. But the cross section for production of boron recoils of more than 100 kev energy is only 1.6×10^{-27} cm^2 if we use the Rutherford formula which has been shown to be approximately correct for the scattering of fast electrons.[35,36] This means a cross section of only 1/1000 of nuclear dimen-

[33] H. Aoki, Proc. Phys. Math. Soc. Japan **21**, 232 (1939).

[34] M. Schein, W. P. Jesse and E. O. Wollan, Phys. Rev. **57**, 68 (1940).

[35] P. M. S. Blackett and J. G. Wilson, Proc. Roy. Soc. **165**, 203 (1938).

[36] W. A. Fowler and Jaquenette Oppenheimer, Phys. Rev. **54**, 320 (1938).

sions, and therefore a negligible number of recoils.

4. Now let us consider the influence of electrons themselves. An electron will be counted if its energy is E_r. The slowest electron which can be counted is one of energy E_r, provided that its range lies entirely within the chamber. The fastest electron to be counted must lose E_r in the chamber. However, if the range of an electron of energy E_r is greater than the maximum dimension of the chamber then no electrons at all will be counted.

Let E_m be the energy of the fastest countable electron; this energy can be determined from the well-known formulae for the energy loss of electrons. Then, if k is the number of shower particles per cm² per min. and N the number of electrons per cm³ of the substance, the number of secondaries of energy between E_r and E_m per cm³ and min. is

$$\frac{2\pi e^4 Nk}{mc^2}\left(\frac{1}{E_r}-\frac{1}{E_m}\right). \tag{15}$$

This number is of the same order as the observed effect from neutrons if E_m is about $2E_r$.

In the case of the experiments of one of us, it was ascertained that the counter did not count in the presence of a strong γ-ray source. Since such γ-rays will produce abundant electrons of all energies inside the counter by various processes, we can conclude that slow cosmic-ray electrons were not counted either in our counter. Furthermore, it follows that the range of an electron of energy E_r is greater than the maximum dimensions of the counter, *viz.*, 20 cm. (at 0.1 atmos. BF_3). The energy corresponding to this range is 40 kv which we thus establish as a minimum value for E_r in our experiments. (Cf. above, after Eq. (14a).)

We can now proceed to a provisional evaluation of the experiments. From the previous discussion it follows that the chief uncertainty lies in the effect of the recoils produced by neutrons. If we would assume, that the whole measured effect (of 0.1 pulse per cc and min. at 1 m H_2O) is to be attributed to α-disintegrations we would obtain from (12)

$$q=0.05 \text{ neutron/g sec. at 1 m } H_2O. \tag{16}$$

Because of the recoils this figure represents an upper limit to q.

On the other hand, we can derive from (16) a lower limit to q_{Nv} (cf. 14) (which in turn is a lower limit to the number of neutrons below 10 Mev produced because such neutrons can only be captured and not be multiplied). Let c_α and c_r be the efficiencies of counting α-disintegrations and recoils, respectively, then the number of counts will be

$$qc_\alpha+q_{Nv}c_r.$$

If the experiments are evaluated assuming only α-disintegrations to be counted, the apparent q will be

$$q_{app}=q+q_{Nv}(c_r/c_\alpha). \tag{16a}$$

But since $q<q_{Nv}$

$$q_{Nv}>q_{app}/(1+c_r/c_\alpha), \tag{16b}$$

where c_r/c_α has the approximate value 0.2 according to (14b).

§ 5. Measurements using hydrogenic material together with a 1/v-detector

A considerable increase of the measurable effects can be achieved by using hydrogen either surrounding or otherwise combined with the detector. Then the hydrogen slows down the incident neutrons so that they can be more easily captured by the detector. Experiments of this type were carried out by v. Halban, Kowarski and Magat. They exposed a vessel filled with ethyl bromide C_2H_5Br to the cosmic radiation and measured the bromine activity by the method of isotope separation.[16] The vessel used was a flat box of 10 cm thickness, which, by number of hydrogen atoms, is equivalent to 6 cm of water.

In order to discuss experiments of this type we must know how many incident neutrons of a given energy E_0 will be slowed down sufficiently in the vessel so that they may be captured. Many of the neutrons will be scattered in such directions that they will leave the vessel again on the same side from which they entered, and others will leave on the far side. The number of neutrons which get lost in this way before being slow enough for capture, will depend on the

shape of the vessel and will increase with increasing number of collisions necessary for slowing down the neutron, i.e., with increasing E_0.

For a flat vessel of thickness D and infinite extension in the two other directions, the probability that an incident neutron of initial energy E_1 is still in the vessel when it has been slowed down to E_2, is

$$p=4\pi^{-1}\sum_{n \text{ odd}}\frac{1}{n}\sin\frac{\pi n a l_H}{D+a l_H}\times\exp\left(-\frac{1}{6}\frac{n^2\pi^2(r^2)_{Av}}{(D+a l_H)^2}\right), \quad (17)$$

where l_H is the mean free path between two collisions with hydrogen (1.5 cm in ethyl bromide), $a=3.14$ is a constant connected with the diffusion of neutrons in ethyl bromide, and $(r^2)_{Av}$ the mean square distance traveled from energy E_1 to E_2. The index n takes all odd integral values but in most cases it is sufficient to consider the term $n=1$. Equation (17) is valid if the thickness D is large compared with $\frac{1}{2}al_H\approx 2.35$ cm ethyl bromide which is not very well fulfilled for the dimensions used in the experiments of v. Halban, Kowarski and Magat ($D=10$ cm). With these dimensions, the probability that a neutron reaches thermal energy in the vessel without being scattered out,[37] is about 87 percent for an initial energy of 1 ev, 65 percent for 100 ev, 40 percent for 10^5 ev, and 16 percent for 1 Mev. It might be thought desirable to increase the thickness of the vessel in order to make $D\gg\frac{1}{2}al_H$. However, faster neutrons ($>10^5$ ev) will then have a considerable probability of being slowed down to the thermal region, and for such neutrons (17) is no longer valid because of the rapid variation of l_H with energy.

If the energy distribution of the incident neutrons is given by (2), the total number of neutrons slowed down in the vessel to thermal energies is

$$N_{th}=\pi^{-3}Mql_AS\left(\frac{D+al_H}{bl_H}\right)^2\sin\frac{\pi a l_H}{D+a l_H}\times\left\{\exp\left(-\frac{1}{6}\frac{\pi^2(r^2)_{Av}(E_{capt})}{(D+a l_H)^2}\right)-\exp\left(-\frac{1}{6}\frac{\pi^2(r^2)_{Av}(E_1)}{(D+a l_H)^2}\right)\right\}, \quad (18)$$

where l_A is the mean free path in air, $b=0.82$ is a factor taking account of the collisions with carbon and bromine in the C_2H_5Br, S is the surface of the flat vessel (on one side) and $(r^2)_{Av}(E)$ the mean square distance traveled by a neutron of initial energy E before it is captured in the vessel. E_{capt} is given by (4a), and E_1 is approximately the energy at which the mean free path $\frac{1}{2}al_H$ becomes larger than D, i.e., about 1 Mev. To obtain Eq. (18) it must be assumed (1) that the mean free paths in the substance and in air are constant for all initial energies which contribute appreciably to the activity produced in the vessel and (2) that there is no appreciable capture in air for neutrons of these energies. We have mentioned above that the probability to be captured in the vessel used by v. Halban *et al.* is about $1/e$ for a 100-kev neutron and falls rather rapidly at higher energy. Now if the mean free path in air, l_A, did not increase with energy, the energy distribution of the neutrons incident upon the measuring vessel would be as dE/E, and then neutrons above 100 kev would give only a small contribution to the number of neutrons detected. Actually we know that l_A *does* increase with energy, and we know that this increase takes place below 150 kev (§1). This will make the neutrons of higher energy more important, and the necessary correction to (18) will be the greater the lower the energy E_S at which the mean free path in air increases to its high energy value. The importance of high energy neutrons will be further enhanced if there is strong capture of neutrons in air for such energies which are still important for the effects detected, because such capture will increase the number of fast neutrons in air relative to the slow ones.

The uncertainties at high energies will be even

[37] In ethyl bromide, the capture does not occur immediately after the neutrons are slowed down to thermal energies. The capture cross section of Br is unknown but probably smaller than 10×10^{-24} cm². This would mean that at least 25 elastic collisions with H occur before capture. The probability that a neutron diffuses out after reaching thermal energy is therefore at least 5 percent. An upper limit of 30 percent is set by the capture in hydrogen.

more important for larger thicknesses D because then faster neutrons will contribute more to the bromine activity. Moreover, Eq. (17) will then become invalid because of the variation of l_H with energy.

Another problem is the behavior of slow neutrons in ethyl bromide. We have assumed thus far that only thermal neutrons are appreciably captured. However, it is also possible that the lower resonance levels of bromine capture an appreciable number of neutrons coming from high energies; in this case, the necessary $(r^2)_{Av}$ for a fast neutron would be reduced and its probability p of capture correspondingly increased.

In spite of these many uncertainties we shall assume (18) to be approximately valid. It is then permissible to replace the first exponential in the curly bracket by 1 and the second by zero, further to replace the sine by its argument and to neglect al_H compared with D. Then (18) reduces to[38]

$$N_{capt}=0.47MqVl_A/l_H, \tag{18a}$$

where $V=SD$ is the volume of the vessel. This simple formula is valid if

$$\tfrac{1}{2}al_H \ll D \ll [(r^2)_{Av}]^{\frac{1}{2}}.$$

Since $(r^2)_{Av}$ is only 5 times $\frac{1}{2}al_H$, this condition is never very well fulfilled but, due to a cancellation of corrections, the difference between (18) and (18a) is only 2 percent for ethyl bromide and $D=10$ cm.

For thicknesses $D \approx (r^2)_{Av}$ Eq. (18) must be used instead of (18a). For $D \gg (r^2)_{Av}$, the number of neutrons captured will become proportional to the surface rather than the volume of the vessel. However, (18) is then no longer correct, because of the uncertainties at high energies discussed above. For still larger thicknesses, we get again a volume effect due to the production of neutrons in the vessel itself; if we assume this production to be q_V per gram and sec., we obtain in this limit:

$$N_{capt}=q_V V\rho_B \tag{18b}$$

(ρ_B the density of ethyl bromide) which is about 7 times smaller than (18a) if we assume $q=q_V$.

[38] It should be noted that in this formula l_A is measured in g/cm² and l_H in cm.

An infinite flat vessel cannot be realized in practice. For a large flat vessel, (18) will still be approximately valid because there will be a compensation of the neutrons which diffuse out by the side walls, and those which come in from the side. For a sphere, the theory gives one-half of the expression in Eq. (18), with D replaced by R. For $l_H 3^{\frac{1}{2}} \ll R \ll [(r^2)_{Av}]^{\frac{1}{2}}$ the final result is then $\frac{3}{4}$ of Eq. (18a).

V. Halban, Kowarski and Magat[16] found about 100 neutrons per cm² and minute at an altitude of 9500 m, corresponding to 3 meters of water pressure. According to (18) this gives $q \approx 0.010$ neutron per gram and second.

The value of q deduced from these experiments is again an upper limit to the actual q because of the effects discussed after Eq. (18). The apparent values of q deduced here and in Eq. (16) are, of course, influenced in different ways by the capture of neutrons in air, etc.

Other arrangements belonging to this category are $1/v$ detectors surrounded by paraffin or by borax. The latter type has been used for the measurement of cosmic neutrons.[10-12] It is, however, less apt to give interpretable results than the bromine method. Some discussion of it will be found in reference 31. In contrast to statements in the literature it must be pointed out, that the absorbing effect of a borax shield is not confined to thermal neutrons. Irrespective of the energy dependence of its sensitivity such an arrangement will give the correct dependence of q on altitude, provided the energy distribution of neutrons does not depend on altitude, i.e., at distances larger than about 1 m water equivalent from the top of the atmosphere as well as from the ground. So far, all the measurements available have been carried out on the ground.

§ 6. Recoil measurements

The investigation of neutron recoils may yield information about the energy distribution of faster neutrons. Such measurements can be made using ionization chambers with linear amplifiers, proportional counters or photographic plates. In evaluating the experiments it must be remembered that the measurements give directly only the energy distribution of the recoil atoms, and that a neutron of energy E produces recoils ranging from zero energy to $(4/M_r)E$. The energy

distribution of the neutrons can therefore only be obtained by a differentiation of the distribution of recoils. Unless the range distribution of the recoils is measured directly by a linear amplifier, it must again be deduced from the number of recoils as a function of the bias which requires another differentiation. A similar evaluation is necessary for photographic plates. The present experiments[39] do not yet allow an analysis along these lines.

The energy distribution which could be deduced from recoil measurements will not give much relevant information for energies below the first excited level of N^{14}, because for these energies the neutron distribution will be determined mostly by the mechanism of slowing down in nitrogen which could more adequately be investigated by laboratory measurements of the cross sections for various energy neutrons. The number of high energy neutrons is very small; moreover measurements of their energy distribution could only be made with heavy recoil nuclei because if hydrogen were used the number of recoil protons from fast neutrons would only be of the same order as the number of protons directly produced by the cosmic radiation.

III. Discussion of the Experimental Results

§ 7. The altitude dependence

We have shown at the end of §2 that the neutron intensity must decrease with altitude at least within a distance L from the top of the atmosphere. The experiments of one of us show, on the other hand, an increase with altitude up to 1 meter water pressure. This means that L must be 1 meter water or less for most of the neutrons observed at high altitudes. In §2, we have found that L is approximately 1 meter for a neutron of initial energy below 30 Mev. Therefore we can conclude that either (1) the neutrons observed at high altitudes are mostly produced with energies below 30 Mev, or (2) the mean free path for inelastic collisions is of the same order for neutrons of higher energies than 30 Mev as for slower neutrons.

Which of the two conclusions is correct cannot be decided. There is no *a priori* argument against either of them; but older theories of nuclear forces predicted[18] a considerable increase of the mean free path for energetic neutrons (above 100 Mev). If these theories were proved correct we should have to draw conclusion (1).

We cannot draw any similar conclusions about the neutrons observed at lower altitudes. E.g., it would be entirely possible that these neutrons are partly or wholly produced by very energetic neutrons which themselves originated near the top of the atmosphere. If such energetic neutrons have a long range, as predicted by the theories of Heisenberg and Williams,[18] they could penetrate to lower altitudes and there produce slower neutrons which then diffuse as discussed in §1, 2. If this should be the origin of the neutrons at lower altitude, we should have to draw conclusion (1) about the neutrons observed at high altitude; and since the neutron intensity is much smaller at lower altitude, we could then say that most of the neutrons produced altogether have moderate initial energies (100 Mev, say). In any case, only a small fraction of the neutrons produced can have long mean free path.

The altitude dependence of neutron intensity permits some further conclusions on the neutron production. According to the experiments of one of us,[15] the neutron intensity increases by about a factor two for each meter of water. This figure may be considered as safe from about 4 to 1 meter water. This result shows that the neutrons cannot be produced by mesons because, according to Schein, Jesse and Wollan,[34] the meson intensity increases only by a factor of 11 over the whole atmosphere. Since the increase seems fairly uniform at the lower altitudes,[40] an increase by a factor of only about 2–2.5 is to be expected from 4 to 1 meter. On the other hand, the soft component of cosmic radiation (electrons +photons) increases with altitude about as much as the neutron intensity.

§ 8. Number of neutrons. Energy considerations

We have shown that there are many uncertainties in the evaluation of the present experiments on neutrons in cosmic radiation, and that they might be to a large extent eliminated by somewhat different experimental arrangements (§4, §3) and by laboratory measurements on the

[39] S. A. Korff, Phys. Rev. **56**, 1241 (1939).

[40] Rossi, Hilberry and Hoag, Chicago Meeting, No. 10 (1939).

interaction of neutrons with nitrogen. At the present time we can only give estimates of the number q of neutrons which escape capture at high energies. The number of neutrons produced originally is difficult to estimate at present (§1, 4). We can only say that q represents a lower limit to the actual number q' of neutrons produced.

The measurements of one of us (S.A.K.) with BF_3 counters give a neutron production 0.05 neutron per gram and second at one meter of water (§4); this figure represents an upper limit to q because part of the counts in the BF_3 chamber will be due to recoil nuclei rather than to boron disintegrations. The evaluation of the measurements of v. Halban, Kowarski and Magat with ethyl bromide at three meters of water gives 0.010 neutron per gram and second. From the experiments with BF_3 counters, it follows that the number of neutrons increases with elevation by about a factor of 2 per meter of water, so that the BF_3 measurements give about the same result as the C_2H_5Br experiments. In view of the many uncertainties, this agreement must be considered as accidental.

The total number of neutrons produced per second in a column of 1 cm² cross section is

$$Q=100q'(1\text{ meter})\int_0^\infty e^{-0.7(x-1)}dx, \qquad (19)$$

where x is the depth in meters of water from the top of the atmosphere. It is uncertain whether the production should be assumed to increase at the normal rate in the top meter as has been assumed in (19). If we take one-half of the value (19) for the top meter, and also replace q' by q we shall certainly get a lower limit to Q; *viz.*,

$$Q>10\text{ neutrons/cm}^2\text{ sec.} \qquad (20)$$

It is interesting to investigate the energetic role of the neutrons. If we assume that the initial kinetic energy of the neutrons is about 10 Mev and if we add another 10 Mev for the binding energy of the neutron in the nucleus it came from, we find that a total of more than 200 Mev must be spent per cm² and sec. to produce neutrons. This is one-twelfth of the total energy[41] spent by the cosmic radiation in producing ionization. However, it would be difficult to measure the total energy spent in *producing* neutrons; it is much more important to know how much the neutrons themselves contribute to the ionization. This quantity will be much smaller, mostly because the binding energy of the neutron in the nucleus it came from will not be transformed back into "visible" energy; the neutrons disappear finally by the $N^{14}(n,\alpha)B^{11}$ or the $N^{14}(n,p)C^{14}$ reaction so that much of the energy resides finally in protons or B^{11} nuclei. Thus cosmic radiation serves to build up nuclei of high internal energy. Only the kinetic energy of the neutrons and the small energy evolved in the n,p process (0.7 Mev) will be transformed into ionization, by producing recoils and by exciting nitrogen nuclei which subsequently emit γ-rays. But even part of the kinetic energy of a fast neutron (>8 Mev) will be consumed in disintegrating N and O nuclei by nuclear reactions in which more than one particle is emitted. Thus the energy which is actually transformed into ionization may well be as low as 5 Mev per neutron, i.e., 50 Mev per cm² and sec. when the figure of Eq. (29) is assumed, or 2 percent of the whole energy in the cosmic radiation. This figure is of course as uncertain as all the figures on neutrons in cosmic radiation.

The production of neutrons has been compared with that of protons by C. G. and D. D. Montgomery,[42] and it seems indeed likely that these particles are produced in the same process. From measurements of Neddermeyer and Anderson on Pike's Peak,[43] we can estimate that there is about 1 proton per 300 lightly ionizing particles. The number of the latter is about 0.2 per cm² and sec. on Pike's Peak. Therefore, if R is the average range of the protons in cm of standard air, the number produced per gram and second is about

$$\frac{0.2}{300R\times1.2\times10^{-3}}=\frac{0.6}{R}$$

(1.2×10^{-3} is the density of standard air). For $R=1$ meter (10-Mev protons) this would give

[41] I. S. Bowen, R. A. Millikan and H. V. Neher, Phys. Rev. **53**, 855 (1938).

[42] C. G. and D. D. Montgomery, Rev. Mod. Phys. **11**, 255 (1939).

[43] S. H. Neddermeyer and C. D. Anderson, Phys. Rev. **50**, 263 (1936).

6×10^{-3} proton/g sec. If we assume the neutron intensity to decrease by a factor 2 per meter water, the neutron production at 6 meters water would be about 10^{-3}/g sec. The agreement is sufficient in view of the uncertain data.

Our considerations show that the total number of neutrons is certainly considerable, and of the same order of magnitude as the total number of electrons or quanta in cosmic radiation. Thus if the neutrons are produced by quanta, each quantum must produce on the average about one neutron. Of course, it is likely that an energetic quantum when it disintegrates a N or O nucleus, produces several neutrons at once so that not every quantum will be concerned in the production process. Moreover, it is as yet unknown whether quanta or other particles are responsible for the neutron production.

APRIL 1, 1940 PHYSICAL REVIEW VOLUME 57

Excitation of the 455-Kev Level of Li^7 by Proton Bombardment

C. M. Hudson, R. G. Herb and G. J. Plain*
University of Wisconsin, Madison, Wisconsin
(Received January 24, 1940)

The yield of gamma-rays from a thin film of lithium bombarded by protons has been investigated up to 2.08 Mev, by recording both single and coincidence counts in G-M tubes. Above 0.85 Mev proton energy most of the radiation is shown to be due to excitation of the 0.455-Mev level of Li^7 without permanent capture of the proton. The yield of 17-Mev radiation does not drop to zero above 0.440 Mev. It falls to a low value and remains approximately constant up to 1.6 Mev. The absorption coefficient in lead for the soft gamma-radiation from lithium was compared to the absorption coefficient of annihilation radiation from N^{13}. A value of 0.459 Mev was obtained for the energy of the soft lithium radiation by assuming monochromatic radiation of 0.511 Mev from N^{13}. This close agreement with the expected energy indicates that not over 10 percent as many 0.28-Mev quanta as 0.511-Mev quanta are present in the radiation from N^{13}.

Introduction

THE excitation of gamma-rays from lithium by proton bombardment was studied three years ago at this laboratory using protons in the energy region 0.4 to 1.9 Mev.[1]

A gamma-ray resonance of lithium had previously been established for protons of 0.440 Mev energy by Hafstad, Heydenburg and Tuve.[2] These gamma-rays were found by Lauritsen and his colleagues to have an energy of approximately 17.5 Mev. The previous work here showed the presence of considerable radiation caused by protons above 0.85 Mev, but no measurements were made of the energy of this radiation.

The work reported upon in this paper shows that most of the radiation above 0.85 Mev proton energy is due to the excitation of an energy level of Li^7 which was found by Rumbaugh, Roberts and Hafstad[3] to be 0.455 ± 0.015 Mev above the ground state. Their paper will hereafter be referred to as RRH.

While this paper was being written, Fowler and Lauritsen[4] reported obtaining from lead absorption measurements similar to ours, a value of 0.495 ± 0.025 Mev for the energy of the radiation due to 1.08- and 1.29-Mev protons on lithium. They attribute this to excitation of the 0.455-Mev level, but have no explanation for the high value they obtained for the gamma-ray energy.

Our values for the absorption coefficient of the radiation agreed with those of Lauritsen, but when corrections were applied for a hard component, the energy obtained for the soft component agrees with the value expected from

* Now at the University of Iowa, Iowa City, Iowa.
[1] Herb, Kerst and McKibben, Phys. Rev. **51**, 691 (1937).
[2] Hafstad, Heydenburg and Tuve, Phys. Rev. **50**, 504 (1936).
[3] Rumbaugh, Roberts and Hafstad, Phys. Rev. **54**, 657 (1938).
[4] W. A. Fowler and C. C. Lauritsen, Phys. Rev. **56**, 841 (1938).

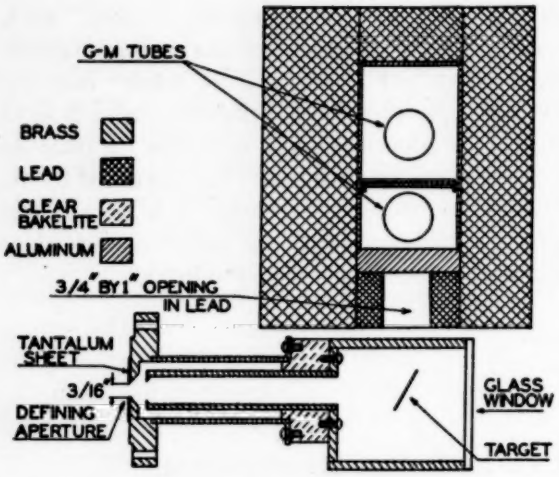

FIG. 1. Target chamber and counter arrangement.

RRH. Excitation curves for the total radiation and for its hard component are also extended up to 2.08 Mev.

EXPERIMENTAL ARRANGEMENT

Figure 1 shows the arrangement of target chamber and counters. Lithium targets were prepared by evaporation of lithium metal onto a sheet of tantalum mounted as shown in the figure. Diaphragms outside the chamber limited the proton beam to a small part of the target so that the film used was fairly uniform. Tantalum was used for these diaphragms and for the target backing since it was found to give no observable gamma-radiation.

Gamma-ray yields were measured by two thin-walled glass G-M tubes enclosed in a lead box as shown in Fig. 1. An aluminum plate on the floor of the shielding box served as a source of secondary electrons. An investigation of the absorption of secondary electrons by taking coincidence yields as a function of the thickness of aluminum between the counters can determine the energy of hard radiation.

The tubes were connected in a circuit such that the single counts in the lower G-M tube were recorded through a scale-of-ten circuit and at the same time coincident discharges of the two Geiger-Mueller tubes were recorded in another scaling circuit.[5] The bombardment current was measured by the current integrator previously described.[1] With this system the counting rate for singles and the counting rate for coincidences could each be expressed in counts per microcoulomb of bombarding protons.

EXCITATION CURVES

The presence of soft radiation emitted by protons on lithium was first noticed in this work when the ratio of coincidence to single counts was found to be very low for radiation due to protons of 1.6 Mev energy striking a thick target. Preliminary measurements of the absorption in lead indicated that most of the radiation was due to excitation of the 0.455-Mev level of lithium.

From a thin film (film I) which was then prepared, singles and coincidence yields were investigated simultaneously over the energy region 0.4 to 1.9 Mev. These data are shown in Fig. 2, with the ordinates for coincidences multiplied by six to make the two curves coincide over the 0.440-Mev region, where only hard radiation is present. Because the two curves remain identical up to almost 0.8 Mev, all radiation in this region is believed to be hard.

The yield curves show that the hard gamma-ray intensity does not drop to zero above the 0.440-Mev resonance, but decreases to a low, constant value (~6 times the counting rate due to background). Above 0.8 Mev the singles yield rises sharply, but the coincidence yield remains practically constant at its low value. The rise in singles yield must therefore be due to radiation so soft that practically none of its secondary electrons can penetrate both counter tubes. These measurements were made with no aluminum between the counters so that in order to cause coincidences, secondary electrons had to traverse two counter walls which gave an equivalent of approximately 0.3 mm of aluminum.

A broad resonance for soft radiation at proton energies around 1.05 Mev has been well traced, both in the earlier publication[1] and in this work. A slight hump near 1.31 Mev reproduced itself in all three curves of Fig. 2, and in the two curves previously published. Between 1.4 and 1.8 Mev, excitation curves for both film I and film II appear to show resonance structure, but since the two do not agree very well the resonances cannot

[5] The arrangement is described in more detail in the paper by Plain, Herb, Hudson and Warren, Phys. Rev. 57, 187 (1940).

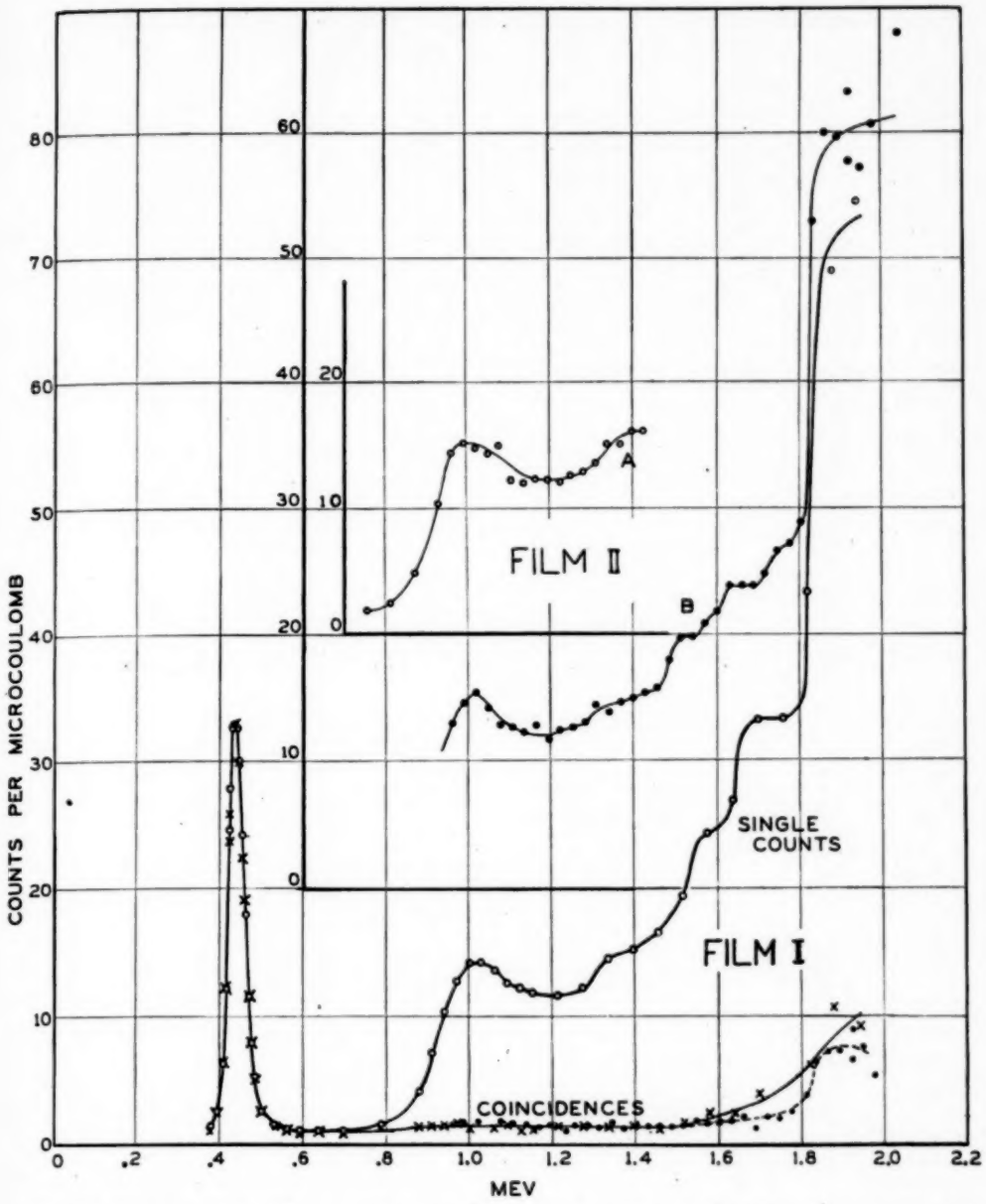

FIG. 2. Single and coincidence yields from thin lithium targets as a function of proton energy. The singles yield measures the total gamma-ray intensity, and the coincidence yield measures the intensity of the hard component.

be considered as definitely established. A large, sharp increase in intensity at 1.83 Mev is unmistakable.

Since the threshold for neutron emission was recently reported by the Westinghouse Research Laboratories group[6] to be at 1.86 Mev, it is thought possible that part of the increase at 1.83 Mev in Fig. 2 may be due to neutrons. In the present work, insufficient precautions were taken to exclude the possibility of an error in the voltage as large as the observed difference. Observations on the nature of the reactions above 1.8 Mev and extension of the excitation curves were cut short to begin revision work on the electrostatic generator.

The form of the singles yield curve does indi-

[6] Haxby, Shoupp, Stephens and Wells, Annual meeting American Physical Society, December 28, 1939.

cate that the observed rise at 1.83 Mev is due principally to gamma-rays, since the curves appear to flatten out above 1.9 Mev. It is thought likely that a neutron yield curve would continue to increase over a considerable voltage region above the threshold. The observed rise in coincidence yield may be due to neutrons, to an increase in the intensity of ~17-Mev gamma-rays, or to resonance excitation of a new component of gamma-radiation of sufficient energy to cause coincidences.

From a consideration of the preceding curves it is seen that the coincidence yield measures the intensity of the hard component. Apparently independently of any changes in the singles yield, the coincidence yield from 0.6 to 1.6 Mev retains its low but measurable value, approximately six times the correction for generator and cosmic-ray background. Accidentals could not be responsible for the observed intensity, according to the measured resolving time of the circuit (6.8×10^{-5} sec.); and besides, the accidentals should increase as the square of the single counting rate, but the observed coincidences do not increase. This leads to the conclusion that the coincidence yield even above 0.8 Mev is a measure of the hard component of the radiation.

The energy of the hard component was measured for radiation from a lithium target which had an absorption thickness of ~0.25 Mev for 0.7-Mev protons. When protons of 0.97 Mev were used for bombardment, a thickness of 6.1 mm of aluminum was required to reduce the coincidences by one-half. For gamma-rays due to 1.64-Mev protons, a half-value thickness of 7.4 mm of aluminum was obtained. The probable error in these values is large because of the high singles counting rate due to the intensity of soft radiation. With a singles counting rate low enough to avoid many accidental coincidences, the true coincidence rate was low, and only 240 counts were taken at each of three points to determine the half-value thickness. Within the probable error these values agree with the half-value thickness obtained for 17.5-Mev radiation from the 0.440-Mev resonance, and indicate that the coincidence yield over the entire voltage region investigated is due to 17.5-Mev radiation.

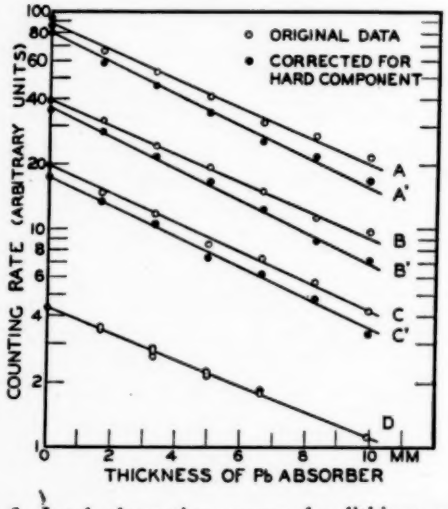

FIG. 3. Lead absorption curves for lithium gamma-radiation (*A*, *B*, and *C*) and for positron annihilation radiation (*D*).

TABLE I. *Lead absorption of gamma-rays.*

	Gamma-rays from Protons on thin Li			Positron Annihilation Radiation
Curve	*A–A'*	*B–B'*	*C–C'*	*D*
Proton energy (Mev)	1.214	1.639	1.032	
Original absorption coefficient (Curves *A*, *B*, & *C*)	1.523	1.490	1.551	1.414
Correction for hard radiation	10.9%	9.0%	7.9%	
Absorption coefficient of soft component (Curves *A'*, *B'*, & *C'*)	1.690	1.690	1.662	
Average value		1.681		
Energy of radiation (Mev)		0.459		0.511

Energy of the Soft Component

The absorption coefficient in lead for radiation emitted from film I at each of several proton energies (see Table I) was obtained by taking the singles yield as a function of the thickness of lead sheets placed just below the window of Fig. 2. These data when plotted on the semi-logarithmic scale of Fig. 3 as curves *A*, *B* and *C* gave the "original absorption coefficients" listed in Table I.

The proportion of hard radiation for each voltage investigated was taken as the ratio at that voltage of the ordinate for coincidences to the ordinate for singles yield from film I (Fig. 2). A lead absorption curve was taken separately for 17.5-Mev radiation to determine how the single counts due to the hard component decreased with thickness of lead. From these data on

the proportion and absorption of hard radiation, corrections for the number of counts due to the hard component were subtracted from the yields shown at each point of curves A, B, and C. The yields resulting from this correction are shown as the points determining curves A', B', and C', for the soft component. The absorption coefficients obtained from these curves are nearly equal, with an average value of 1.681 cm^{-1}.

Determination of the energy of radiation with this absorption coefficient had to be made by comparison with the absorption coefficient of a known radiation under identical conditions. Annihilation radiation, due to positrons from N^{13}, was used for this purpose as follows:

Radioactive nitrogen was prepared by deuteron bombardment of a carbon target, which was placed in the same position as the lithium target. After bombardment the chamber was flushed with air and was open at atmospheric pressure during the measurements. The measurements over 39 min. gave a value of 11.1 min. for the half-life. This agrees[7] with Ellis and Henderson's value of 11.0 min., which Livingston and Bethe adopted, but recent results of careful work by Ward give a value for the half-life of 9.93±0.03 min. The source of error in our work is not understood. If it is caused by contaminants it is possible that the use of this radiation for calibration may have caused error in the value obtained for the energy of the soft radiation from lithium.

A brass plate was laid on the surface of the target so that positron annihilation radiation was produced very nearly in the same position as the lithium target.

Measurement of the absorption coefficient of positron recombination radiation in lead gave a value of 1.414 cm^{-1}. By use of this absorption coefficient and Heitler's theoretical curves[8] for the variation of absorption coefficient with energy, an energy of 0.459 Mev is obtained for the soft component of lithium radiation.

Since no transmutation seems capable of explaining these gamma-rays, and since RRH have observed an energy level 0.455 Mev above the ground state in Li^7, it appears certain that the observed rays must be due to excitation of this energy level without permanent capture of the proton.

In these computations it was assumed that radiation from N^{13} consisted only of annihilation radiation, with an energy of 0.511 Mev. This procedure may be questioned since several observers have reported some 0.28-Mev radiation in addition to a negligible amount of radiation harder than 0.511 Mev. From his latest work with a cloud chamber Richardson[9] reported that 21 percent as many quanta of 0.28 Mev as of 0.511 Mev were emitted, with an uncertainty factor of two. Lyman[10] obtained 10±7.5 percent, using gamma-gamma coincidences, and 12 percent from β-ray spectrum analysis. Watase and Itoh[11] find similar results. In contradiction to these results, Valley,[12] working with a magnetic spectrograph with x-ray film as a detector, reported nothing in the region 0.28±0.03 Mev, with 2.5 percent as an upper limit (i.e., <0.05 quanta of 0.28 Mev per disintegration). Since our value for the Li^7 energy level agrees closely with that of RRH, it was thought worth while to compute the possible effect of soft radiation and from estimates of the probable errors to set some upper limit to the amount of such radiation present.

Upper limits for the proportion of 0.28-Mev radiation are indicated in two ways by the present work. First, the lead absorption curve labeled D in Fig. 2 is straight. The absorption coefficient for 0.28-Mev radiation in lead is 3.4 times the coefficient for 0.511 Mev, according to Heitler's curves. From a graph drawn to include various proportions of 0.28-Mev radiation it seems probable that some curvature would have been observed if there had been more than 30 percent as many 0.28-Mev quanta as 0.511-Mev quanta. The radiation from annihilations producing only one quantum (1 Mev) is known to be negligible, and computations show that radiation harder than 0.511 Mev, from positrons annihilated while in motion is also negligible

[7] C. D. Ellis and W. J. Henderson, Nature **135**, 429 (1935); M. S. Livingston and H. A. Bethe, Rev. Mod. Phys. **9**, 359 (1937); A. G. Ward, Proc. Camb. Phil. Soc. **35**, 523 (1939).

[8] W. Heitler, *Quantum Theory of Radiation* (Oxford, 1936), pp. 124, 160 and 216.

[9] J. R. Richardson, Phys. Rev. **55**, 609 (1939).

[10] E. M. Lyman, Phys. Rev. **55**, 1123(A) (1939).

[11] Watase and Itoh, Proc. Phys. Math. Soc., Japan **21**, 389 (1939).

[12] G. E. Valley, Phys. Rev. **56**, 838 (1939).

ible. The straightness of the lead absorption curve is therefore an indication of the maximum possible proportion of radiation with energy appreciably different from 0.511 Mev.

A second indication is the fact that the energy of the Li^7 gamma-radiation (0.459 Mev) measured here agrees with the value 0.455 ± 0.015 Mev obtained by RRH in an entirely different way. The probable error in the whole determination was figured from estimates of: first, the errors in measuring the absorption coefficients of the positron radiation and of the soft component of the lithium radiation; second, the errors in reading slopes and absorption coefficients from Heitler's curves; and third, the error given by RRH for the energy of the excited level. The over-all probable error is taken as the square root of the sum of the squares of the individual probable errors. It is about the same as the error that would have been made in determining the energy of the lithium level if there had been 10 percent as many 0.28-Mev quanta as 0.511-Mev quanta in the radiation from N^{13} and its positrons.

This upper limit of 10 percent is on the low side of Lyman's 10 ± 7.5 percent but since it was obtained in such a devious way, it must be considered only as supplementary evidence that very little 0.28-Mev radiation is emitted.

Mr. R. E. Warren and Mr. D. L. Bobroff have aided in taking data and making drawings. Professor G. Breit has given valuable discussions of the nuclear processes involved. The Wisconsin Alumni Research Foundation and the Penrose Fund of the American Philosophical Society have furnished financial support.

APRIL 1, 1940 PHYSICAL REVIEW VOLUME 57

Positive Excess and Electron Component in the Cosmic-Ray Spectrum

DONALD J. HUGHES
Ryerson Physical Laboratory, University of Chicago, Chicago, Illinois

(Received January 25, 1940)

The sea-level cosmic-ray energy spectrum has been determined, using a 30-cm counter controlled cloud chamber in a 12,400-oersted magnetic field. The spectrum of mesotrons alone is obtained by inserting a 10-cm lead filter in the counter train, the total spectrum is obtained with no filtering, and the spectrum of the soft (electron) component is then the difference between these two spectra. An excess of positive particles exists both with and without the lead, the ratio of positives to negatives being 1.21 ± 0.08 (standard error) in the former, and 1.18 ± 0.08 in the latter case. Comparison of the spectra with and without lead shows the presence of an absorbable component (electrons) in the energy region 2 to 8×10^8 ev but no absorbable particles of higher energy. The spectra have been corrected for the distortion at low energies caused by the magnetic field. The corrected mesotron spectrum possesses a maximum and a rapid decrease below the maximum while the total spectrum shows no maximum but a continuous increase in number with decreasing energy.

IN June, 1939, at the Chicago cosmic-ray symposium H. Jones[1] reported on the energy distribution of mesotrons. The energy spectrum was obtained with the large cosmic-ray magnet at the University of Chicago, using a 10-cm lead filter to remove electrons. The results showed a greater number of positive than negative particles, the excess, amounting to 29 percent, being spread rather uniformly throughout the spectrum. Such an excess might mean either a greater absorption of negatives in the lead or a real positive excess in the energy spectrum incident on the magnet. Blackett's[2] work on the unshielded energy spectrum showed a small positive excess which was interpreted by him as being probably of no significance. Ringuet,[3] using a lead absorber, found a large positive excess at high energies but no excess without the lead. Pair production of mesotrons would of course result in an equality in regard to sign, and such an equality

[1] H. Jones, Rev. Mod. Phys. **11**, 235 (1939).

[2] P. M. S. Blackett, Proc. Roy. Soc. **A159**, 1 (1937).

[3] L. Leprince-Ringuet and J. Crussard, J. de phys. et rad. **8**, 207 (1937).

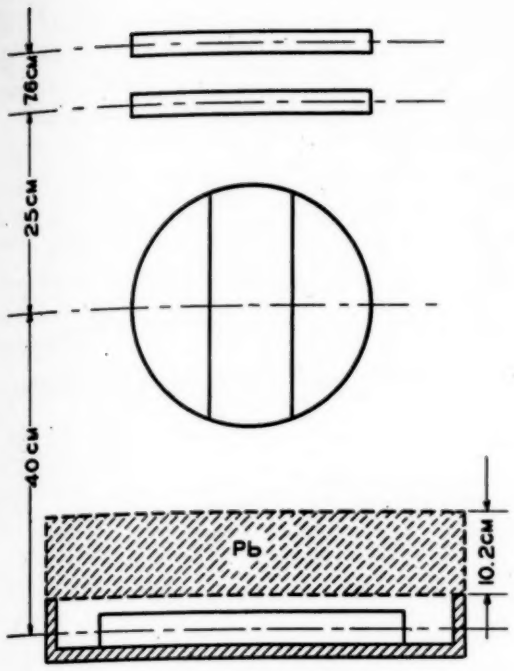

FIG. 1. Diagram of apparatus.

is usually assumed. However, explanation of the observed excess in terms of absorption of negatives is very difficult, for the lead absorbers used should have practically no effect on the high energy rays which are involved in these experiments. Because of the open nature of this question it seemed desirable to us to continue the experimental work, having two objects in view, (1) to remove as far as possible any instrumental asymmetry which might give rise to a spurious effect and (2) to determine the relation of the lead absorber to the positive excess.

APPARATUS

The apparatus is shown diagrammatically in Fig. 1. Details of construction and operation of the cloud chamber and electromagnet have been given elsewhere.[4] Expansions of the 30-cm chamber are controlled by the triple coincidence G-M counters, the average interval between expansions being of the order of 2 min. When the lead filter is in place, only those particles with a residual range greater than 10-cm lead, namely, the mesotrons, are recorded. With the filter removed, the absorbable particles (the electrons) as well as the mesotrons are obtained.

It is of great importance that the effect of any systematic curvature introduced by distortion be removed. If gas motions in the chamber tend to curve tracks more in one direction than the other, a spurious excess of one sign would of course develop. Before taking the present series of photographs, therefore, we have attempted to reduce and balance the distortions as much as possible. Accurate control of the motion of the chamber diaphragm by material used, placement, and pressure regulation, has been found to be of primary importance in controlling distortion. Reference 4 gives a more complete description of these measures, and Fig. 2 shows the distortions now present in the chamber. Here are plotted the observed curvatures (caused by distortion) of 110 tracks photographed with no magnetic field during the course of the present experiment. d is the central displacement for a 20-cm track length, while E is the energy which would be inferred from d if the 12,400-oersted field were present. The distribution of d's about the correct value zero gives the probable error in d which is shown in the figure—0.012 cm. This probable error applied to the measurements with magnetic field represents an error of 6 percent at 10^9 ev and 100 percent at 1.6×10^{10} ev, thus fixing the maximum detectable energy at the latter value. The curve shows no asymmetry which might cause an apparent excess of particles of one sign.

Measurement of the distortions with zero field,

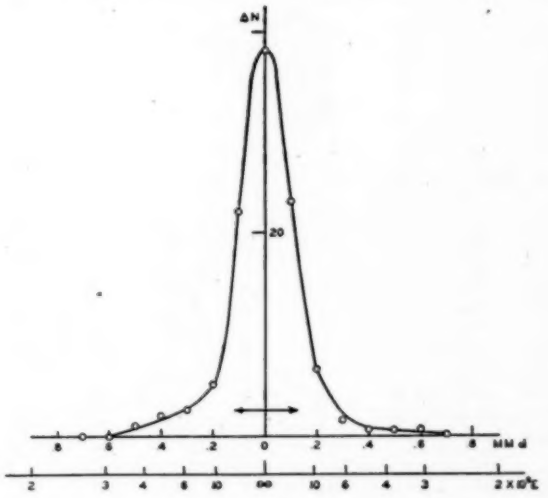

FIG. 2. Curvature of zero field tracks.

[4] H. Jones and D. Hughes, Rev. Sci. Inst. 11, 79 (1940).

of course, does not take into account those additional distortions which may be present only when the magnet is on, for instance those arising from convection currents caused by heating. To reduce convection currents, the temperature of the chamber has been controlled by reducing the exciting current of the magnet so that the pole pieces and chamber can be kept quite accurately at room temperature by the cooling oil. While the field strength has been lowered only from 16,000 to 12,400 oersteds, the power consumption and heat produced is reduced by 75 percent. This temperature control is effective in stopping the mass motion of gas that sometimes develops when the apparatus is not at temperature equilibrium.

However, to average out any asymmetry that might be present in spite of the symmetrical shape of Fig. 2, the magnetic field has been periodically reversed throughout the experiment. This procedure should nullify the asymmetrical effect of any distortions which are present with the magnetic field but absent without it.

The Positive Excess

A total of 1334 tracks with magnetic field has been measured, 674 with, and 660 without the lead absorber. The results form two separate energy spectra, which are given in Table I. Here are listed the number of positive and negative particles in each 5×10^8 ev energy interval for both the unfiltered and the filtered spectrum.

Table I. *Energy distribution of tracks.*

Range in 10^9 ev	With lead			Without lead		
	+	−	Total	+	−	Total
0 to 0.5	13	15	28	35	30	65
0.5 1.0	58	48	106	55	49	104
1.0 1.5	69	53	122	50	48	98
1.5 2.0	39	40	79	53	48	101
2.0 2.5	36	24	60	38	34	72
2.5 3.0	36	32	68	31	20	51
3.0 3.5	17	11	28	10	12	22
3.5 4.0	10	12	22	7	10	17
4.0 4.5	14	7	21	14	2	16
4.5 5.0	7	6	13	3	5	8
5.0 5.5	10	3	13	6	2	8
5.5 6.0	7	1	8	3	1	4
6.0 6.5	0	2	2	2	2	4
6.5 7.0	0	2	2	1	1	2
7.0 7.5	2	2	4	1	1	2
7.5 8.0	2	1	3	4	0	4
8.0 8.5	3	1	4	4	0	4
8.5 9.0	0	3	3	2	2	4
9.0 9.5	0	1	1	1	0	1
9.5 10.0	0	0	0	0	1	1
10.0 ∞			87			72
	323	264	674	320	268	660

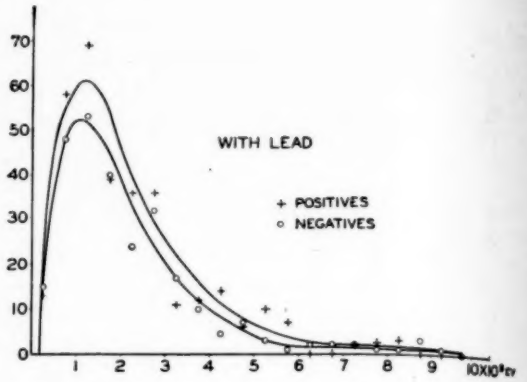

Fig. 3. Positive-negative spectra with lead absorber.

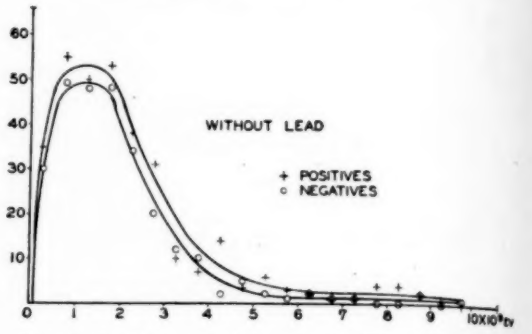

Fig. 4. Positive-negative spectra without absorber.

Considering the total number of positives and negatives for each spectrum, it is seen that the positive excess is present both with and without lead, the ratio (R) of positives to negatives having the following values:

With lead: $R=1.21\pm0.08$ (standard error)
Without lead: $R=1.18\pm0.08$.

Thus the value is the same within experimental error whether the absorber is present or not. The presence of the excess with lead confirms Jones' result, and the equality of R in both cases shows that the excess is real, i.e., is present in the sea-level cosmic-ray spectrum, and is not of instrumental origin.

If the tracks are grouped according to the direction of the magnetic field ("direct" or "reversed"), it is found that both with and without lead, the positive excess is smaller with the field reversed. This difference is less than the experimental error but may be indicative of an

asymmetry which occurs only with the magnet on, but which is averaged out by the field reversals.

The positive-negative spectra are compared graphically for the data with lead absorber in Fig. 3 and for that without the absorber in Fig. 4. Although the separation of the positive and the negative curves is not great, it is evident in each case that the positive excess is spread throughout the spectrum rather than localized in any one

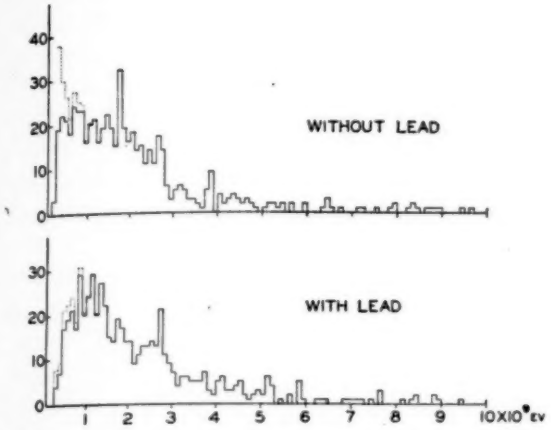

FIG. 5. Positives and negatives combined; 10^8 ev energy intervals.

region of it. This rough constancy of R, which was also found in Jones' work, is not in accord with Ringuet's finding that the excess increases with energy.

The experimental results, of course, give no information concerning the origin of the observed excess. It is well known that the primary rays which give rise to the mesotrons are predominantly positive, and it may be that this initial excess of positives is in some way propagated to sea-level.

THE ELECTRON COMPONENT

If the positives and negatives are grouped together, we have two energy spectra, one of the mesotrons alone and another of the total spectrum. The raw data comprising these are shown by the solid line in the block diagrams of Fig. 5. The presence of an absorbable component at energies less than 10^9 is immediately obvious upon comparing the two curves. Both spectra are somewhat distorted below 10^9 by magnetic deflection of rays, but the ratio of the ordinates of the two curves at any energy is unaffected by such distortion.

Comparison of the spectra with and without lead shows the location in the spectrum of the rays absorbed by the lead. The counting rate *in the magnetic field* is increased by 10 percent when the lead is removed. This means that of those rays capable of passing the magnetic barrier and setting off the counters, about 10 percent are absorbed by the lead. (The counting rate increases by 39 percent with removal of the lead when the magnet is off, hence most of this 39 percent soft group is of energy below the magnetic cut-off value.) In order to compare the spectra, therefore, it is necessary to adjust the areas under the two curves, the area under the unshielded spectrum being made 10 percent greater than the other.

The adjusted spectra are shown together in Fig. 6 (energy intervals of 5×10^8 ev), and the low energy end in more detail in Fig. 7 (energy intervals of 1×10^8 ev). It is seen that there is no significant difference between the spectra for high

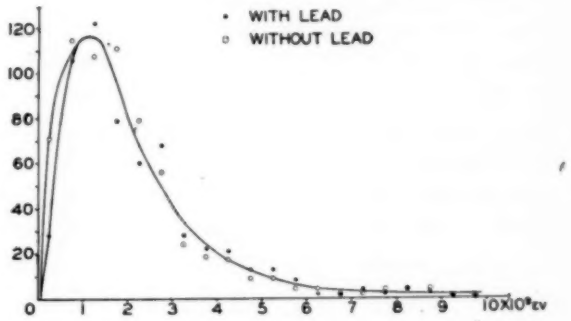

FIG. 6. Spectra with areas adjusted; 5×10^8 ev energy intervals.

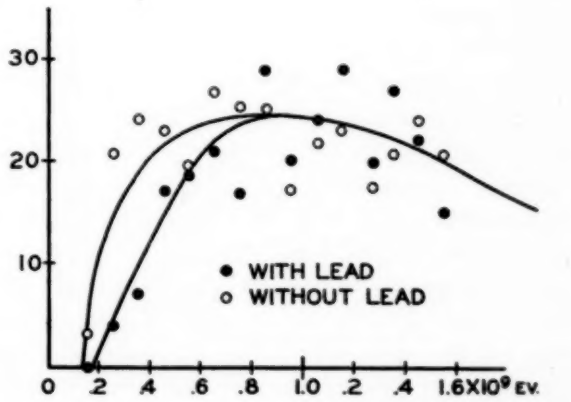

FIG. 7. Low energy region of Fig. 6; 10^8 ev energy intervals.

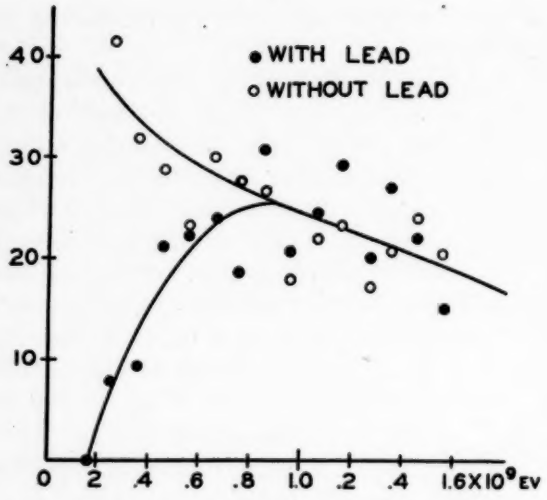

FIG. 8. Low energy spectra corrected for magnetic distortion.

energies, while for energies less than about 8×10^8 ev there is a definite absorbable group. It must be remembered that the difference between the two curves at low energies is in reality greater than it appears, for at such energies both curves are lowered by magnetic deflection. An actual count of the tracks in the spectra of Figs. 5 and 6 shows that for energies less than 8×10^8 ev there are 186 tracks in the unshielded spectrum and 134 in the shielded, while for energies greater than this value, the numbers are 506 and 505, respectively. Thus, there are 52 particles absorbed in the low energy region of the spectrum and none, within experimental error, at higher energies.

The rays stopped by the lead must represent electrons of sufficient energy to pass the magnetic barrier. They cannot be mesotrons, losing energy by ionization only, for a mesotron with residual range less than 10–14 cm lead has less than the magnetic cut-off energy. If the supposition of the preceding sentence is untrue—if mesotrons in the interval 2 to 8×10^8 ev lose energy by some process in addition to ionization—then the absorbable group may be composed in part of mesotrons. Analysis shows that the number of particles removed by scattering in the lead block is less than $\frac{1}{4}$ percent and hence does not affect the results appreciably. The scattering is small because the upper counters are close together and at a great distance from the lower counter, because the lower counter is larger than the upper two, and because the lead block is very close to the lower counter.

It is possible to calculate the fraction of the rays of a given energy which are deflected away from the chamber and hence to correct the low energy end of the spectra for this magnetic deflection. This has been done by tracing the paths of representative rays through the apparatus, finding the "allowed cone" and, taking into account the zenith angle distribution, calculating the number of rays at each energy which pass through the chamber. The correction is inappreciable for energies greater than 1.2×10^9 ev and increases with decreasing energy until it becomes 100 percent between 1 and 2×10^8 ev. The dotted line of Fig. 5 shows the raw data corrected for the magnetic deflection, and Fig. 8 the corrected low energy region of Fig. 7. The spectrum of the penetrating rays changes only slightly with the correction, still showing a maximum and a rapid decrease below the maximum. The total spectrum on the other hand shows no maximum at all, but a continuous increase in number with decreasing energy. Because the correction becomes indeterminate between 1 and 2×10^8, the extreme low energy ends of the spectra are unknown.

Counting rates taken with no magnetic field support the correctness of this calculation. The change in the area under each spectrum due to the calculated correction should, of course, be equal to the change in the measured counting rate when the field is removed. The counting rate without lead increases by 28 percent when the field is removed, while that with lead increases by only 3 percent, which is in accord with the calculated increases in area.

The results thus show that there are very few electrons of energies greater than about 8×10^8, while from this energy to about 2×10^8 there is a transition region in which the predominating particles change from mesotrons to electrons, which other work has shown are dominant at lower energies. Blackett and Wilson's experiments on the energy loss in metal plates has shown the sudden decrease in the electron spectrum, and Wilson has placed the transition region at 1 to 3×10^8 ev. The present work, involving a larger number of photographs, shows the same

behavior but indicates that the electron component extends to appreciably higher values than that given by Wilson.

It must be emphasized that this experiment, using a high field, was not primarily intended for work in this transition energy region. More accurate information, not involving the necessity of so stringent a correction, could be obtained by using an experimental set-up with a lower field such that the magnetic correction would set in at an energy lower than the one of primary interest.

It is not only a pleasure but a privilege for me to acknowledge at this point the ever-present help and inspiring guidance of Professor A. H. Compton which have made this work possible. Dr. Haydn Jones has been directly responsible for the construction of most of the apparatus used, and I wish to express my great indebtedness to him. In all the work of taking the photographs and measuring the tracks Mr. F. Leslie Code has been of very great assistance. The help of Mr. Ralph Meagher is also gratefully acknowledged.

APRIL 1, 1940 PHYSICAL REVIEW VOLUME 57

A Theoretical Study of the Diffuse Scattering of X-Rays by Crystals*

W. H. ZACHARIASEN
Ryerson Physical Laboratory, University of Chicago, Chicago, Illinois

(Received January 22, 1940)

A new derivation is made of the intensity expression for the coherent scattering of x-rays by a small crystal. The accepted intensity formula for the diffuse scattering—the well-known Debye formula—is shown to be incorrect and is replaced by a more complicated expression. According to the revised theory the intensity of the diffuse scattering varies much more rapidly with the scattering direction and exhibits a series of diffraction maxima. These maxima are found in the directions $\mathbf{k}_m$ satisfying equations of the type $(1+\lambda\tau_{\min})\mathbf{k}_m=\mathbf{k}_0+\mathbf{B}_H$, where $\mathbf{k}_0$ is the direction of incidence (with $k_m=k_0=1/\lambda$, the reciprocal wave-length) and $\mathbf{B}_H$ a reciprocal lattice vector. The consequences of the theory are discussed in detail.

INTRODUCTION

WHEN a beam of parallel and monochromatic x-rays falls on a crystal scattering processes take place. Disregarding the thermal agitation of the atoms in the crystal lattice the intensity of the coherent part of the scattered radiation is given by the well-known Laue expression

$$J_0=Sf^2\prod_i\frac{\sin^2[N_i\pi(\mathbf{k}-\mathbf{k}_0)\cdot\mathbf{a}_i]}{\sin^2[\pi(\mathbf{k}-\mathbf{k}_0)\cdot\mathbf{a}_i]}. \qquad (1)$$

The equation holds for a small crystal (linear dimensions of the order 10^{-4} cm, for instance) containing N atoms with one atom per unit cell. S is the familiar J. J. Thomson formula for the intensity of scattering from a single free electron, f is the atomic scattering power and $\mathbf{a}_i$ $(i=1,2,3)$ are the edges of the unit cell. The vectors $\mathbf{k}_0$ and $\mathbf{k}$, where $k_0=k=1/\lambda$, represent the directions of incidence and of scattering. According to Eq. (1) there are sharp intensity maxima in the Laue directions which are given by

$$\mathbf{k}-\mathbf{k}_0=\mathbf{B}_H\equiv H_1\mathbf{b}_1+H_2\mathbf{b}_2+H_3\mathbf{b}_3, \qquad (2)$$

where H_i designate three integers, $\mathbf{b}_i$ the vector set reciprocal to $\mathbf{a}_i$. For other directions the intensity is zero.

In the famous paper of P. Debye[1] the effect of the thermal vibrations was studied theoretically, and it was found that Eq. (1) had to be replaced by

$$J=J_1+J_2,\quad J_1=J_0e^{-2M},\quad J_2=NSf^2(1-e^{-2M}), \qquad (3)$$

where M is a function of temperature and scattering angle. While the first term like the original Laue expression exhibits sharp maxima

* The results given in this article were presented in a paper before the American Physical Society at the Chicago meeting December 1, 1939.

[1] P. Debye, Ann. d. Physik **43**, 49 (1914).

in the Laue directions and is zero elsewhere, the part J_2 changes slowly with the scattering angle and represents diffusely scattered x-rays.

From theoretical side objections were raised to Debye's treatment[2] and on the basis of later investigations[3] it was claimed that the diffuse radiation was concentrated under the maxima due to the term J_1 of Eq. (3).

Extensive experimental studies of the diffuse scattering from crystals have been made by G. E. M. Jauncey[4] and collaborators and their results were found to be in general agreement with Debye's formula. It seems that the theoretical conclusions reached by Brillouin, Faxén and Waller never have been seriously considered while the Debye formula on the other hand has been confirmed by more recent theoretical derivations due to Jauncey and Harvey[5] and to Woo.[6]

The writer has made a simplified derivation of the intensity formula for the scattering of x-rays by a small crystal. It is found that the Debye expression for the diffuse scattering is not correct. The new form for J_2 leads to intensity maxima in certain specific directions. These diffraction maxima may coincide with the Laue maxima (as claimed by Brillouin, by Faxén and by Waller). However, under proper conditions the maxima will not coincide with the Laue directions, thus giving rise to new diffraction spots in x-ray photographs. In the following sections the theory of this new effect will be developed and discussed while a preliminary experimental study will be reported upon in a following article.

1. Derivation of the Intensity Expression for the Coherent Scattering of X-Rays by a Small Crystal

For the sake of convenience let it be supposed that the small crystal is a parallellepiped with edges $(N^{\frac{1}{3}}-1)\mathbf{a}_i$ (where $N^{\frac{1}{3}}-1$ is assumed to be an even number) and that there is one atom per unit cell. The equilibrium positions of the atoms may consequently be described by the vectors

$$\mathbf{r}_l=\sum_i l_i\mathbf{a}_i, \quad -\tfrac{1}{2}(N^{\frac{1}{3}}-1)\leqq l_i\leqq\tfrac{1}{2}(N^{\frac{1}{3}}-1), \tag{4}$$

where $l_1l_2l_3$ is a set of integers. If $\mathbf{\Delta}_l$ is the displacement of the atom at $\mathbf{r}_l$ the intensity of the coherent scattering is

$$J=Sf^2\sum_l\sum_{l'}\exp\left[i2\pi(\mathbf{k}-\mathbf{k}_0)\cdot\mathbf{r}_{ll'}\right]\times\langle\exp\left[i2\pi(\mathbf{k}-\mathbf{k}_0)\cdot(\mathbf{\Delta}_l-\mathbf{\Delta}_{l'})\right]\rangle_{Av} \tag{5}$$

with

$$\mathbf{r}_{ll'}=\sum_i(l_i-l_i')\mathbf{a}_i.$$

One finds readily

$$\langle\exp\left[i2\pi(\mathbf{k}-\mathbf{k}_0)\cdot(\mathbf{\Delta}_l-\mathbf{\Delta}_{l'})\right]\rangle_{Av}=\exp\left\{-s^2[\langle(\mathbf{u}\cdot\mathbf{\Delta}_l)^2\rangle_{Av}-\langle(\mathbf{u}\cdot\mathbf{\Delta}_l)(\mathbf{u}\cdot\mathbf{\Delta}_{l'})\rangle_{Av}\right], \tag{6}$$

where $s=2\pi|\mathbf{k}-\mathbf{k}_0|=4\pi\sin\theta/\lambda$ while $\mathbf{u}$ is a unit vector along $\mathbf{k}-\mathbf{k}_0$. With the abbreviations

$$2M=s^2\langle(\mathbf{u}\cdot\mathbf{\Delta}_l)^2\rangle_{Av}, \quad P_{ll'}=s^2\langle(\mathbf{u}\cdot\mathbf{\Delta}_l)(\mathbf{u}\cdot\mathbf{\Delta}_{l'})\rangle_{Av} \tag{7}$$

and with $e^{P_{ll'}}\approx1+P_{ll'}$ (which is justifiable except for very high temperatures) Eq. (5) becomes

$$J=J_1+J_2, \quad J_1=J_0e^{-2M},$$
$$J_2=Sf^2e^{-2M}\sum_l\sum_{l'}P_{ll'}\exp\left[i2\pi(\mathbf{k}-\mathbf{k}_0)\cdot\mathbf{r}_{ll'}\right]. \tag{8}$$

The two terms J_1 and J_2 correspond to Laue scattering and diffuse scattering; but while J_1 agrees with the expression found by Debye (compare Eq. (3)) a different formula is obtained for J_2.

The problem of finding the normal coordinates for the vibrations of a simple lattice is well known[7] and needs but little discussion. By means of a Fourier series expansion the displacement function $\mathbf{\Delta}_{(r,\,t)}$ (which is given physical significance only at the lattice points since an atom is assumed to be displaced as a whole) is represented as a superposition of elastic waves

$$\mathbf{\Delta}_{(r,\,t)}=\sum_j\sum_p{}'\mathbf{A}_{p,\,j}(t)\exp\left[i2\pi\tau_p\cdot\mathbf{r}\right]. \tag{9}$$

In this expansion the index j refers to the three waves associated with each propagation vector

[2] E. Schrödinger, Physik Zeits. **15**, 79 and 497 (1914); H. Faxén, Ann. d. Physik **54**, 615 (1918).

[3] L. Brillouin, Ann. de physique (9) **17**, 120 (1922); H. Faxén, Zeits. f. Physik **17**, 266 (1923); I. Waller, Diss. Uppsala (1925), Zeits. f. Physik **17**, 398 (1923).

[4] A great many articles in *The Physical Review*, particularly during the last 10 years.

[5] G. E. M. Jauncey and G. G. Harvey, Phys. Rev. **37**, 1203 (1931).

[6] Y. H. Woo, Phys. Rev. **38**, 1 (1931) and **41**, 21 (1932).

[7] M. Born and Th. v. Kármán, Physik. Zeits. **13**, 294 (1912); *ibid.* **14**, 15 and 65 (1913). M. Born, *Dynamik d. Kristallgitter* (Leipzig, 1915). I. Waller, reference 3.

τ_p. The vectors τ_p are given by

$$\tau_p=\sum_i \frac{p_i}{N^{\frac{1}{3}}-1}\mathbf{b}_i, \tag{10}$$

where p_i denotes an integer. Because of the periodicity the integers p_i may be restricted to lie within the limits $-\frac{1}{2}(N^{\frac{1}{3}}-1)\leq p_i\leq\frac{1}{2}(N^{\frac{1}{3}}-1)$. Accordingly all propagation vectors τ_p lie within a corresponding region—the Brillouin zone—which in the present case is the unit cell of the reciprocal lattice. There are two standing waves for every set of values (τ_p,j) and one verifies readily that the combination $(-\tau_p,j)$ gives the same two waves. It suffices consequently to consider the τ_p-values lying in one-half of the Brillouin zone. (The summation over half the Brillouin zone is indicated in Eq. (9) by the symbol $\sum_p'$, while $\sum_p$ will be used for summation over the entire Brillouin zone. Clearly $\sum_p'=\frac{1}{2}\sum_p$.)

Since Eq. (9) corresponds to the introduction of normal coordinates it follows that

$$\begin{aligned}&\langle(\mathbf{u}\cdot\boldsymbol{\Delta}_l)^2\rangle_{Av}=\tfrac{1}{2}\sum_j\sum_p\gamma_{p,j}{}^2\langle A_{p,j}{}^2\rangle_{Av},\\ &\langle(\mathbf{u}\cdot\boldsymbol{\Delta}_l)(\mathbf{u}\cdot\boldsymbol{\Delta}_{l'})\rangle_{Av}\\ &\quad=\tfrac{1}{2}\sum_j\sum_p\gamma_{p,j}{}^2\langle A_{p,j}{}^2\rangle_{Av}\cos 2\pi\tau_p\cdot\mathbf{r}_{ll'}.\end{aligned} \tag{11}$$

$\gamma_{p,j}$ is cosine of the angle between $\mathbf{A}_{p,j}$ and $\mathbf{u}$. The average energy associated with one vibrational mode is $\frac{1}{2}Nm_a\omega_j{}^2\langle A_{p,j}{}^2\rangle_{Av}$, m_a being the atomic mass. (The factor of $\frac{1}{2}$ enters because there are two standing waves for every term of Eq. (9).) Accordingly one has

$$\langle A_{p,j}{}^2\rangle_{Av}=\frac{Q_j}{2\pi^2Nm_a\nu_j{}^2},\quad Q_j=\frac{h\nu_j}{e^{h\nu_j/kT}-1}+\tfrac{1}{2}h\nu_j. \tag{12}$$

The density of points τ_p in the Brillouin zone is NV, where $V=(\mathbf{a}_1\mathbf{a}_2\mathbf{a}_3)$ is the volume of the unit cell. The summation over the discrete points in the Brillouin zone may conveniently be replaced by an integration over a continuous distribution having the same density. One finds then

$$2M=\frac{s^2V}{4\pi^2m_a}\sum_j\int\gamma_j{}^2\frac{Q_j}{\nu_j{}^2}dv, \tag{13}$$

$$P_{ll'}=\frac{s^2V}{4\pi^2m_a}\sum_j\int\gamma_j{}^2\frac{Q_j}{\nu_j{}^2}\cos[2\pi\tau\cdot\mathbf{r}_{ll'}]dv. \tag{14}$$

Upon substitution of Eq. (14) in Eq. (8) and summation over all pairs of atoms in the crystal the intensity J_2 becomes

$$J_2=Sf^2e^{-2M}\frac{s^2V}{4\pi^2m_a}\sum_j\int\gamma_j{}^2\frac{Q_j}{\nu_j{}^2}\times\left\{\prod_i\frac{\sin^2[N^{\frac{1}{3}}\pi(\mathbf{k}-\mathbf{k}_0+\tau)\cdot\mathbf{a}_i]}{\sin^2[\pi(\mathbf{k}-\mathbf{k}_0+\tau)\cdot\mathbf{a}_i]}\right\}dv. \tag{15}$$

The integrand in Eq. (15) is zero unless $\mathbf{k}-\mathbf{k}_0+\tau\approx\mathbf{B}_H$ and it is therefore convenient to introduce a small vector $\epsilon=\sum_i\epsilon_i\mathbf{b}_i$ defined by

$$\epsilon=\tau-\tau_0,\quad \mathbf{k}-\mathbf{k}_0+\tau_0=\mathbf{B}_H. \tag{16}$$

Noting that $\nu_j=\tau v_j$ (where v_j is the propagation velocity) and that $Vdv=d\epsilon_1d\epsilon_2d\epsilon_3$ Eq. (15) may be given the form

$$J_2=Sf^2e^{-2M}\frac{s^2}{4\pi^2m_a}\sum_j\int\int\int\frac{\gamma_j{}^2Q_j}{v_j{}^2|\tau_0+\epsilon|^2}\times\prod_i\frac{\sin^2[N^{\frac{1}{3}}\pi\epsilon_i]}{\sin^2\pi\epsilon_i}d\epsilon_i. \tag{17}$$

The velocities v_j are in general functions of the vibration direction; but (unless the anisotropic character of the crystal is pronounced) the range of variation is rather small, so that the velocities to a first approximation may be treated as constants. As a rule the three velocities v_j are not greatly different from one another, and as an admittedly rough approximation it will be assumed therefore that $v_1=v_2=v_3=v=$ a constant. With these assumptions the integration of Eq. (17) may be carried out approximately[8] and the following result is obtained

$$J_2\approx I_0\left(\frac{e^2}{mc^2R}\right)^2\frac{1+\cos^2 2\theta}{2}f^2e^{-2M}N\frac{4\sin^2\theta}{\lambda^2m_av^2}\times\frac{2\pi(NV)^{\frac{1}{3}}Q(\tau_0)}{1+2\pi(NV)^{\frac{1}{3}}\tau_0{}^2}. \tag{18}$$

The corresponding approximate expression for $2M$ is obtained from Eq. (13) when the Brillouin zone is replaced by a sphere of equal volume. The radius of this sphere is $\tau_m=(3/4\pi V)^{\frac{1}{3}}$ and

[8] Each of the three sine functions $\sin^2[N^{\frac{1}{3}}\pi\epsilon_i]/\sin^2\pi\epsilon_i$ of the integrand was replaced by smoothing functions $N^{\frac{1}{3}}\exp[-\pi N^{\frac{1}{3}}\epsilon_i{}^2]$.

the formula for $2M$ becomes

$$2M=\frac{s^2V\tau_m kT}{\pi m_a v^2}\{\phi_{(x_m)}+\tfrac{1}{4}x_m\}, \qquad (19)$$

where

$$x_m=\frac{h\nu\tau_m}{kT} \quad \text{and} \quad \phi_{(x)}=\frac{1}{x}\int_0^x \frac{d\xi}{e^\xi-1}.$$

The customary form is obtained when the characteristic temperature Θ is introduced by means of the relation $h\nu\tau_m=k\Theta$.

2. Discussion

The intensity of the diffuse scattering changes according to Eq. (18) rapidly with the scattering angle and exhibits maxima in the directions for which τ_0 assumes minimum values. This result contrasts sharply with the slow variation with scattering angle predicted on the basis of the Debye formula, but agrees with the statements made by Faxén and Waller[3] that the main part of the diffuse scattering is to be found in the Laue directions. The lack of confirmation of Debye's equation is not surprising since Debye at one stage in the derivation incorrectly assumed neighboring atoms to scatter independently. (The same mistake was made in the later derivations of the Debye formula by Jauncey and Harvey and by Woo.) In the notation of this article Faxén's expression for the diffuse scattering becomes

$$J_2=Sf^2e^{-2M}N\frac{kT}{V\tau_0^4}\left\{\frac{(\mathbf{B}_H\times\boldsymbol{\tau}_0)^2}{c_{44}}+\frac{(\mathbf{B}_H\cdot\boldsymbol{\tau}_0-\tau_0^2)^2}{c_{11}}\right\},$$

where c_{44} and c_{11} are elastic constants. It is readily seen that Faxén's equation agrees rather well with the first approximation to Eq. (18) when $2\pi(NV)^{\frac{1}{3}}\tau_0^2\gg 1$ and when $h\nu\tau_0/kT\ll 1$. Faxén's discussion of the physical significance of the formula he obtained is unfortunately incomplete and some of the most interesting consequences escaped his notice.

Let an incident beam of parallel, monochromatic x-rays fall on a stationary crystal. The vector $\mathbf{k}_0$ is then sharply defined relative to the crystal lattice and Eq. (18) gives the intensity of the diffuse scattering as function of the scattering direction $\mathbf{k}$. The quantity τ_0 is defined by the relation $\mathbf{k}-\mathbf{k}_0+\boldsymbol{\tau}_0=\mathbf{B}_H$, where as stated the vector $\mathbf{B}_H$ is unique. Consider a particular scattering direction $\mathbf{k}$. The vector $\mathbf{B}_H$ associated with it is readily found from a construction in the reciprocal lattice as shown in Fig. 1. (Cf. the article by Faxén.[3]) It is seen that the sought vector $\mathbf{B}_H$ is the reciprocal lattice vector having the shortest separation from the vector $\mathbf{k}-\mathbf{k}_0$, this separation being the vector $\boldsymbol{\tau}_0$. Consider next the direction of scattering as variable. The terminus of $\mathbf{k}$ describes then a sphere of radius $1/\lambda$ about the terminus of $-\mathbf{k}_0$; this is the "sphere of reflection." The points on the surface of the sphere of reflection which lie closer to $\mathbf{B}_H$ than to any other lattice point define a sector of the solid angle 4π, such that the same vector $\mathbf{B}_H$ is associated with all directions $\mathbf{k}$ within the sector. In this manner all scattering directions are grouped into a finite number of sectors, each sector being characterized by a different vector $\mathbf{B}_H$. The number of different sectors is approximately

$$n\approx 8\pi V\tau_m/\lambda^2=15.6\ V^{\frac{1}{3}}/\lambda^2. \qquad (20)$$

As $\mathbf{k}$ varies within a given sector, τ_0 varies with it by virtue of $\mathbf{k}-\mathbf{k}_0+\boldsymbol{\tau}_0=\mathbf{B}_H$ and the intensity changes accordingly. It is important to note that τ_0 can become zero only by proper adjustment of the incident wave vector $\mathbf{k}_0$. Since $\mathbf{k}_0$ and $\mathbf{B}_H$ are considered fixed vectors while $\mathbf{k}$ has the definite length $1/\lambda$, τ_0 assumes a

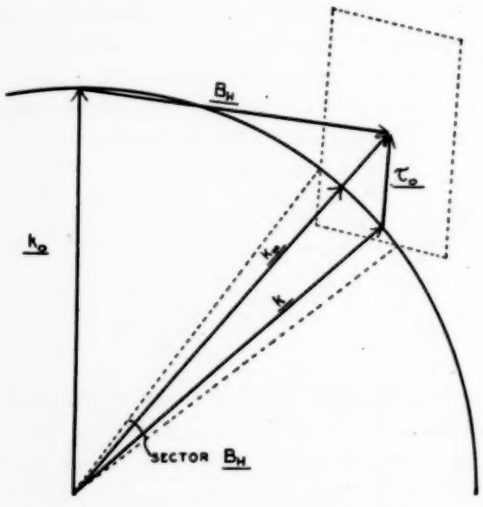

FIG. 1. Showing a section of the reciprocal lattice and illustrating the geometrical interpretation of Eqs. (16) and (22).

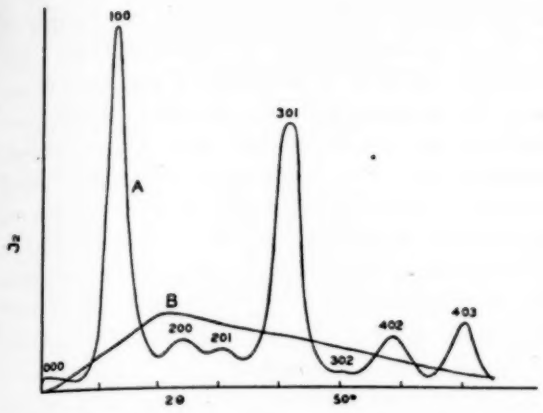

Fig. 2. Showing the intensity distribution of the diffuse scattering for KCl. The crystal is treated as a simple cubic structure with lattice constant $a=3.14$A and one atom per unit cube. The direction of incidence is assumed to be along $\mathbf{a}_3$, while the intensity distribution in the plane $\mathbf{a}_2=0$ is given in the figure. The wave-length is taken to be $\lambda=0.71$A. The curve A is calculated from Eq. (18), curve B from the Debye formula. The three integers affixed to the maxima of curve A are the Miller indices of the active lattice planes. The different behavior of the two intensity curves as the scattering angle goes to zero is of interest. As the scattering angle decreases to small values the intensity according to Eq. (18) approaches first the constant value $J_2=NSZ^2kT/m_0v^2$ (Z being the atomic number) and drops then rapidly to zero in the exact forward direction.

minimum value when $\mathbf{k}$ is parallel to $\mathbf{B}_H+\mathbf{k}_0$. If $\tau_{\min}$ is this minimum value one has consequently

$$\tau_{\min}=|\mathbf{B}_H+\mathbf{k}_0|-|\mathbf{k}|$$

or

$$\lambda\tau_{\min}=\left[1+8\sin\theta_B\cos\frac{\theta_B+\theta_i}{2}\sin\frac{\theta_B-\theta_i}{2}\right]^{\frac{1}{2}}-1\approx-\Delta\sin 2\theta_B, \quad (21)$$

where θ_B is the Bragg angle and $\theta_i\equiv\theta_B+\Delta$ the glancing angle of incidence relative to the sequence of lattice planes normal to $\mathbf{B}_H$. The intensity of scattering reaches a maximum value when τ_0 is a minimum and the direction of the intensity maximum, $\mathbf{k}_m$, is therefore given by

$$[1+\lambda\tau_{\min}]\mathbf{k}_m=\mathbf{B}_H+\mathbf{k}_0. \quad (22)$$

Thus the direction of maximum intensity lies in the plane of incidence, but the glancing angle of scattering is in general not equal to the glancing angle of incidence. When $\theta_i-\theta_B\equiv\Delta$ is small the scattering angle, $2\theta_m$, corresponding to the maximum becomes

$$2\theta_m\approx 2\theta_B+2\Delta\sin^2\theta_B. \quad (23)$$

For scattering directions $\mathbf{k}$ near a maximum, $\mathbf{k}_m$, one may set

$$(\lambda\tau_0)^2=(\lambda\tau_{\min})^2+\chi^2, \quad (24)$$

where χ is the angle between $\mathbf{k}$ and $\mathbf{k}_m$. According to Eqs. (18) and (24) the intensity distribution is symmetrical about a maximum (in the immediate neighborhood of the maximum). The half-width at half-maximum is evidently

$$\chi_{\frac{1}{2}}=\lambda[\tau_{\min}^2+1/2\pi(NV)^{\frac{1}{3}}]^{\frac{1}{2}}\approx\lambda|\tau_{\min}|=|\Delta|\sin 2\theta_B. \quad (25)$$

The number of different intensity maxima of J_2 corresponding to a fixed incident wave is given by Eq. (20) since there is one maximum for every sector $\mathbf{B}_H$.

The difference between the Debye formula and ours is well illustrated in Fig. 2 which shows the diffuse (coherent) scattering for a concrete example as calculated according to the two formulas. It becomes clear from this figure that the Debye formula cannot even be considered as a fair approximation. With this fact in mind it is surprising that the extensive experimental studies of the diffuse scattering by Jauncey and collaborators not only failed to reveal the presence of the intensity maxima but even led to confirmation of the Debye expression which we now know to be incorrect. However, reference to the articles describing these experiments shows that the observations were made with highly divergent incident beams and that in all but a few cases continuous rather than monochromatic radiation was used. The aperture of the ionization chamber corresponded furthermore to a large solid angle and it seems that the precaution to remove the warped surface layers of the crystals by etching was not taken. Under these circumstances neither $\mathbf{k}_0$ nor $\mathbf{k}$ are well defined, and the observations should accordingly be compared with the average value of J_2 over large variations of the vector $\mathbf{k}-\mathbf{k}_0$. Suppose that the variation in $\mathbf{k}-\mathbf{k}_0$ is so large that the vector τ_0 traces out the entire Brillouin zone. The average value J_2 is then obtained when the quantity

$$\frac{2\pi(NV)^{\frac{1}{3}}Q(\tau_0)}{1+2\pi(NV)^{\frac{1}{3}}\tau_0^2}$$

in Eq. (18) is replaced by its average value.

One finds readily

$$\left\langle \frac{2\pi(NV)^{\frac{1}{3}}Q(\tau_0)}{1+2\pi(NV)^{\frac{1}{3}}\tau_0^2} \right\rangle_{Av} \approx 4\pi kTV\tau_m[\phi_{(x_m)}+\tfrac{1}{4}x_m] \quad (26)$$

and hence with reference to Eq. (19)

$$\langle J_2\rangle_{Av} = NSf^2e^{-2M}2M \approx NSf^2[1-e^{-2M}], \quad (27)$$

which is the Debye expression. The experimental results of Jauncey and co-workers are consequently useless as a means of distinguishing between Eq. (18) and the Debye formula. Further detailed studies of the diffuse scattering with well defined x-ray beams are therefore desirable and have been begun in this laboratory.

According to Eq. (22) the directions of the intensity maxima of J_2 are uniquely fixed only if the incident wave is monochromatic and if the crystal is stationary. The directions $\mathbf{k}_m$ vary with the rotation angle when the crystal is rotating and wave-length held fixed, so that the diffuse scattering maxima will be recorded as streaks on rotating crystal photographs.[9]

If the crystal is held stationary while the wave-length is varied continuously (as in the Laue method of crystal analysis) the directions $\mathbf{k}_m$ remain in the fixed planes defined by $\mathbf{k}_0$ and the active vectors $\mathbf{B}_H$, but the scattering angles, $2\theta_m$, change with the wave-length. The diffraction maxima J_2 accordingly appear as sections of radial straight lines on a photographic plate placed normal to the incident beam. Such radial streaks have been observed in Laue photographs of various crystals[10] and different interpretations have been suggested. The radial streaks should according to our theory be a general feature of all Laue photographs; but whether they are observed or not is a question of exposure times since the intensity of the streaks is small, particularly for crystals with high characteristic temperatures. The suggestion that the radial streaks of Laue photographs might be due to the temperature effect was first made by Faxén in his paper of 1923.[3] Quite recently this suggestion was experimentally confirmed by Preston[10] who showed that the intensity of the streaks increased with the temperature. Preston's conclusion that the thermal vibrations of the lattice breaks the crystal up into groups consisting of an atom and its next neighbors cannot be accepted, however.[11]

The exact treatment of the theory as applied to crystals containing different kinds of atoms becomes very complicated and will not be attempted in this article. A first approximation may, however, be obtained by assuming that the atoms of a unit cell vibrate as a single particle, and one finds then

$$J_2 \approx I_0\left(\frac{e^2}{mc^2R}\right)^2 \frac{1+\cos^2 2\theta}{2} |F|^2 e^{-2M} N \times \frac{4\sin^2\theta}{\lambda^2 v^2 \sum m_a} \frac{2\pi(NV)^{\frac{1}{3}}Q(\tau_0)}{1+2\pi(NV)^{\frac{1}{3}}\tau_0^2}, \quad (28)$$

where

$$F = \sum f \exp\left[i2\pi(\mathbf{k}-\mathbf{k}_0)\cdot\mathbf{r}\right]$$

is the structure factor, $\sum m_a$ the mass of the unit cell and N the number of unit cells contained in the crystal, while the expression for M must be correspondingly modified.

[9] These streaks of rotating crystal photographs are not to be confused with another set of streaks due to Laue scattering (J_1) of a continuous component of the incident radiation.

[10] See for instance: W. Friedrich, Physik. Zeits. **14**, 1082 (1913); A. P. R. Wadlund, Phys. Rev. **53**, 843 (1938); G. D. Preston, Proc. Roy. Soc. **172**, 116 (1939).

[11] In a few instances the observed radial streaks must be attributed to disorders in the lattice tending to produce essentially two-dimensional super-lattices. The present writer suggested (Phys. Rev. **53**, 844 (1938)) that Wadlund's observations on rocksalt might be explained as two-dimensional lattice effects. In view of the results of this article it is quite certain that the streaks observed by Wadlund are due to diffuse scattering.

Intensity Distribution in X-Ray and Electron Diffraction Patterns

X-Ray Atom Factors of Zinc in Zinc Oxide and Chemical Binding*

C. H. EHRHARDT** AND K. LARK-HOROVITZ
Purdue University, Lafayette, Indiana

(Received November 15, 1939)

Electron diffraction patterns of zinc oxide show intensities markedly deviating from the ones calculated under the assumption of a spherically symmetrical electron distribution in the atom. Possible explanations were suggested on the basis of a shift of the electron cloud with respect to the nucleus, a distortion of the crystal lattice, a distortion of the electron cloud, and particularly of the valence electrons, or effects of dynamical reflection of the electron waves not taken into account in the kinematic theory. For a final decision between these possibilities, x-ray diffraction patterns from a flat sample of zinc oxide have been obtained photographically, with monochromatic Cu $K\alpha$ radiation, and the relative intensities measured. From these results it is possible to calculate the x-ray atom factors for zinc, and thus to construct theoretical electron diffraction curves. These reproduce the essential features of the electron diffraction experiments of K. Lark-Horovitz and H. J. Yearian. Therefore, the observed intensity anomaly must be due to anomalous F factors in the expression for electron diffraction intensity $(Z-F)^2[(\sin\theta)/\lambda]^{-4}$ rather than to effects of dynamical reflection neglected in the kinematic theory. This is also in agreement with the explanation by James and Johnson since the x-ray intensities of our experiments are in better agreement with the theoretical values obtained by using the distorted charge distribution as calculated by James and Johnson, than they are with values based upon the symmetrical distribution of Pauling and Sherman. Discrepancies at larger values of $(\sin\theta)/\lambda$ are discussed in connection with temperature and order-disorder effects: the combination of electron diffraction and x-ray patterns allows one to distinguish between intensity anomalies due to distortion of the electron cloud and effects due to some other factors such as order-disorder.

1. X-RAY AND ELECTRON ATOM FACTORS

IT is possible to determine atom factors not only from x-ray, but also from electron diffraction patterns. The intensity distribution in an electron diffraction pattern is much more sensitive to changes in the F factor than it is in an x-ray pattern. In the case of electron diffraction the intensity is determined by the quantity $(Z-F)$ where Z is the atomic number of the scattering atom. For small values of $(\sin\theta)/\lambda$, F is of the order of Z, and small changes in F can therefore produce comparatively large changes in $Z-F$ and, accordingly, in the intensity distribution of the diffraction pattern. Investigations of electron diffraction patterns of zinc oxide,[1, 2] have shown that the intensity distribution differs markedly from the intensity distribution of the corresponding x-ray pattern and from the intensities calculated under the assumption of spherical distributions of electrons around the zinc and oxygen nuclei. It was shown that this intensity anomaly cannot be due to trivial experimental factors such as impurities, preferred orientation, or crystal growth nor to a distortion of the crystal lattice,[3] but must be due either to an intrinsic change in the F factor resulting from distortion of the electron cloud[4] by the crystal bonds, or to some dynamic effect unaccounted for in the kinematical theory of electron diffraction. Since the lines predicted by the dynamical theory, but forbidden by the ordinary structure factor, have only been found occasionally and with extremely small intensity, the first alternative seemed preferable.

Since the *apparent* intensity distribution in the x-ray pattern, when estimated visually, agrees with that expected for the accepted structure, (Wurtzite) the problem was to explain the intensity anomaly of the electron diffraction pattern without changing the qualitative character of the predicted intensity distribution of

* Presented at the Washington meeting of the American Physical Society, December, 1938, Phys. Rev. **55**, 605 (1939). Submitted as a thesis to the Faculty of Purdue University by C. H. Ehrhardt.

** Now with Universal Oil Products Company, Riverside, Illinois.

[1] H. J. Yearian and K. Lark-Horovitz, Phys. Rev. **42**, 905 (1932).

[2] H. J. Yearian, Phys. Rev. **48**, 631 (1935).

[3] V. A. Johnson and L. W. Nordheim, Phys. Rev. **51**, 1002 (1937).

[4] V. A. Johnson and H. M. James, Phys. Rev. **53**, 327 (1938); H. M. James and V. A. Johnson, Phys. Rev. **56**, 119 (1939); V. A. Johnson, this issue.

the x-ray pattern. It seems possible to explain the main intensity anomalies without violating the qualitative x-ray data by assuming a model in which the zinc and oxygen atoms are linked together along the c axis in a similar way as are the atoms in a diatomic molecule; that is, by assuming that two of the valence electrons are smeared out over an ellipsoid along the c axis.[4]

To decide definitely whether this explanation is correct or whether the dynamic theory must be taken into account, it is necessary to find the x-ray atom factor for zinc in zinc oxide. This would allow direct comparison with the theoretical considerations, and should also make it possible to construct electron diffraction intensities from the experimental x-ray atom factors.

2. Experimental Problem

For this purpose it is necessary to measure the scattered intensities, eliminate geometric and pure structural factors common to both electron diffraction and x-ray patterns, and finally to compare the x-ray atom factor obtained: (a) with the calculated values, and (b) with the observed intensities in the electron diffraction pattern.

The experimental procedure consists, therefore, of the following steps: (a) Photographic registration of diffraction patterns with exposure chosen for different intensity regions such that the photometric density, $D \leqq 1$; (b) Construction of the most probable photometer curve from the diffraction pattern; (c) Reduction of this curve to density; (d) Correction for absorption; (e) Reduction to relative atom factors by eliminating the structure factor and correcting for temperature motion.

For comparison with the electron diffraction pattern, it is only necessary to determine relative values of the atom factors. These can be computed from the observed relative intensity. We can write for the intensity I:

$$I = KH|S|^2 f(\theta) T,$$

where K is a constant containing experimental factors due to the geometry of the arrangement; H is a frequency factor for the different planes; S is the crystal structure factor, $\Sigma_n F_n \exp[2\pi i(hx_n + ky_n + lz_n)]$; hkl are the Miller indices of the reflecting plane; xyz are the coordinates of the nth atom in the unit cell; $F(n)$ is the quantity in which we are primarily interested: the atom factor; $f(\theta)$ is a pure function of angle and contains the polarization factor and the Lorentz factor; θ is the Bragg angle for reflection; T is the temperature factor (see later).

3. Experimental Procedure

(a) X-ray source and camera

As a source of CuKα x-rays, a demountable tube[5] was used in connection with a rocksalt monochromator. Exposures of 8 to 60 hours were made in a cylindrical camera of 270 mm circumference. The camera could be rotated about its own axis, and was mounted on a brass plate pivoted on the axis of the monochromator so that proper adjustment could be easily made. For simplicity of absorption correction, a flat sample was used of such thickness that the incident beam was completely absorbed.

As a check on previous work on the geometrical structure, the diffraction pattern of a sample of ZnO paste on a silk thread was investigated. The spacings found were in agreement with those of previous investigations.[6]

(b) Photographic density determination

The pattern used for intensity measurements were recorded on a microphotometer of the Moll type. To eliminate possible effects of grain in the film a number of microphotometer traces were superimposed and a most probable trace constructed. This trace (Fig. 1) was then converted into optical density with the logarithmic protractor.[7] By using only those portions of the film for which the density was directly proportional to the incident x-ray intensity ($D \leqq 1.0$), the area of the peaks on the density trace could be taken as a measure of the intensity. In order to cover the complete diffraction pattern so that the strong peaks would not lie outside the range of unit density and still get an appreciable density for weaker reflections, overlapping exposures were used. In this procedure, a film was taken

[5] E. P. Miller, Rev. Sci. Inst. **4**, 379 (1933).
[6] W. L. Bragg, Phil. Mag. **39**, 647 (1920); L. Weber, Zeits. f. Krist. **57**, 398 (1922); G. Aminoff, Zeits. f. Krist. **57**, 204 (1922).
[7] An improved form of the instrument described by Yearian, H. J. Yearian, Rev. Sci. Inst. **4**, 407 (1933).

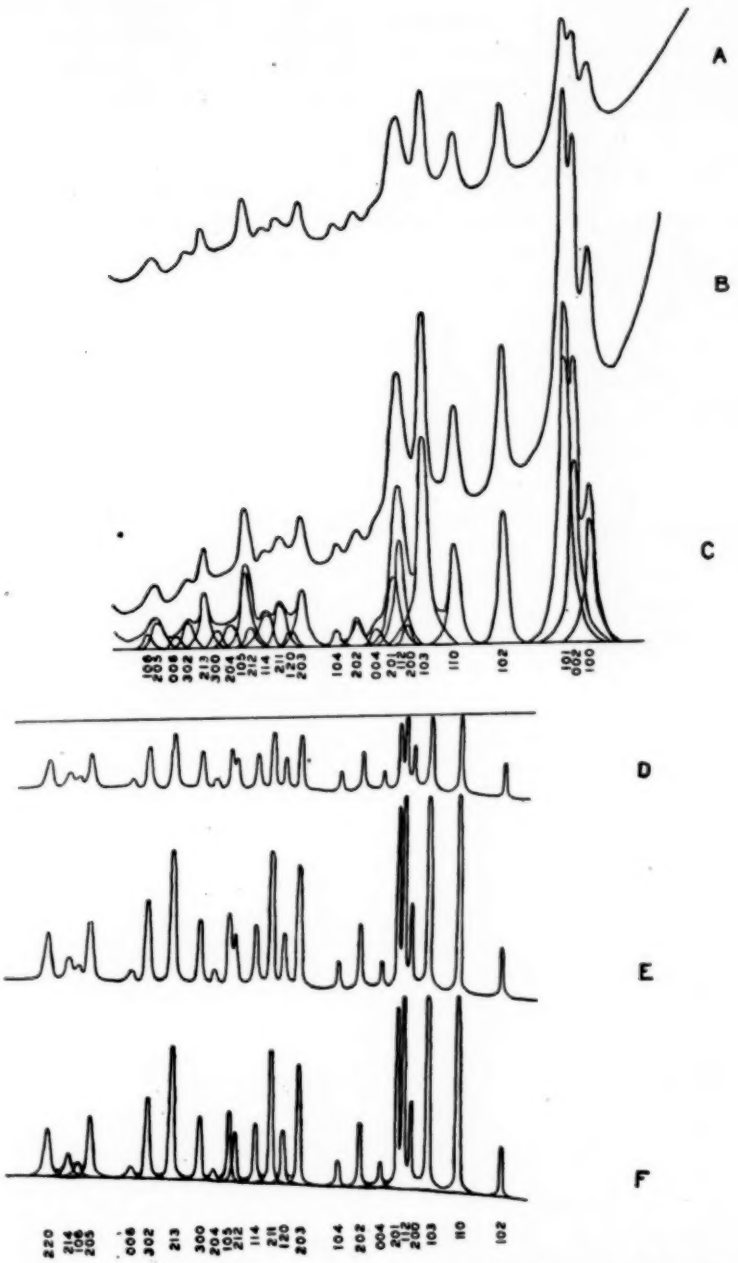

FIG. 1. Electron diffraction and x-ray photometer traces. A. Electron diffraction photometer trace; B. Curve *A* reduced to density; C. Curve *B* reduced to flat background and resolved; D. X-ray photometer trace (reduced by ¼ relative to *A*); E. Curve *D* reduced to density; F. Curve *E* resolved.

such that the strongest peak did not exceed unit density, and the ratio of its intensity to other weaker peaks was determined. A second picture was then taken in which the strongest peak was highly over-exposed, but in which the weaker peaks of the first picture were brought up nearly to unit density. The ratio of their intensities to those of still weaker peaks was determined, thus giving, indirectly, the ratio of intensities with respect to the strongest lines.

4. Corrections

(a) Absorption correction

Before any interpretation of the intensities can be made, several corrections have to be applied. For a flat sample of infinite thickness, the absorption correction is given by the expression:

$$I=[1-\cos\beta/\cos(\phi+\beta)]^{-1},$$

where ϕ is the angle between the scattered beam and incident beam and β is the angle between the incident beam and the normal to the sample. Choosing the value at the point $\phi=\pi-\beta$ as unity, the relative absorption correction for all other angles can be evaluated. The measured areas were multiplied by the appropriate absorption correction to give the corrected relative intensities.

(b) The temperature correction

The atom factor F_T for an atom bound in a crystal at a temperature T is related to the atom factor for a free atom F_0 by the relation

$$F_T=F_0\cdot e^{-M},$$

where M is a function of Θ/T and $\sin^2\theta/\lambda^2$, Θ being the characteristic temperature of the crystal. The form of the temperature correction depends on whether the crystal is isotropic or anisotropic and whether it contains only one type of atom or different atoms. The temperature correction is well known theoretically for the case of isotropic crystals[8] and for certain cases of anisotropic crystals[9] (Zn,[10] Cd,[11] and others). The anisotropy is most important for crystals strongly deviating from complete symmetry,[12] but, since zinc oxide has an axial ratio of 1.599 as compared to the ideal ratio 1.633, a simple temperature correction has been used. However, the fact that the crystal is somewhat distorted, and that it contains two types of atoms, makes the application of this simple correction an approximate one. We have used as a characteristic temperature 355°K, a value used success-

[8] P. Debye, Ann. d. Physik **43**, 49 (1914); I. Waller, Ann. d. Physik **83**, 154 (1927).
[9] C. Zener, Phys. Rev. **49**, 122 (1936).
[10] E. O. Wollan and G. G. Harvey, Phys. Rev. **51**, 1054 (1937).
[11] G. W. Brindley, Proc. Lond. Phil. Soc. **3**, 200 (1936).
[12] G. W. Brindley and P. Ridley, Proc. Phys. Soc. Lond. **50**, 751 (1938).

Table I. *Calculation of molecular structure factor S_1^0 from observed intensities.*

hkl	$\frac{\sin\theta}{\lambda}$	Mean observed intensity	Absorption correction	Corrected intensity	H	$\lvert S_2\rvert^2$	$f(\theta)$	obs. S_1^2	e^{-M}	S_1^0
					$\beta=75°$					
100	0.178	1335	1.505	2010	6	1	20.96	4.00	0.982	4.07
002	.193	895	1.412	1263	2	4	17.74	2.98	.978	3.05
101	.203	2045	1.357	2760	12	3	15.85	2.21	.977	2.26
102	.263	600	1.175	705	12	1	8.901	2.56	.960	2.67
110	.309	1114	1.103	1231	6	4	6.13	2.89	.940	3.08
103	.340	945	1.071	947	12	3	4.925	2.31	.93	2.48
					$\beta=60°$					
200	0.357	385	1.235	476	6	1	4.42	4.23	0.92	4.6
112	.364	1480	1.204	1785	12	4	4.19	2.97	.92	3.23
201	.370	900	1.177	1058	12	3	4.09	2.67	.915	2.93
004	.386	184	1.155	213	2	4	3.74	2.65	.906	2.93
202	.406	396	1.107	438	12	1	3.37	3.29	.900	3.76
104	.425	141	1.092	154	12	1	3.13	2.03	.890	2.28
203	.460	705	1.052	742	12	3	2.83	2.67	.870	3.07
120	.472	267	1.041	278	12	1	2.76	2.89	.862	3.35
211	.482	780	1.033	807	24	3	2.74	2.02	.858	2.35
114	.494	460	1.028	473	12	4	2.71	1.91	.850	2.24
212	.510	359	1.021	367	24	1	2.72	2.37	.840	2.82
203	.514	515	1.013	523	12	3	2.73	2.31	.837	2.76
204	.525	141	1.008	142	12	1	2.77	2.07	.830	2.49
300	.535	450	1.004	452	6	4	2.84	2.57	.825	3.12
213	.553	1126	1.001	1127	24	3	3.02	2.27	.813	2.79
302	.569	603	1.000	603	12	4	3.25	1.96	.805	2.44
006	.579	95	1.002	95	2	4	3.50	1.84	.796	2.31
205	.599	544	1.010	550	12	3	4.13	1.92	.785	2.45
106	.605	128	1.015	130	12	1	4.40	1.57	.782	2.00
214	.609	210	1.019	214	24	1	4.62	1.39	.78	1.78
220	.617	402	1.030	415	6	4	5.23	1.82	.775	2.34

fully before[2] and we have therefore, $M=0.68\times10^{-16}\sin^2\theta/\lambda^2$. Recent experimental investigations of the temperature correction by electron diffraction[13] indicate that our assumption is justified, and the temperature function can be well approximated by a monotonic function using $\Theta=355°$K.

(c) Correction for anomalous dispersion

Since Cu $K\alpha$ radiation has been used it is necessary to take into account the correction in atom factor for anomalous dispersion due to the K-absorption edge of the zinc atom. This atom factor defect can be calculated theoretically[14] from the theory of anomalous dispersion of x-rays as $\Delta F=F_0-F$, and it is found, in our case, that $\Delta F=2.15$. Since there is no apparent variation of ΔF with $\sin\theta$, it is possible, for comparison of the experimental values with the theoretical values, to subtract the atom factor defect from the theoretical values.

5. Structure Factor

Zinc oxide crystallizes in a hexagonal structure of the Wurtzite type, consisting of a hexagonal close-packed lattice of Zn, and another of O displaced a distance u along the c axis. The coordinates of the Zn atoms are (000), (1/3, 2/3, 1/2), and the coordinates of the oxygen are (00u) and (1/3, 2/3, 1/2+u). The axial ratio is $c/a=1.599$ with $c=5.18$, $a=3.24$ (as compared with an ideal ratio $2(2/3)^{\frac{1}{2}}=1.633$). Former x-ray investigations of ZnO have led to the assumption of a value for the parameter $u=3/8$, since this value leads to no apparent conflict with the observed intensities. Parameter values between 0.36 and 0.39 lead to only small changes in the intensities which cannot be determined from powder photographs alone, since the intensity anomalies must also be considered. For the purpose of this investigation the parameter value was therefore assumed to be 3/8. With this value, the distance Zn−O along the c axis is 1.94A and the distance to the three other oxygens surrounding the Zn atoms is 2.04A. The lattice, therefore, deviates somewhat from the ideal structure.

[13] R. M. Whitmer and H. J. Yearian, Phys. Rev. **55**, 1114 (1939).
[14] H. Hönl, Ann. d. Physik **16**, 625 (1933).

Table II. *Comparison of experimental values of S_1^2 with theoretical values.*

hkl	$\frac{\sin\theta}{\lambda}$	Expt. normalized	Average deviation	P–S spherical distribution	J and J 3 valence electrons	J and J 2 valence electrons
100	0.178	30.3	0.4	29.2	32	31.1
110	.309	23.7	.3	22.3	24.8	23.9
200	.359	20.2	.5	19.8	22.1	21.3
120	.472	15.3	.5	14.5	16.3	15.7
300	.535	13.4	.5	12.2	13.7	13.2
220	.607	10.5	.4	10.1	11.2	10.9
101	.203	17.8	.04	18.5	19.4	19.1
201	.369	12.1	.6	14	14.6	14.2
211	.481	10.1	.25	10.4	11.0	10.8
002	.193	22.8	.4	23.2	24	23.7
102	.263	20.6	.3	20.4	20.9	20.8
112	.364	13.6	.12	16.6	17.1	16.8
202	.405	14.3	1.0	14.9	15.3	15.2
212	.509	11.7	.3	11	11.2	11.1
302	.568	10.4	.04	9.5	9.7	9.6
103	.339	19	.05	19.9	18.9	19.2
203	.459	13.3	.2	14.5	13.6	13.9
213	.553	11.5	.2	11.1	10.1	10.9
004	.386	12.4	.2	12.4	12.2	12.2
104	.425	10	.3	11.2	11	11
114	.494	9.5	.2	9.3	9.1	9.2
204	.525	10.2	.7	8.5	8.3	8.4
214	.609	7.3	.45	6.7	6.5	6.6
105	.514	11.7	.4	12.3	12.6	12.5
205	.600	10.1	.3	10.1	10.5	10.4
006	.579	9.9	.7	9.3	9.6	9.5
106	.606	8.0	.45	8.7	9	8.9

The structure factor for ZnO is given by

$$S=(F_{Zn}+F_Oe^{2\pi iul})[1+\exp(2\pi)i(1/3h+2/3k+1/2l)]=S_1\times S_2.$$

S_1 (a function of $\sin\theta/\lambda$ and l) is the structure factor of the ZnO molecule and S_2 takes into account the two molecules in the unit cell. From the observed intensities I we can calculate relative values of S_1 from*

$$S_1=\left(\frac{I}{KH|S_2|^2f(\theta)}\right)^{\frac{1}{2}},$$

where the symbols have the meaning defined above.

Out of the total of about 50 pictures the average results of the best nine have been evaluated

* Since we have used a monochromater the polarization factor is not the simple factor $\frac{1}{2}(1+\cos^2 2\theta)$ but is given by $\frac{1}{2}(1+\cos^2 2x\cos^2 2\theta)$ where $\cos^2 2x$ for CuK and NaCl(100) is equal to 0.724

$$f(\theta)=\frac{1+0.724\cos^2 2\theta}{\sin^2\theta\cos\theta}.$$

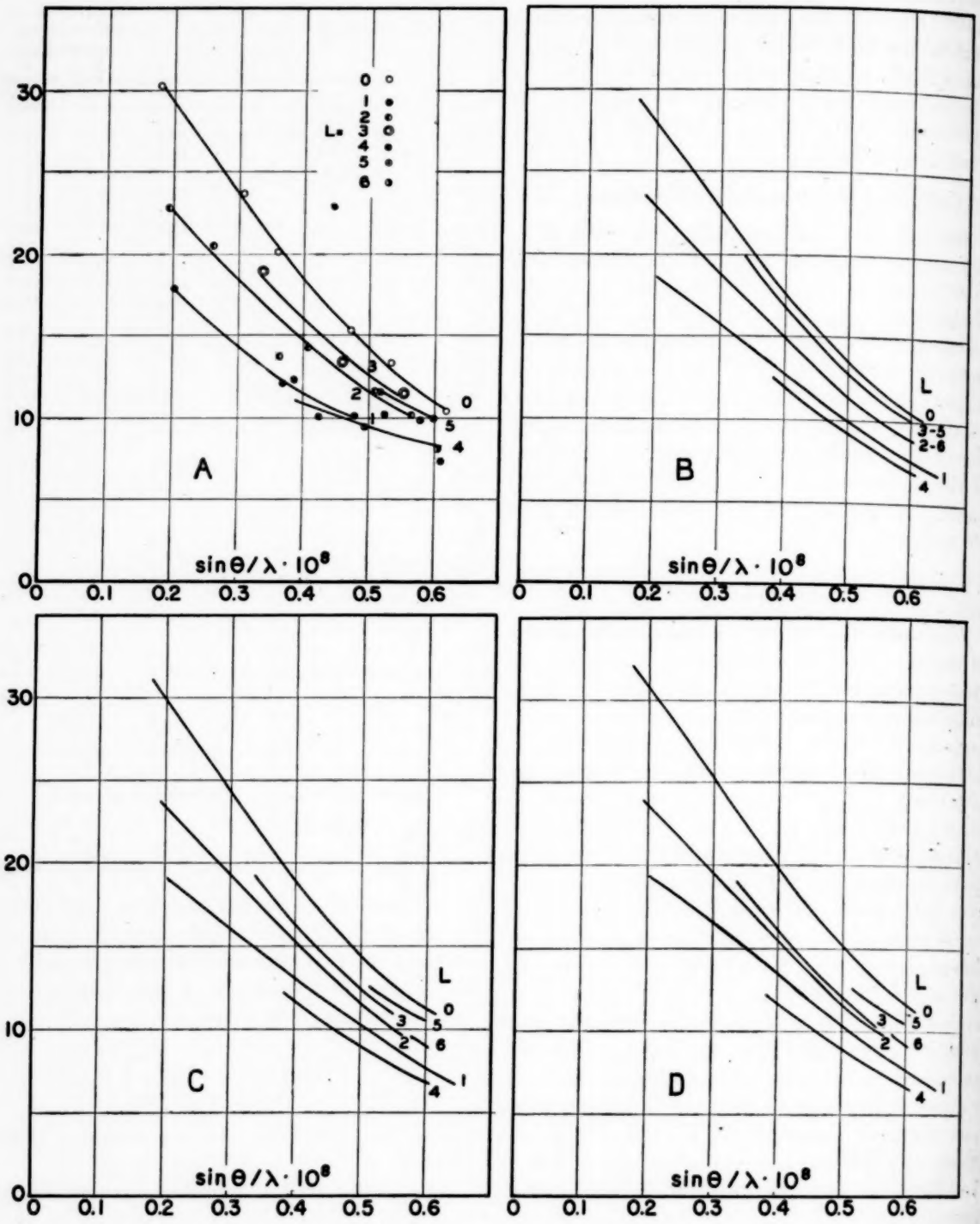

FIG. 2. X-ray structure factor S_1^0 for the zinc oxide molecule. A. Experimental curves; B. Theoretical curves based on spherically symmetric electron distribution (Pauling-Sherman); C. Theoretical curve based on ellipsoidal distribution of 2 of the valence electrons (James and Johnson); D. Theoretical curve based on ellipsoidal distribution of 3 of the valence electrons (James and Johnson). *Note:* L in the figure has the same significance as l in the text.

and the results are shown in Table I. The last column of Table I gives S_1^0, the observed structure factor for the ZnO molecule corrected for temperature.

6. Atom Factors Evaluated from S_1^0

(a) X-ray F factors for ZnO

The values obtained for S_1^0 can now be used for comparison with the theoretical calculations and the experimental electron diffraction curves. This is more satisfactory than complete reduction to individual atom factors, which is a rather difficult, and not always unique, procedure.

For this purpose the experimental values were normalized to the theoretical values, computed with a spherical electron distribution function and a parameter $u=3/8$. We divided the experimental values into the theoretical values and in this way obtained an average multiplying factor which was then used to place the experimental values on a common basis.

Since the different contributions of O and Zn can be calculated for any particular Miller index l, the results for S_1^0 are listed in the order $l=0, 1, 2 \cdots$ in Table II. This table shows the average deviations and the comparison with theoretical values based upon a spherical electron distribution (Pauling-Sherman), and upon a distribution distorted by valence electrons (James and Johnson).

Computed intensities of the lines are affected, of course, also by the choice of the parameter, u. Assuming atom factors calculated from a spherical charge distribution, values of S_1^2 have been calculated as a function of the parameter between the limits $0.36<u<0.39$. The changes in intensity, for a range of ± 0.005 in the parameter, are not greater than the average deviations in the observed intensities, and no uniform improvement of the results is obtained by introducing a parameter deviating markedly from 0.375.* In comparing the experimental values with the ones calculated from a spherical charge distribution and with the results of the calculations for an asymmetrical distribution of electrons, one sees that the experimental results are in better agreement with the distorted charge distribution. This becomes still more evident from Fig. 2 which shows the experimental x-ray values as compared with the theoretical calculations. In comparing these results we see that while the spherical distribution gives one curve only for $l=3$, and $l=5$, and for $l=2$ and $l=6$, the distribution of the valence electrons produces a splitting of these curves. Still more striking is the displacement of $l=3$ and of $l=2$ with respect to $l=0$.

Two distributions of the valence electrons have been considered, in which either two or three of the valence electrons were placed in a prolate ellipsoid along the c axis and the remaining two or one were distributed at random. The general character of the observed intensities is represented better by the curves obtained from the model assuming two valence electrons (particularly at large values of $\sin\theta/\lambda$). While the

TABLE III. *Comparison of experimental electron diffraction values of S_{1e} with values obtained from x-ray data*
$S_{1e}=Z_{Zn}-F_{Zn}+(Z_O-F_O)e^{2\pi i u l}$
$Z_{Zn}=30$, $Z_O=8$, $u=3/8$.

hkl	$Z_{Zn}-F_{Zn}$	Z_O-F_O	S_{1e} CALCULATED FROM X-RAY DATA	S_{1e} EXPT. VALUES
100	3.2	2.35	5.5	3.8
110	8.	4.15	12.2	9.4
200	11	4.65	15.6	12.1
120	14.9	5.6	20.5	18.9
300	16.5	5.95	22.4	21.4
220	19.1	6.25	25.35	18
101	6.9	2.8	5.3	3.4
201	13.7	4.8	10.85	8
211	16.3	5.65	12.9	10.6
002	5.7	2.6	6.3	4.7
102	7.7	3.65	8.5	8.4
112	14.7	4.75	15.4	11.1
202	13.9	5.1	14.7	13.1
212	16.4	5.8	17.4	16.7
302	17.7	6.1	18.8	18.4
103	11.5	4.5	15	14.7
203	16.4	5.5	20.6	16
213	17.9	6.0	22.7	19.1
004	12.3	4.85	7.5	12.8
104	15.1	5.3	9.8	12.8
114	16.1	5.75	10.4	12.9
204	15.6	5.9	9.7	14
214	18.7	6.2	12.5	13.3
105	17.8	5.85	22.3	22.4
205	19.1	6.2	23.8	22.7
006	18.1	6.15	19.1	18
106	20	6.2	20.9	19.4

* As seen from Table I of Johnson's paper, this issue, the main difference between the valence electron model, accounting for our results, and the spherical distribution is in the slope of the curve for $l=0$, which is independent of the parameter u.

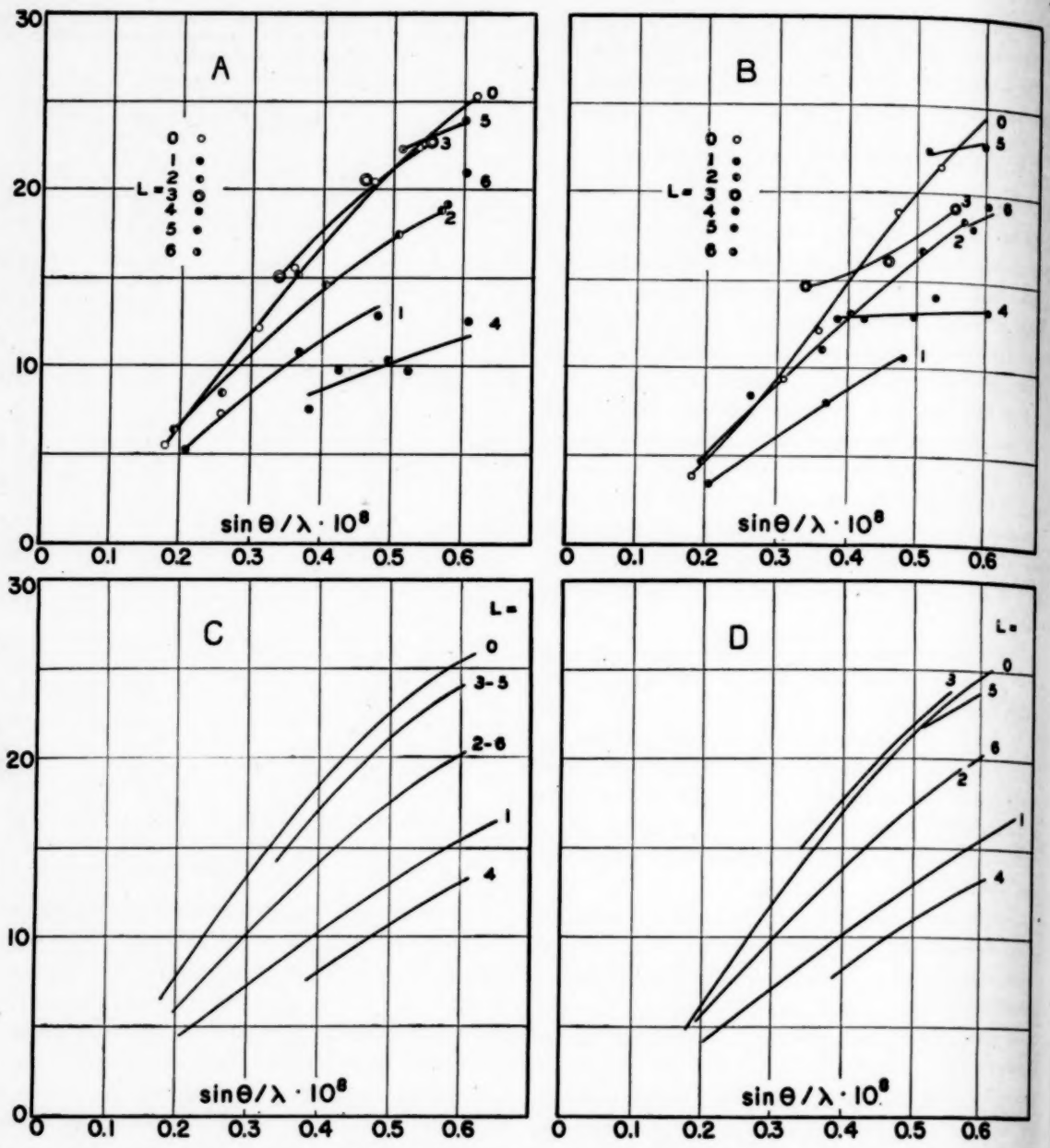

FIG. 3. Electron diffraction structure factor S_{1l}' for the zinc oxide molecule. A. Derived from experimental x-ray data; B. Determined experimentally by electron diffraction; C. Theoretical curves calculated from spherically symmetric electron distribution (Pauling-Sherman); D. Theoretical curves calculated from an ellipsoidal distribution of 2 of the valence electrons (James and Johnson).

assumed deviations from spherical distribution reproduce the experimental curves, in the main, there are still some anomalies, particularly in the intensities of the lines corresponding to $l=5$ and $l=4$. The line belonging to $l=4$ should be much lower in respect to $l=1$ than is actually observed. We will discuss this point in greater detail in connection with the electron diffraction curves.

(b) Comparison of x-ray and electron diffraction scattering curves: derived electron *F* factors

The quantitative evaluation of the x-ray intensities reveals anomalies which can be explained in the main by the assumption of a quasi molecular binding in the crystal, but the differences are so small that one would hesitate to

postulate, on this basis alone, the existence of a distortion due to bonding.

The electron diffraction pattern, however, shows a behavior which cannot be reproduced to any extent by the assumption of a spherical electron distribution. It is then the combination of x-ray and electron diffraction investigations which makes it possible to recognize small changes in electron distribution. They appear as anomalies in the intensities of the electron diffraction pattern and can be diagnosed by investigating the corresponding x-ray pattern.

The electron diffraction structure factor for the ZnO molecule, S_{1e}, is given by

$$S_{1e}=(Z_{Zn}-F_{Zn})+(Z_O-F_O)e^{2\pi iul}.$$

In order to make a detailed comparison of the x-ray results with those obtained from electron diffraction, we have solved the corresponding equation for x-rays:

$$S_1=F_{Zn}+F_Oe^{2\pi iul}$$

for values of F_{Zn}, using the theoretical spherical distribution values of the atom factor for O and the experimental x-ray values of S_1.[15] To these values we add the atom factor defect due to the use of Cu $K\alpha$ radiation, to obtain an experimental value of the atom factor for Zn in the ZnO lattice. Using these atom factors for Zn we constructed the electron diffraction factor S_{1e} as defined above.[16]

The results of these calculations are shown in the Table III, together with the experimental electron values, which have been normalized in the same manner as the x-ray values. The Figs. (3A and 3B) show the electron diffraction factor S_{1e} as obtained from x-ray data and the experimental electron diffraction results.

A comparison of Fig. 3A with Fig. 3B shows that it is possible to reproduce the main features of the electron diffraction pattern from x-ray data.[17] In both cases the curves for $l=2$, 3, 5, cross the curve for $l=0$, and $l=2$ and $l=6$ lie on separate curves.

7. Discussion

The satisfactory agreement between the scattering curves obtained directly from electron diffraction and those derived from experimental x-ray atom curves, shows that the explanation of the anomalous intensities as produced by scattering from an asymmetric charge distribution is essentially correct. At the outset it is surprising that the x-ray intensities estimated by visual inspection, or from a microphotometer trace, seem to be normal, whereas the electron diffraction intensities are, even visually, entirely different from what the structure factor would lead us to expect. In the light of our results the cause of this apparent discrepancy becomes clear. It is evident that even monotonous x-ray S curves can produce a crossing over in the corresponding electron diffraction curves. Such an effect is produced if the valence electrons are distributed in an ellipsoidal fashion as in the model calculated by James and Johnson.

Figures 3C and 3D show the theoretical electron scattering curves as obtained from the assumption of a symmetrical charge distribution and from a model assuming an asymmetric distribution as discussed before. The principal characteristics of the experimental results are reproduced only in the curves obtained from the asymmetric charge distribution.

In comparing the experimental values as derived from x-ray scattering with the theoretical curves, one finds that the experimental value for $l=5$ lies closer to $l=0$ than $l=2$, and $l=3$ lies somewhat lower than the theoretical curve. This shift of the experimental curve is, however, in agreement with the experimental electron diffraction curves of Fig. 3B. That the curve for $l=3$ does not intersect the curve for $l=0$ as found experimentally is due to the model chosen in the theory. The charge distribution ρ is a function of Z only.† While the distortion of the valence electron distribution gives an adequate

[15] This procedure is justified by the fact that the O has a much smaller effect than the Zn. If one calculates the atom factor of O from the experimentally observed scattering power, using James' and Johnson's calculations for Zn, one obtains unreasonable results. This is due to the fact that such an interpretation puts all experimental errors into O.

[16] This procedure is strictly correct only if the electron cloud is spherically symmetric. Any asymmetry will introduce a small phase factor in the electron diffraction calculation. Trial calculations, using a graphical method have shown, however, that the error made in this simplification is less than the experimental error.

[17] The similar procedure: calculating theoretical x-ray atom factor from the electron diffraction data is subject to much greater error. See reference 18.

† See Section II, Part 3 of Johnson's paper, this issue.

explanation for the main trend of the picture, there are still some anomalies which remain unexplained. Such anomalies occur mostly at large values of $\sin\theta/\lambda$. The electron diffraction curve for $l=3$ lies much higher as compared with $l=1$ than does the one from x-ray results. The two points for $l=6$ do not permit an accurate determination of the curve on account of the very weak[18] intensity of the reflections for $l=6$, but they are high in respect to $l=2$ whereas the corresponding electron diffraction values are low.

To understand these remaining discrepancies between theory and experiment a more detailed discussion is necessary. The ellipsoidal distribution of the valence electrons determines the slope for the different curves and thus produces the crossing over of the S curves for different values of l, in agreement with the experimental results. If, however, we consider the position of separate points along one of the curves, then we frequently find that the position of the x-ray and electron diffraction points are displaced in opposite direction with respect to the average curve itself. For a certain plane (hkl) we find that an x-ray point with high intensity, with respect to the average curve, corresponds to an electron point with low intensity. Such points are all those belonging to $l=4$ (x-ray 004 low, 104 high, 204 low, 214 high; electron 004 high, 104 low, 204 high, 214 low). Other such points are 203, 102.

Since the intensities in electron diffraction depend on $(Z-F)^2$, and the x-ray intensities on F^2, we see that any effect which influences these intensities in the same direction will produce errors of opposite sign in the F values deduced from them. Any effect such as preferred orientation, preferred crystal growth, impurities, temperature disturbance, or a state of order-disorder in the crystal, which changes the structure factor, could produce such a result. We conclude that the residual differences between the F values deduced from the charge distributions and those deduced from intensity measurements are not due principally to imperfections in the assumed charge distribution, but to some factor affecting x-ray and electron intensities in the same direction.

As already mentioned,[1] impurities and preferred orientation are not responsible for any of the observed anomalies. The effect of crystal form due to the methods of preparation was considered. We have investigated powder obtained from single ZnO crystals by crushing, but did not find any deviation from the patterns obtained from ZnO powder made by other methods. The effect of anisotropic heat motion cannot be completely excluded before x-ray measurements have been made. Preliminary electron diffraction experiments[13] at liquid-air temperature, room temperature and above 350°C show, however, that the same intensity anomaly exists at all temperatures without any appreciable change, indicating that the temperature correction cannot be the main reason for the remaining discrepancies.

Although zinc oxide is an insulator at ordinary temperatures, it becomes electrically conducting at elevated temperatures. This conductivity is of the electronic type, indicating a tendency to a state of disorder in the crystal. Such a disorder would influence x-ray and electron patterns in the same way and in the calculation of F would therefore produce an apparent inversion of the different points in respect to the main curve as we have observed.[19] Intensity anomalies found in silver iodide, which has a structure similar to zinc oxide, (Wurtzite) have been explained primarily on the basis of order-disorder.[20] In some of the x-ray investigations in alloys it is not quite clear how far order-disorder or the possible effect of a distortion of the electron cloud will determine the intensities.

It would seem that the combination of x-ray and electron diffraction investigations points the way to the possibility of determining the cause of observed intensity anomalies. Anomalies due

[18] The determination of the weak intensities is, however, less uncertain in the x-ray pattern than in the electron diffraction pattern as can be seen by an examination of the electron diffraction microphotometer trace. (Fig. 1). The diffraction peaks in this case are much broader, ovelap to a greater extent, and are superimposed upon a rather steep background. The construction of this background is somewhat arbitrary.

[19] Depending upon the type of order-disorder, it is also possible, as has been pointed out recently by L. H. Germer and F. E. Haworth, Phys. Rev. **56**, 212 (1939), ordering effects appear in the electron diffraction, but not in the x-ray pattern due to the different size of the domain investigated. This, however, does not apply in the case of vagabond ions as assumed here.

[20] L. Helmholtz, J. Chem. Phys. **3**, 740 (1935).

to structural properties would influence x-ray and electron diffraction in the same way, and therefore, produce in the F curve an apparent inverted behavior. The anomalies due to an intrinsic change in the electron cloud of the atom due to bonding, or anisotropic lattice distortions, since they affect primarily the F factor, would not cause difficulty in reproducing electron diffraction curves from x-ray experiments.

To investigate the remaining discrepancies from this point of view we have started experiments at different temperatures, using ionization methods to refine the technique of intensity measurements.

The present experiments alone do not allow a a definite decision as to order-disorder in the zinc oxide crystal. It is possible, however, to derive the type of binding from the F factor curves for electron diffraction and x-rays combined and to separate the effects of electron cloud distortion from those of structural factors which change both electron diffraction and x-ray intensities in the same direction.

We wish to thank Professors James and Yearian, and Dr. Johnson for many interesting discussions; we wish also to thank Dr. R. K. Waring of the New Jersey Zinc Company for the gift of the spectroscopically pure zinc from which the zinc oxide has been prepared.

APRIL 1, 1940 PHYSICAL REVIEW VOLUME 57

The Effect of Valence Electrons and Electron Cloud Distortion upon Intensities in Electron and X-Ray Scattering*

(Applied to Zinc Oxide)

VIVIAN A. JOHNSON
Purdue University, Lafayette, Indiana

(Received December 28, 1939)

An extensive investigation of electron scattering by zinc oxide has been carried out by Lark-Horovitz and Yearian. The intensity distribution, determined by photographic methods, showed marked anomalies with respect to the intensity distribution of the corresponding x-ray pattern. The visually estimated x-ray intensities seem to be in general agreement with values calculated from approximate Fermi or Pauling-Sherman wave functions, and the marked anomalies appear only in the electron diffraction pattern. The observed intensities have been formally accounted for by assuming a polarization of the M shell of the zinc atom. This hypothesis has been tested by calculating the charge distribution of the M shell in zinc under the effect of the electrostatic fields arising from a partly ionic character of the lattice and its deviation from perfect tetrahedral symmetry. The calculated distortion is too small by a factor of $\frac{1}{160}$ to account alone for the observed anomalies. Then the effect due to the valence electrons is considered. A rough agreement with experimental values is obtained with a model in which two valence electrons of each zinc-oxygen pair of nearest neighbors are assumed to be placed in a uniform linear distribution between these neighboring nuclei and the other two in a uniform distribution through the crystal. A more refined model, in which two valence electrons of each zinc-oxygen pair of nearest neighbors are assumed to be distributed over the surface of an ellipsoid with major axis axis along the c axis of the crystal, accounts for the principal anomalies in the electron diffraction intensities, and at the same time gives results which are in agreement with measured x-ray intensities. The importance of the method used as a tool for determining the type of binding in a crystal is discussed.

INTRODUCTION

A LARGE number of electron diffraction patterns of zinc oxide have been obtained by Lark-Horovitz and Yearian.[1, 2] The intensity distribution was determined by the photographic method and was found to show marked anomalies with respect to the corresponding x-ray pattern. The scattering of x-rays is not influenced by the nucleus of the scattering atom, but electron diffraction is affected by both the nucleus and the electronic cloud. Therefore it should be possible to use electron diffraction to locate the positions of nucleus and electrons in a crystal lattice. It was for this reason that Yearian and

* The investigation reported here is based in part upon a doctoral thesis submitted to the Faculty of Purdue University.

[1] H. J. Yearian and K. Lark-Horovitz, Phys. Rev. **42**, 905 (1932); K. Lark-Horovitz, H. J. Yearian and E. M. Purcell, Phys. Rev. **45**, 123 (1934); K. Lark-Horovitz, H. J. Yearian and J. D. Howe, Phys. Rev. **47**, 331 (1935).

[2] H. J. Yearian, Phys. Rev. **48**, 631 (1935).

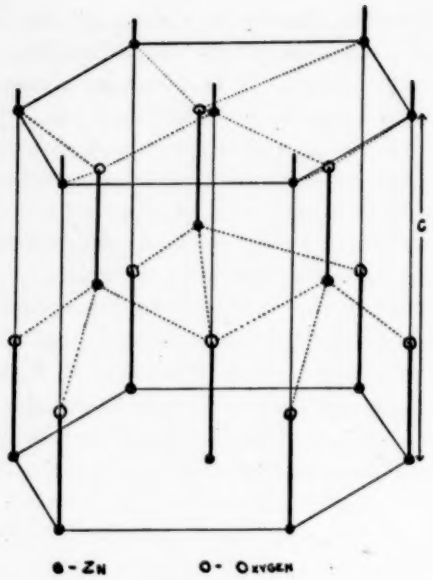

FIG. 1. Structure of zinc oxide.

Lark-Horovitz carried out their study of scattering of high speed electrons by zinc oxide powder. The positions of the rings in the patterns obtained agree very closely with those calculated from x-ray data, but a comparison of estimated with observed intensities shows large discrepancies. According to Mott,[3] electron intensities should differ from x-ray intensities, but only as a monotonous function of $\sin\theta/\lambda$ (where θ is the half-angle of scattering, and λ the de Broglie wave-length of the electrons), and not irregularly from peak to peak.

In order to account for the observed intensity anomalies, Yearian and Lark-Horovitz considered the possibility that the effect was caused by impurities, preferred orientation, the method of depositing the powder, or an incorrect application of the kinematical theory of diffraction. They concluded that the above factors could not account for the observed anomalies. Yearian found that this discrepancy can be formally accounted for by assuming that the atomic electron clouds are drawn out from a spherical form into an ellipsoidal form with the major axis along the c axis of the crystal.[2]

The structure[4] of zinc oxide (Fig. 1) has been found by x-ray data to be in agreement with a single space group, $C_{6v}4$. In an ideal hexagonal close packed lattice with axial ratio $c/a=1.633$ and the parameter $u=0.375$, each atom is at the center of a tetrahedron formed by atoms of the opposite kind. The actual zinc oxide lattice is distorted so that the axial ratio $c/a=1.599$ and $u=0.375$ (this latter value is now being tested by Lark-Horovitz and collaborators). The zinc-oxygen distances along the c axis (1.94A) are less by about five percent than in the other directions (2.04A).

It is reasonable to assume that some shift of the center of the electronic cloud might arise in order to maintain equilibrium in such a distorted lattice. Yearian found that satisfactory scattering curves are obtained by assuming that only the outer shells (M and N) are displaced. If the centers of the $3s$ and $3p$ shells of the zinc atoms are displaced by $0.01c$ (0.05A), and the $3d$ by $0.04c$ (0.20A), this distortion is sufficient in itself to account for the observed intensity anomalies.

In the present investigation, (1) the distortion of the M shell of the zinc atom has been computed by wave mechanical methods, and (2) the effect of the valence electrons upon the electron scattering intensities has been calculated.

I. The Distortion of the M Shell by the Intra-Crystalline Field

A distortion may be produced in the electronic clouds surrounding the zinc nuclei by the electrostatic field due to a partly ionic character of the zinc oxide lattice. The electrostatic potential is considered as a perturbation potential to be applied to the unperturbed wave functions for the various electrons in the M shell of a zinc atom. After the perturbed wave functions have been found, the corrected charge density and charge distribution in the M shell are computed. Then the results of the theoretical calculation are compared with the experimental data.

1. Estimate of the intra-crystalline field

The potential field due to the arrangement of atoms in the zinc oxide crystal may be split into two parts: (1) a tetrahedrally symmetric part that would be set up by a perfect tetrahedral arrangement, and (2) since the arrange-

[3] N. F. Mott, Proc. Roy. Soc. **A127**, 658 (1930).
[4] P. P. Ewald and C. Herman, *Strukturbericht* (Leipzig, 1931) pp. 78, 119. W. L. Bragg, Phil. Mag. **39**, 647 (1920). R. W. G. Wyckoff, *The Structure of Crystals* (Chemical Catalog Company, 1924), p. 273–275.

ment is not perfectly tetrahedral, a linear field set up by the deviation from perfect symmetry.

The simplest form for a potential of tetrahedral symmetry is:

$$V_T = ax'y'z',$$

where a is a constant to be determined by an estimate of the lattice potential, and x', y', z' are coordinates with respect to a set of rectangular axes, with origin at the nucleus of the central zinc atom, which pass through the midpoints of the edges of the tetrahedron. It is more convenient to use a system of coordinates with the origin at the nucleus of the central zinc atom, the Z axis in the line joining the zinc nucleus to the nearest oxygen atom (c axis of the crystal) and the X axis parallel to one of the sides of the base of the tetrahedron. In this coordinate system, the tetrahedral potential becomes:

$$\begin{aligned} V_T &= a\left[\frac{1}{3\sqrt{3}}z^3+\frac{1}{3\sqrt{6}}y^3-\frac{1}{2\sqrt{3}}y^2z \right. \\ &\qquad \left. -\frac{1}{\sqrt{6}}x^2y-\frac{1}{2\sqrt{3}}x^2z\right], \\ &= ar^3\left[\frac{5}{6\sqrt{3}}\cos^3\theta-\frac{1}{2\sqrt{3}}\cos\theta \right. \\ &\qquad \left. -\frac{1}{3\sqrt{6}}\sin^3\theta\sin 3\varphi\right], \\ &= V_1'+V_2'+V_3'. \end{aligned} \tag{1}$$

V_3' has been neglected as it would produce no first-order change in the charge distribution along the Z axis, which is alone of interest for the following discussion.

The linear field, being produced by a distortion in the direction of the c axis, has the form:

$$V_L = bz = br\cos\theta. \tag{2}$$

To estimate the constants a and b, one must assume values for the effective charges of the ions in the lattice. The actual values are not known; to fix maximum values a purely ionic lattice with the ions Zn^{++} and O^{--} is assumed. The Coulomb potential of the lattice is

$$V_C(x, y, z) = \sum_i \frac{e_i}{[(x_i-x)^2+(y_i-y)^2+(z_i-z)^2]^{\frac{1}{2}}},$$

where x_i, y_i, z_i are the coordinates of the ith particle in the lattice. By expanding this function for points along the Z axis and by considering that the even powers of z drop out, one obtains:

$$\begin{aligned} V_C(0, 0, z) = \sum_i \frac{e_i}{r_i}\left[\cdots+\frac{z_i}{r_i^2}z+\cdots \right. \\ \left. +\left(\frac{5z_i^3}{2r_i^6}-\frac{3z_i}{2r_i^4}\right)z^3+\cdots\right]. \end{aligned} \tag{3}$$

By requiring that the sum of the tetrahedral and linear potentials cannot exceed such a Coulomb lattice potential one obtains maximum value expressions for a and b:

$$\frac{1}{3\sqrt{3}}a = \sum_i \frac{5e_iz_i^3}{2r_i^7}-\sum_i\frac{3e_iz_i}{2r_i^5},$$

$$b = \sum_i \frac{e_iz_i}{r_i^3}.$$

These sums are evaluated by using the known positions of the atoms in the crystal. The results, accurate to within 1 percent, are:

$$a = 0.109(a_H)^{-4}, \qquad b = 0.020(a_H)^{-2}, \tag{4}$$

where a_H = Bohr radius.

2. Calculation of the distortion produced

As soon as the coefficient b is evaluated, one can make a rough estimate of the average displacment along the c axis produced in the M shell by the linear field (the tetrahedral field does not influence such a displacement). By applying the conditions of equilibrium to an electron in the Thomas-Fermi potential field alone and then to the same electron under the influence of both the Thomas-Fermi field and the linear field, one finds that the displacement produced by the

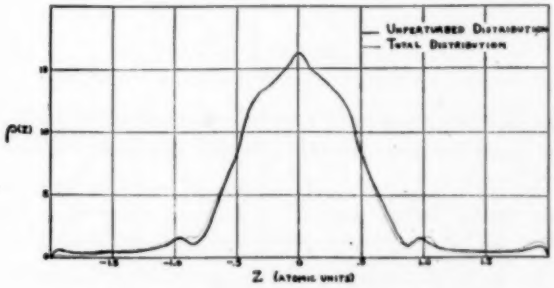

FIG. 2. Projection of the charge distribution on the Z axis.

linear field is

$$\mathbf{z}=\frac{bR^3}{Z\varphi(R/\mu)}.$$

R, the mean distance of the electrons in the M shell from the nucleus, certainly does not exceed a_H. By setting $R=a_H$, one gets $\mathbf{z}\leqq 0.004a_H$. Hence one obtains as a rough estimate of the dipole moment of the M shell:

$$D\leqq 18(0.004)=0.07 \text{ atomic unit.} \quad (5)$$

As will appear later, this is about $\frac{1}{10}$ the dipole moment required to explain the experimental results.

Actually it is not necessary to rely upon this estimate alone, inasmuch as the maximum distortion and dipole moment have been calculated by the following method:[5]

The unperturbed wave functions for the $3s$, $3p$ and $3d$ orbits in zinc are computed by the methods of numerical integration developed by Hartree.[6] The Thomas-Fermi potential[7] is used. Then the perturbation functions due to both the tetrahedral and the linear fields are evaluated numerically. The charge density associated with the M shell is expressed as the sum of the unperturbed density, the perturbation of the charge distribution due to V_T, and the perturbation of the charge distribution due to V_L. The projection of this charge distribution along the Z axis is computed and compared with the projection of the unperturbed charge distribution (see Fig. 2).

The adequacy of the distortion of the M shell as an explanation of the intensity anomalies in ZnO can be tested by comparing the computed dipole moment of the atom with that found by Yearian to be required to explain the observations, 4.7 atomic units. The calculated value is:

$$D_{\text{calc}}=\int \rho z d\tau=\int \rho r\cos\theta d\tau. \quad (6)$$

The distortion due to the tetrahedral field makes no contribution to the dipole moment, which becomes

$$D_{\text{calc}}=\frac{8}{3}b\int_0^\infty B(r)r^3dr=0.028 \text{ atomic units,} \quad (7)$$

where $4/(3\pi)^{\frac{1}{2}}bB(r)$ represents the perturbation of the charge distribution due to V_L.

Thus the calculated value is only about $\frac{1}{160}$ of that required to account for the observed intensity anomalies. Since the wave functions employed probably have too great a range in r and hence probably too high a polarizability, and since the estimated value of b is surely a maximum, it seems clear that the discrepancy is not due to the method of calculation. Hence, it must be concluded that the experimentally observed anomalies of the electron diffraction intensities cannot be accounted for by the deviation from spherical symmetry of the charge distribution in the M shell.

II. Effect of Valence Electrons on Electron Scattering Intensities

Previous discussions of the intensity anomalies in the electron scattering of ZnO have neglected the distortion of the oxygen atom and the effect of the valence electrons of the zinc atom. In view of the preceding results, it is still reasonable to neglect the polarization of the oxygen atom; hence one is led to look for the origin of the effects in the behavior of the valence electrons of Zn and O. Since a spherical distribution of electrons would not give the desired effect, it is necessary to use part of the electrons in a distribution over a definite direction and the remaining electrons smeared out at random. Electrons occupying an essentially uniform distribution through the crystal cannot contribute to the diffraction maxima, but distortions of the electron distributions of the atoms in the crystal comparable to those known to occur in diatomic molecules would have the right qualitative character to produce the observed effects. Therefore it seems desirable to test whether such distortions can account for the intensity observations and to see what might be deduced concerning the binding within the crystal.

Since the direct computation of the distribution of electrons in the zinc oxide crystal is

[5] Vivian A. Johnson and L. W. Nordheim, Phys. Rev. **51**, 1002 (1937). More refined calculations show that the factor $\frac{1}{30}$ given in this abstract should be changed to $\frac{1}{160}$. See last paragraph, Section 2.

[6] D. R. Hartree, Mem. and Proc. of the Manchester Lit. and Phil. Soc. **77**, 1 (1932)..

[7] E. Fermi, Zeits. f. Physik **48**, 73 (1928). L. H. Thomas, Proc. Camb. Phil. Soc. **23**, 542 (1927).

impracticable, it has been possible only to test the effectiveness of simple model electron distributions in explaining observed intensities. Linear distributions of charge along the internuclear lines[8] and distributions over ellipsoids of revolution with the internuclear axis as the major axis have been used as models for electron concentrations. The problem is to determine whether models in which reasonable numbers of electrons are assigned to such distributions can account for the observed x-ray and electron diffraction intensities,[9] and to find the character of the assumed bonding distributions.

1. Calculation of corrected atom factors

In calculating values of the x-ray atom factors F_{Zn} and F_O from models, it is convenient to divide the charge distribution in the model into three parts: a spherical distribution about the oxygen nucleus, computed from the Pauling-Sherman wave function for O and giving rise to F_O; a spherical distribution about the Zn nucleus computed from the Pauling-Sherman wave function for Zn^{++} and giving rise to $F_{Zn^{++}}$; a model distribution of the "valence electrons" giving rise to the structure factor F_V, a function of $(\sin\theta/\lambda)$ and the Miller indices, h, k and l.

In computing the form factor F_V the usual methods, applicable only to spherical distributions, cannot be applied. It is necessary to use the fundamental expression for the form factor:

$$F(\mathbf{k})=\int \rho \exp\left[i\mathbf{k}\cdot\mathbf{r}\right]d\tau,$$

where $\mathbf{k}$ is a vector perpendicular to the reflecting plane, of magnitude $(4\pi\sin\theta/\lambda)$, $\mathbf{r}$ is the radius vector to the volume element, and ρ is the density of the charge distribution. For a charge distribution over an ellipsoid of revolution,[10] the integration offers some difficulty. Following a method developed by James, this problem is conveniently treated by relating the atom factor for a distribution of charge over a sphere to the atom factor of the distribution over

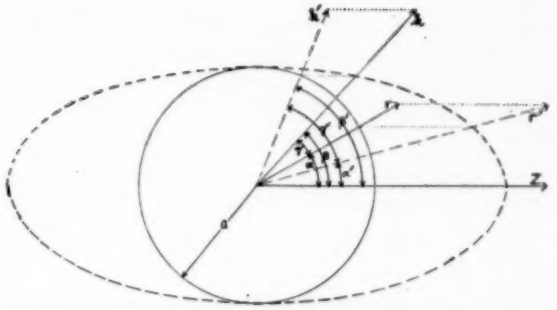

FIG. 3. Transition from spherical to ellipsoidal distribution.

an ellipsoid of revolution obtained by stretching that spherical distribution in the Z direction.

Let the charge distribution over the surface of a sphere, of surface density σ, be considered as a volume distribution of density ρ between spheres of radii a and $a+da$. Then

$$\sigma=\rho da.$$

Let ρ depend only on the angle α between the Z axis and the radius vector to the point considered. Then ρ can be developed in spherical harmonics:

$$\rho(\alpha)=\frac{1}{4\pi a^2}\sum_m A_m P_m(\cos\alpha).$$

To evaluate the form factor for such a distribution, the exponential may be expanded as

$$\exp\left[i\mathbf{k}\cdot\mathbf{r}\right]=\exp\left[ikr\cos\gamma\right]$$
$$=\sum_{n=0}^{\infty}(2n+1)i^n P_n(\cos\gamma)f_n(kr), \qquad (8)$$

where $f_n(kr)=(\pi/2kr)^{\frac{1}{2}}J_{n+\frac{1}{2}}(kr)$,

and γ is the angle between $\mathbf{r}$ and $\mathbf{k}$. Making use of the transformation:

$$P_m(\cos\alpha)=P_m(\cos\beta)P_m(\cos\gamma)$$
$$+\sum_{s=1}^{m}2\frac{(m-s)!}{(m+s)!}P_m^s(\cos\beta)P_m^s(\cos\gamma)\cos\varphi_{rz},$$

where β is the angle between $\mathbf{k}$ and the Z axis, one can readily carry out the integration over the sphere, to find:

$$F(k,\cos\beta)=\sum_n A_n i^n P_n(\cos\beta)f_n(ka). \qquad (9)$$

The next step is to find how Eq. (9) is modified if the sphere is stretched uniformly in the Z direction so that the scattering takes place from a surface distribution over an ellipsoid instead of

[8] Vivian A. Johnson and Hubert M. James, Phys. Rev. **53**, 327 (1938).

[9] An attempt to account for the intensity anomaly by considering the valence electrons was made earlier by Yearian and Lark-Horovitz; but their model also gave an appreciable anomaly in the observed x-ray intensities and hence was not used.

[10] H. M. James and V. A. Johnson, Phys. Rev. **56**, 119 (1939).

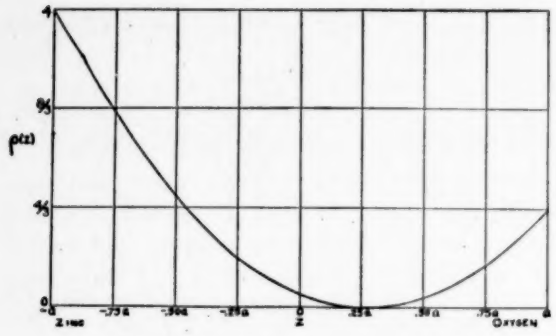

FIG. 4. Projection of valence electron distribution.

over a sphere. Consider all distances parallel to the Z axis to be multiplied by a factor s. Let the quantities relating to the modified problem be distinguished by primes. From the geometry of the problem (Fig. 3) the following relations are found to hold:

$$x=x',\quad y=y',\quad z=z'/s;$$

$$r'\sin\alpha'=r\sin\alpha,\quad r'\cos\alpha'=sr\cos\alpha;$$

$$\rho'(x',y',z')=(1/s)\rho(x',y',z'/s)=(1/s)\rho(x,y,z);$$

$$r'=r\{1+(s^2-1)\cos^2\alpha\}^{\frac{1}{2}}; \tag{10}$$

$$k_x=k_x',\quad k_y=k_y',\quad sk_z'=k_z;$$

$$k=k'\{1+(s^2-1)\cos^2\beta'\}^{\frac{1}{2}};$$

$$\cos\beta=\frac{s\cos\beta'}{\{1+(s^2-1)\cos^2\beta'\}^{\frac{1}{2}}}.$$

These relations are now used to find the form factor for the ellipsoidal distribution:

$$F'(k',\cos\beta')=\int\rho'(x',y',z')\exp\left[i(k_x'x'+k_y'y'+k_z'z')\right]dx'dy'dz',$$

$$=\int\frac{1}{s}\rho(x,y,z)\exp\left\{i[k_xx+k_yy+(k_z/s)\cdot sz]\right\}dxdyd(sz),$$

$$=\int\rho(x,y,z)\exp\left[i\mathbf{k}\cdot\mathbf{r}\right]dxdydz,$$

$$=F(k,\cos\beta),$$

$$=F[k'\{1+(s^2-1)\cos^2\beta'\}^{\frac{1}{2}};\ s\cos\beta'/[1+(s^2-1)\cos^2\beta']^{\frac{1}{2}}],$$

or

$$F'(k',\cos\beta')=\sum_{n=0}^{\infty}A_ni^nP_n\left(\frac{s\cos\beta'}{[1+(s^2-1)\cos^2\beta']^{\frac{1}{2}}}\right)f_n(ak'[1+(s^2-1)\cos^2\beta']^{\frac{1}{2}}). \tag{11}$$

This result means that the scattering from an ellipsoidal charge distribution is the same as that from a corresponding spherical distribution for a modified k' and β'.

The coefficient A_0 is equal to the total charge assumed to be distributed over the ellipsoid, and the other coefficients A_n describe the lack of uniformity in the distribution. Here it is sufficient to consider terms with $n=0$, 1, 2; that is, to consider the distribution as the sum of constant, linear, and quadratic terms. The projection of the charge density on the Z axis is given by:

$$\rho(z)=\frac{A_0}{2a}+\frac{A_1}{2a^2}z+\frac{A_2}{4}\left(\frac{3z^2}{a^3}-\frac{1}{a}\right). \tag{12}$$

The projection on the Z axis of the charge distribution used in the final calculations is shown in Fig. 4.

2. Examination of possible models

Calculations of F_V were first made with linear distributions of charge over all or part of the internuclear lines connecting each zinc to the four oxygens which surround it tetrahedrally. It was found that rough agreement with the observed intensities could be obtained by distributing two electrons over the line connecting each zinc to the nearest of these oxygens, along the c axis.[8] This agreement is destroyed if any attempt is made to treat the four nearest oxygen neighbors as equivalent. Hence it seems clear that any distribution of charge in the crystal involving "valence electrons" must have these largely

concentrated along the c axis if it is to be compatible with observed intensities.

Hence, in seeking more satisfactory models for the distribution of the valence electrons, attention has been restricted to distributions over ellipsoids with the c axis as the axis of revolution. These models involve various values of the minor axis $2a$, the major axis $2sa$, and the parameters A_0, A_1, A_2. A_0 is the number of "valence electrons" in the model, and A_1 and A_2 are chosen so as to keep the electron density everywhere positive. Reasonably extensive trials gave for the best model:

$$A_0=2; \quad A_1=-8/3; \quad A_2=-10/3 \quad (13)$$
$$s=6; \quad a=0.175\text{A}.$$

No quantitative significance is to be attached to these figures, but one may hope that the qualitative character of the distribution will give some indication as to the situation in the crystal.

With the parameter values of (13), $F_V(k, \beta)$ is evaluated for values of k and β corresponding to the reflecting planes from which scattering has been observed. The values of F_V are added to the values of $F_{Zn}{}^{++}$ to give the values of F_{Zn} used in calculating $|S_1|$, the molecular form factor, from Eq. (14):

The comparison of theory and experiment is

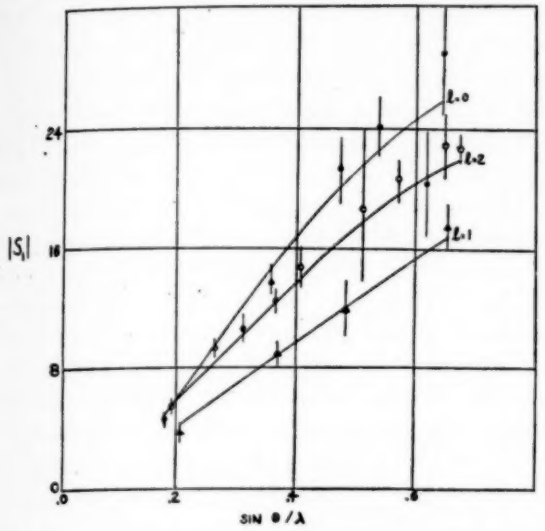

FIG. 5a. Comparison of experimental and calculated values of $|S_1|$. The vertical lines indicate the average deviation in the experimental values determined by electron diffraction methods.

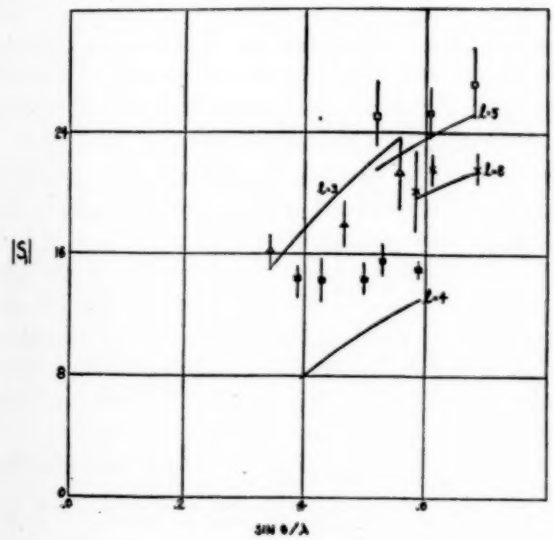

FIG. 5b. Comparison of experimental and calculated values of $|S_1|$.

TABLE I. *Values of the molecular structure factor* $|S_1|$.*

hkl	$\frac{\sin\theta}{\lambda}$	Calculated: Valence Electron Method	Calculated: Pauling-Sherman Method	Observed: X-Ray Methods[14]	Observed: Electron Diff. Method[2, 15]
100	0.178	4.8	6.5	5.5	4.3
110	.309	12.0	13.7	12.2	10.5
200	.356	14.6	16.3	15.6	13.6
120	.472	20.2	21.4	20.5	21.2
300	.535	22.7	23.6	22.4	[24.0]
220	.617	25.0	25.8	25.3	[20.2]
310	.642	25.7	26.4		[29.0]
101	.203	4.2	4.5	5.3	3.7
201	.369	9.0	9.2	10.8	9.0
211	.481	12.4	12.5	12.9	11.9
311	.650	16.4	16.4		17.4
002	.193	5.3	5.8	6.3	5.3
102	.263	8.3	8.5	8.5	9.4
112	.364	12.2	12.6	15.4	12.5
202	.405	13.9	14.3	14.7	14.7
212	.509	17.7	17.9	17.4	[18.7]
302	.568	19.4	19.4	18.8	20.6
222	.647	21.2	21.1		[23.0]
312	.671	21.5	21.4		[22.6]
103	.339	14.9	14.2	15.0	16.3
203	.459	20.2	19.6	20.6	18.0
213	.553	23.7	22.8	22.7	21.4
004	.386	7.7	7.6	7.5	14.4
104	.425	8.9	8.7	9.8	14.4
114	.494	10.8	10.6	10.4	14.4
204	.525	11.5	11.4	9.7	15.7
214	.609	13.3	13.2	12.5	15.0
105	.514	21.6	21.6	22.3	25.1
205	.600	23.7	24.0	23.8	[25.4]
215	.674	25.2	25.5		[27.2]
006	.579	19.6	19.7	19.1	[20.2]
106	.606	20.2	20.3	20.9	[21.7]
206	.680	21.4	21.6		[21.4]

* The less reliable values in column 6 are bracketed.

most conveniently made through the molecular structure factor. The total structure factor for electron scattering by zinc oxide is given[2] by:

$$S=S_1\times S_2=[(Z_{Zn}-F_{Zn})+(Z_O-F_O)e^{2\pi iul}]\times[1+e^{2\pi i(h/3+2k/3+l/2)}], \quad (14)$$

where h, k, l are the Miller indices of the scattering plane, $u=0.375$, and F_{Zn} and F_O are the x-ray atom factors.[2]

In their experiments, Yearian and Lark-Horovitz measured the relative intensities and positions of the rings obtained, then calculated the molecular form factors, S_1, by use of the relation:

$$|S_1|=C\left(\frac{\sin\theta}{\lambda}\right)^3\left[\frac{I}{f|S_2|^2}\right]^{\frac{1}{4}}, \quad (15)$$

where C is a proportionality factor and f the frequency factor. Column 6 of Table I gives the values of $|S_1|$ calculated from the observed intensities.[11]

$|S_1|$ can be calculated from (14) if the values of F_{Zn} and F_O are known. Pauling and Sherman[12] have calculated F values for all atoms on the assumption of a spherically symmetric electron distribution. The values of $|S_1|$ obtained by putting these F values for zinc and oxygen in (14) are given in column 4 of Table I.

Furthermore, values of $|S_1|$ can be computed by substituting in (14) values of F_{Zn} and F_O determined by x-ray measurements. Ehrhardt and Lark-Horovitz[13, 14] have obtained photographically x-ray diffraction patterns from zinc oxide, from these calculated the x-ray atom factors for zinc, and then constructed the corresponding $|S_1|$ curves. The values of $|S_1|$ obtained by Ehrhardt and Lark-Horovitz are given in column 5 of Table I.

In Fig. 3 of Ehrhardt and Lark-Horovitz the calculated values are shown in comparison to the values obtained by the x-ray measurements,[14] and in Fig. 5 of this paper, they are shown in comparison to the values obtained by the electron diffraction measurements.[2, 15]

3. Discussion of results

As shown by Table II and Fig. 2 of reference 14, there is no outstanding discrepancy between experimental and calculated values. The general agreement between the calculated and experimental structure factors at small values of $\sin\theta/\lambda$ is probably within the limits of experimental error. There is no outstanding discrepancy between the observed x-ray and calculated values. The principal disagreement between calculated and observed electron diffraction values is that between the sets of values for $l=4$. A possible explanation of this discrepancy lies in the fact that the intensities corresponding to scattering from planes for which $l=4$ are weak and the corresponding peaks are poorly resolved.[16] In comparing the calculated and observed electron diffraction values the following results should be noted: the model used gives better agreement than the Pauling-Sherman model for the reliably determined points corresponding to low values of $\sin\theta/\lambda$ and $l=0$ and 2, the curves for $l=0$ and 2 cross near $\sin\theta/\lambda=0.2$ as do the experimental curves, and the curves for $l=2$ and $l=6$ are separated, as are the curves for $l=3$ and $l=5$. The high axial ratio of the ellipsoid used in the model indicates a charge distribution concentrated primarily along the Z axis. This accounts for the fact that the experimentally observed intersection of the curves for $l=0$ and $l=3$ at large $\sin\theta/\lambda$ is not reproduced, since such a charge distribution influences reflection from the prism zones rather uniformly.

From the results obtained by the use of the model here considered, it appears that the intensity anomalies in the electron scattering from ZnO are due principally to the unsymmetrical distribution of a few weakly bound electrons from each Zn−O pair.

The concentration of electrons between the

[11] The intensities were corrected for temperature effect. At the suggestion of K. Lark-Horovitz, Whitmer and Yearian (Phys. Rev. **55**, 1114 (1939)) have investigated the temperature correction for zinc oxide by electron diffraction methods, and have found that the temperature correction is a monotonous function, corresponding to a Debye temperature of 350°K in an isotropic body.

The values of $|S_1|$ given in the table are 2.02 times the corresponding values given in Yearian, Phys. Rev. **48**, 631 (1935). This factor is used to transform the arbitrary scale to a scale comparable with that of the calculated values.

[12] L. Pauling and J. Sherman, Zeits. f. Krist, **81**, 1 (1932).

[13] K. Lark-Horovitz and C. H. Ehrhardt, Phys. Rev. **55**, 605 (1939). Washington meeting, December 27–29, 1938.

[14] C. H. Ehrhardt and K. Lark-Horovitz, Phys. Rev., this issue.

[15] At large values of $\sin\theta/\lambda$ the resolution in electron diffraction curves becomes unreliable. See Fig. 5 of this paper and Fig. 1*C* of reference 14.

[16] In this connection see discussion of this point in C. H. Ehrhardt and K. Lark-Horovitz, Phys. Rev., this issue.

zinc-oxygen pairs along the c axis might be due either to the electric field arising from the deviation of the crystal from perfect symmetry or to the existence of some homopolar binding between the zinc-oxygen pairs of nearest neighbors. The most successful model considered places some excess of electrons in the neighborhood of the zinc nucleus (Fig. 4), and hence certainly does not approximate a lattice of the ions Zn^{++} and O^{--}. The indicated intra-crystalline field would be much smaller than that estimated in Section I 1; *it seems then that the concentration of charge indicates that there is homopolar binding of the zinc-oxygen neighbors along the c axis.* Such a binding would account for the deviation of the zinc oxide crystal from perfect symmetry. According to this idea, a zinc oxide molecule would retain its individuality within the crystal, in contrast to the situation in such purely ionic crystals as sodium chloride. These zinc-oxygen pairs, or molecules, are not completely electrically symmetrical; the binding of these molecules into the crystal would thus include electrostatic as well as polarization forces, and possibly some further contribution from homopolar binding as well.

This study of electron scattering from zinc oxide shows that electron diffraction offers a powerful method for the investigation of the structure of crystals, such as zinc oxide, for which the type of binding is not indicated by other methods available.

I wish to express my sincere appreciation to Dr. K. Lark-Horovitz for his suggestion of the problem and for his constant encouragement, to Dr. L. W. Nordheim for many important suggestions relating to Part I, to Dr. H. M. James for valuable assistance with Part II, to Drs. H. J. Yearian and C. H. Ehrhardt for information concerning the experimental results, and to Dr. H. A. Bethe for helpful comment during the progress of the work.

APRIL 1, 1940 PHYSICAL REVIEW VOLUME 57

X-Ray Dispersion in Copper Crystals

E. M. McNatt*
Wayman Crow Hall of Physics, Washington University, St. Louis, Missouri
(Received January 26, 1940)

The diffuse scattering of Cu $K\alpha$ radiation ($\lambda=1.54$A) from single crystals of copper ($\lambda_k=1.38$A) has been measured for various scattering angles from $\phi=40°$ to 120°. Atomic structure factors, calculated from these measurements by combining them with the average temperature-modified structure factor values obtained by other workers using the powdered crystal reflection method, have been compared with Hartree theoretical atomic structure factor values for $\lambda\to 0$ to obtain the decrement caused by dispersion. The average decrement was found to be $\Delta f=1.75$ as compared with the Hönl value of 2.8 for this ratio of incident to critical absorption wave-length, $\lambda/\lambda_k=1.12$. No evidence for a dip in the atomic structure factor curve such as found with zinc was noted. Since copper is a cubic crystal the atomic electron clouds are presumably spherically symmetrical and hence no dip in the S or f curves should be expected.

I. Introduction

In a recent paper[1] the writer published experimental results showing the effect of dispersion and atomic electron cloud distortion on the diffuse scattering of Zn and Cu $K\alpha$ radiation from single crystals of zinc. During the course of that experiment similar measurements were made on single crystals of copper ($\lambda_k=1.38$A), using copper $K\alpha$ radiation ($\lambda=1.54$A), to determine whether analogous effects exist in the case of copper. Measurements of the decrement in the reflecting power of copper crystals for Cu $K\alpha$ rays have been made by Rusterholtz[2] and others, using the powdered crystal method. From these measurements the decrement in the atomic structure was calculated with the aid of the Debye-Waller theoretical formula for the temperature correction. However the Debye-Waller formula involves the "characteristic" tempera-

* Now with The Carter Oil Company, Tulsa, Oklahoma.
[1] E. M. McNatt, Phys. Rev. **56**, 406 (1939).
[2] A. A. Rusterholtz, Zeits. f. Physik **65**, 226 (1930).

ture, and the uncertainties in the specific heat data from which this is calculated make its use unsatisfactory. On the other hand diffuse scattering measurements combined with experimental reflection intensity data permit the direct calculation of atomic structure factors without the use of the temperature factor. Furthermore, diffuse scattering measurements not only require no corrections for the effects of extinction, but are in general less dependent upon surface conditions than are powdered crystal reflection data because the half-absorption depth in diffuse scattering experiments is from three to thirty times as great as the dimensions of powdered crystals used in reflection experiments.

II. Experimental Method

The apparatus and method of measurement used in this research have been described before.[1] Copper crystals used in the experiment were small sections cut from cylindrical single crystals of copper.[3] In order to obtain the required flat surfaces, the crystal rods were first cut lengthwise by slow sawing with a fine jewelers, saw. Next the surface was carefully ground flat with emery powder, and finally the crystal was etched to remove distortion caused by the sawing and grinding. The etching was done by a method described by Underwood,[4] in which the metal is etched with HNO_3, first with 55 percent and then with 74 percent solution. When the stronger solution was not preceded by the weaker, a red oxide which resisted further etching was formed. After the crystal had been properly etched it had the matte surface characteristic of etched crystals, and, if the sample was not single, the different orientations present were clearly distinguishable because of the difference in reflecting power for light incident at various angles. Some of the first crystals so prepared showed small "islands" of polycrystalline copper which made the specimens unsuitable for diffuse scattering measurements, since a Bragg reflection from one or more of the "islands" was likely to occur at almost any angle of scattering. As a result of such stray reflections the experimental diffuse scattering would be too high, of course, since the reflections might not be strong enough to be detected as such.

[3] The single crystal copper rods from which the samples were cut were presented to the Physics Department through the courtesy of Dr. Foster C. Nix of the Bell Telephone Laboratories, New York.

[4] N. Underwood, Phys. Rev. **47**, 502 (1935).

III. Temperature-Modified Structure Factors from Reflection Data

Experimental values of the diffuse scattering are obtained from electrometer readings and instrumental constants through the formula[1]

$$S=\frac{4R^2Wm^2c^4}{ANZe^4(1+\cos^2\chi\cos^2\phi)}\times\frac{D(\phi,\theta)}{D_0u(\phi,\theta)}\times\frac{\mu}{\rho}. \quad (1)$$

The theoretical value of S is given by Jauncey's formula[5]

$$S=(f-\Delta f)^2(1-e^{-2M})/Z + [1-(1/Z)\Sigma E_r^2]/R, \quad (2)$$

where f is the atomic structure factor, F is the atomic structure factor modified by the effects of thermal vibrations, E_r is the electronic structure factor for the rth electron, and R is the so-called Breit-Dirac factor to take account of Compton scattering processes. Δf and ΔF are the decrements due to dispersion in the f and F values, respectively.

From Eq. (2) we may express $(f-\Delta f)$ in terms of the measured quantities S and $(F-\Delta F)$, and the incoherent term $[1-(1/Z)\Sigma E_r^2]/R$. This last term is not an experimentally measured datum, and values of E_r^2 are those obtained by James and Brindley[6] using the Hartree distribution function. Fortunately R is nearly equal to unity, and the contribution of the ΣE_r^2 term is small enough so that a large percentage error in it would but slightly affect the final result. In the case of zinc, measurements of F, S, and the temperature factor have been made for wavelengths considerably shorter than that for the K-absorption edge, in which measurements the effect of the natural frequencies of the electrons is small. Therefore we can say that we know f fairly well, and hence measurements made with $\lambda\approx\lambda_k$ will show the effect of these natural frequencies (anomalous dispersion). However such complete data have not been obtained for copper. Thus to find $(f-\Delta f)$ from the measured S values

[5] G. E. M. Jauncey, Phys. Rev. **56**, 644 (1939).

[6] R. W. James and G. W. Brindley, Phil. Mag. **12**, 104 (1931).

we need to know temperature-modified structure factors found using the same wave-length and at the same temperature as that employed in obtaining the diffuse scattering results. Because there are variations in such $(F-\Delta F)$ values published for copper, it was important to investigate the sources of the discrepancies in order to know the best set of values to use.

Perhaps the most conspicuous feature of the published $(F-\Delta F)$ data is that they are not absolute measurements, but have been standardized by comparison with reflections from a standard substance. The fact that the temperature-modified structure factor values of different authors agree well if they are made equal for one value of $(\sin\theta)/\lambda$ indicates that in the standardization of the experiental results lies an important source of error. Several measurements were based on absolute measurements of F for a particular crystal of NaCl, made by James and Firth[7] in 1927. These measurements are not independent of the particular crystal used because of the variation of extinction effects from one crystal to the next, according to James, Brindley and Wood.[8] Consequently measurements standardized by comparison with any other rocksalt crystal may be in error. Another source of uncertainty in the experimental $(F-\Delta F)$ values lies in the preparation of the powders which were used for these experiments. It has been found by Brindley and Spiers[9] for example, that different methods of preparation lead to different results with some materials. Furthermore, the process of packing the powder into briquettes may produce preferred crystal orientation, which would change the experimental results because the orientation is assumed to be random in the calculation of $(F-\Delta F)$ values from the reflection coefficients.

TABLE I. *Δf values calculated from experimental S values.*

ϕ	$(\sin\frac{1}{2}\phi)/\lambda$	S_{EXP}	$(F-\Delta F)_{AV}$	$(f-\Delta f)_{EXP}$	fH	Δf
40°	0.222A^{-1}	2.09	17.50	18.8	20.55	1.75
60°	0.324	2.40	13.55	15.4	17.10	1.70
70°	0.372	2.42	11.95	14.0	15.90	1.90
80°	0.417	2.76	10.60	13.2	14.80	1.60
120°	0.562	1.62	9.00	10.4	12.20	1.80

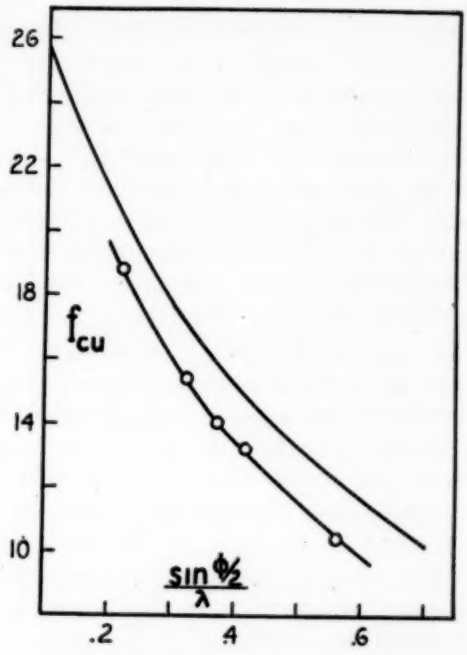

FIG. 1. Atomic structure factors for copper. Upper curve, Hartree theoretical values for $\lambda/\lambda_k \to 0$. Lower curve joins experimental points for $\lambda = 1.54$A.

One of the earliest measurements of copper $(F-\Delta F)$ values using Cu $K\alpha$ radiation was made by Armstrong[10] in 1929. Miss Armstrong used blocks of powdered crystal which had been compressed and then scraped to remove the preferred orientation effect, and standardized her relative values by comparison with the (220) reflection from a NaCl crystal. As mentioned above, this reflection had been calibrated by James and Firth, but with molybdenum $K\alpha$ radiation. She assumed that $(F-\Delta F)$ was independent of wave-length and a function of $(\sin\theta)/\lambda$, and used their absolute value as standard. The powder used was fine enough so that she believed a correction for extinction was unnecessary. In 1930 Wyckoff[11] restandardized the copper (220) reflection and used Armstrong's data to give a new set of $(F-\Delta F)$ values. Rusterholtz[2] used the absolute calibration of aluminum powder by James, Brindley and Wood[8] to standardize his relative measurements on copper using Cu $K\alpha$ radiation. He neglected extinction effects.

[7] R. W. James and Elsie M. Firth, Proc. Roy. Soc. **117**, 62 (1928).
[8] R. W. James, G. W. Brindley, and R. G. Wood, Proc. Roy. Soc. **121**, 154 (1928).
[9] G. W. Brindley and F. W. Spiers, Phil. Mag. **20**, 882 (1935).
[10] A. H. Armstrong, Phys. Rev. **34**, 931 (1929).
[11] R. W. G. Wyckoff, Phys. Rev. **36**, 1116 (1930).

Brindley and Spiers[12] in 1935 published $(F-\Delta F)$ data obtained by measurements made on copper powder which was produced by adding finely powdered zinc to $CuSO_4$ solution. The resulting precipitate was carefully washed, dried, and sieved through a screen of 350 mesh per inch. Microscopic examination showed the particle size to be of the order of 5×10^{-4} cm. The measurements were standardized by comparison with reflections from precipitated KCl. In 1936, however, Brindley [13] recalculated these values on the basis of a standardization employing aluminum powder as standard rather than KCl. Brindley makes his aluminum values "absolute" by fitting them to the theoretical curve at one point. This procedure seems hardly to be justified in the light of the uncertainties mentioned above. At any rate, his new values of f for copper turned out to be about ten percent higher than those previously published.

IV. Experimental Results

In view of the nature of the discrepancies noted, it was judged that an unweighted average of the values obtained by the authors cited above constitute the best set of $(F-\Delta F)$ values available. This average set was consequently used in calculating $(f-\Delta f)$ values from the experimental diffuse scattering (S) values and Eq. (2). Table I shows the experimental values of S, the average $(F-\Delta F)$ values and f values calculated therefrom. Also shown are the atomic structure factors calculated by Hartree's method. The values of Δf shown in the last column are obtained using the Hartree factors as standard. The average value is $\Delta f=1.75$ as compared with $\Delta f=2.8$ from Hönl's theory for $\lambda/\lambda_k=1.12$.

No high degree of accuracy is claimed for the value of Δf obtained, but it is consistent with results from other methods. (See, for example, Fig. 3 of reference 1, which is a plot of results for Δf by various authors.) As shown in Fig. 1 there is no evidence for such a dip in the atomic structure factor curve as was found for zinc. However the experimental difficulties—chiefly low scattered intensity—made it necessary to limit the number of values of $(\sin\theta)/\lambda$ for which the diffuse scattering measurements were made, and additional data would be helpful in proving more conclusively that no such dip exists. The absence of the dip in the curve for a copper crystal adds support to the opinion that the dip in the $\psi=0°$ curve for a zinc crystal is a result of a similar dip in the corresponding f values for zinc.

The author is indebted to Dr. Foster C. Nix of the Bell Telephone Laboratories for furnishing several single crystal copper rods which were used in this experiment, and to Professor G. E. M. Jauncey of this department for his helpful interest in the research.

[12] G. W. Brindley and F. W. Spiers, Phil. Mag. **20**, 865 (1935).
[13] G. W. Brindley, Phil. Mag. **21**, 778 (1936).

Anode Effect as a Function of Temperature

PAUL L. COPELAND
Armour Institute of Technology, Chicago, Illinois
(Received January 9, 1940)

The anode effect has been investigated as a function of temperature first with a diode in which the plate could be separately heated and then with a triode in which a grid maintained at a controlled temperature could be charged by passing an electron current to it. The results indicate: (1) that with the grid at or near room temperature, its surface charge may be high enough to shift its effective contact potential by as much as two or three volts, and (2) that the magnitude of the surface charging decreases rapidly with temperature, being limited to about a tenth of a volt at 600°K, and not being detected at all above 675°K. Time studies for the drift of contact potential were made. It was found that if the contact potential shift was plotted against the logarithm of the time, the resulting graphs were nearly linear. This fact suggests that the drifts involve groups of electrons with different binding forces; so that the effective time constant of the discharge of the surface varies continuously during the history of the drift.

INTRODUCTION

WHEN a relatively high current of low energy electrons (from 0 to 50 electron volts) is incident upon the cold plate of a vacuum tube containing an activated cathode, the contact potential of the plate relative to the cathode is shifted in a negative sense. If the plate current is reduced, there is a drift toward the normal contact potential as measured with low plate current. It is these phenomena, first discussed by W. B. Nottingham,[1] to which we are applying the term "anode effect" as previously proposed.[2] From the outset it was evident that the "decay curve" of the contact potential as a function of the time was not a simple exponential, and Nottingham analyzed his results as the sum of two exponentials, one giving a "mean life" of 200 seconds for the electrons in the trap, and the other giving 5000 seconds. Nottingham[3] also showed that the normal state could be restored rapidly if light were allowed to fall on the anode. Furthermore 100-volt electrons were effective in removing electrons from the surface layer. By the latter means the contact potential could be shifted 0.1 volt or so positive to the normal state. The time then required to return to normal was very long, unless a large current of low energy electrons was supplied from the filament or unless photoelectrons were supplied from the metal of the anode itself. It would seem that very interesting information concerning these effects could be obtained by controlling the temperature of the anode, and the writer has performed a number of such experiments.

For the first experiments of this type the writer[4] built a diode, having a straight tungsten wire for the cathode and a spiral of nickel ribbon for the plate. The spiral could be heated to a controlled temperature by passing a current through it and its temperature determined from its resistance. After insulating layers of organic material had been evaporated from the spiral by heating it to 900°K, no charging effects were noted even though the sensitivity was such that a drift of 0.0001 volt should have been detectable. The pure tungsten filament was replaced by a thoriated tungsten wire. No anode effect was observed until this tube, after heat treatment, had been sealed from the pumps and the filament carried through an activation cycle. Then, if with the spiral cold, the electron current to it were suddenly altered, drifts similar to those studied by Nottingham were observed. As the temperature of the spiral was increased, the magnitude of these contact potential shifts decreased. If the temperature of the anode was as high as 675°K, it was not found possible to detect any drifts by the use of a sensitive galvanometer having a period of about 5 seconds. The results obtained appeared to be quite reproducible for increasing and decreasing anode temperatures. Hence it was concluded that the shifts were due entirely to variations of charge in surface layers, and that the heating of the anode reduced the time which the surface charge remained.

[1] W. B. Nottingham, Phys. Rev. **39**, 183 (1932).
[2] W. B. Nottingham, Phys. Rev. **49**, 78 (1936).
[3] W. B. Nottingham, Phys. Rev. **44**, 311 (1933).
[4] P. L. Copeland, Phys. Rev. **55**, 1145 (1939).

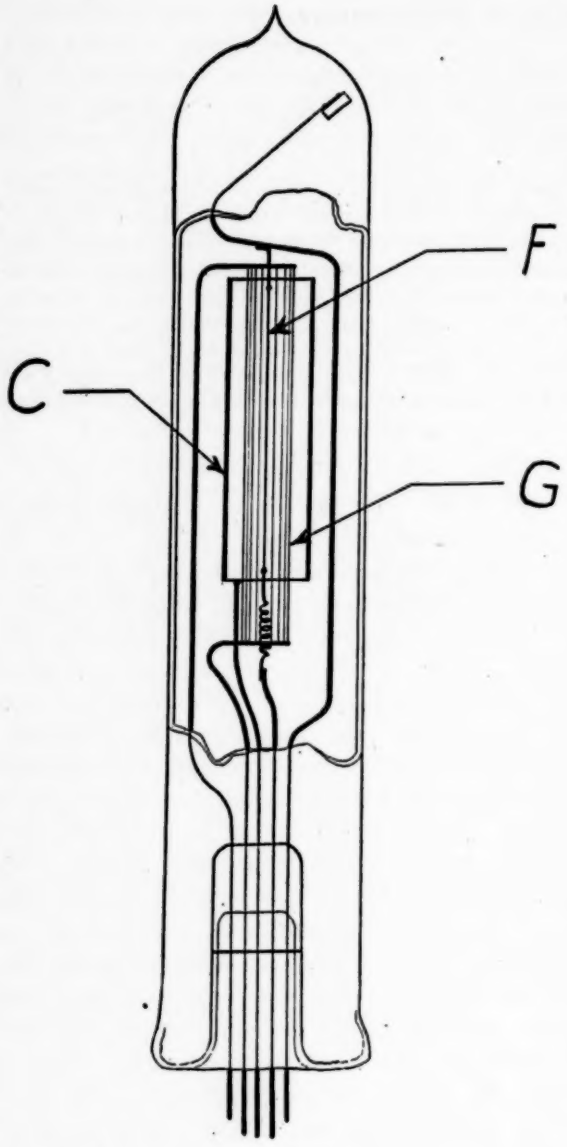

FIG. 1. Details of tube construction.

These results were considered sufficiently reliable to justify a report,[4] but they are not entirely above objection. The metal in the spiral subtends only 70 percent of the surface area about the filament; so that outside effects have some influence. Furthermore there are insulators just beyond the spiral which might become charged, and hence alter the results. The data obtained were not of the desired accuracy, and it was decided to make a triode in which all of these objections could be overcome.

DESCRIPTION OF THE EXPERIMENTAL TRIODE

To secure high sensitivity and other advantages, it was decided to investigate the behavior of the surface charges on the grid of a triode. In one of the tubes constructed, the grid consisted of 13 strands of No. 35 nickel wire (0.0142 cm in diameter). These wires were spaced about equally on the surface of a circular cylinder 1.3 cm in diameter. Fig. 1 shows the details of the construction. At the center of the experimental arrangement we have the filament *F*, which is a 7.2-mil thoriated tungsten wire kept under tension by being doubled and twisted into a spiral at one end. As shown in the drawing, a doubled section of the filament extends well within the grid structure at both ends. The section of the filament emitting appreciable quantities of electrons is a length of about 7 cm lying well inside both the grid and plate structures. The plate, *C*, is a nickel cylinder 10 cm long and 2.8 cm in diameter. All parts are spot-welded directly onto connecting wires and the insulators nearest the experimental region are the glass walls of the envelope. The wire running to the top of the grid structure is of 50-mil tungsten, and the strands of the grid are kept under tension, even when hot, by the natural springiness of this support. Because the expansion of the 13-cm grid wires was quite appreciable at the temperatures required in these experiments and because as the grid expanded the upper ring was pulled off center as well as upward, the symmetry was not perfect under all conditions. An effort was made to secure symmetry under average operating conditions. The tungsten press included one grade of glass between the Pyrex walls and the tungsten wires.

The functions of the parts and the advantages of this design are quite apparent. We may note the following points:

1. The grid can be heated to a controlled temperature by passing a current through it, and its resistance under these conditions can be used as a measure of its temperature.

2. The considerable length of the grid structure is advantageous in two ways. (*a*) As a result of it the electrostatic shielding of the experimental region is very nearly perfect. (*b*) The portion of the grid opposite the emitting part of the fila-

ment is far enough from the supporting rings at the ends to make end effects relatively unimportant in determining the effective grid temperature.

3. The grid, while exerting an electrostatic control on the plate current, can be made sufficiently negative to stop the flow of electrons to it. Under such conditions no electrons are being trapped in the grid, and we are able to measure the true decay curve for the previously acquired charges.

4. The current density to the grid wires may be made high without the necessity of large cathode power.

5. Since the current measurements from which the average contact potential shift of the grid is deduced are made in the plate circuit, the device acts as an amplifier, and precise measurements can be made without great difficulty.

The final stage in the preparation of the tube was its evacuation. It was sealed to the pumping system through two re-entrant type cold traps in series. The evacuation was accomplished by a two stage mercury diffusion pump backed by a Hyvac. During the first 12 hours on the pumping system only the trap nearest the pump was cooled with dry ice. This period was used for the preliminary outgassing of the metal parts. The filament was flashed at 2900°K, and was maintained for 30 minutes at 2600°K. The grid wires were heated to a temperature of 1000°K for one hour. The plate was repeatedly heated by high frequency induction to temperatures in the neighborhood of 1400°K. The heat treatment of the plate was continued over a period of six hours in this way. The processing schedule of the tube for the final day on the pumping system included baking the whole tube in an electric oven maintained at a temperature of 763°K for three hours. During the first part of this baking, only the trap nearest to the pump was cooled; the other trap and the connections leading to it were thoroughly torched. Before the oven was turned off, dry ice and acetone were inserted in the second trap. The filament was again flashed and operated for 15 minutes at 2400°K. The grid was heated to 900°K for 10 minutes. The plate was heated to temperatures ranging between 900°K and 1300°K for 30 minutes. The getter cup was then heated by high frequency induction until it began to give up gas, and was allowed to cool before the pellet had been discharged. This was repeated several times. Following this, the filament was flashed, the grid was heated, and the plate was again heated. The getter was then liberated, and the tube was sealed from the pumps as rapidly as possible. Because of the known photosensitivity[2] of the charges in the anode effect, both ends of the glass bulb were painted with a heavy coat of black Glyptal and the middle section was wrapped in a heavy black cloth for the exclusion of light. After carrying the filament through a complete activation cycle, the triode was ready for the making of observations.

Experimental Procedure and Results

1. Determination of grid charging through amplification factor measurements

The control of the grid potential over the plate current is of an electrostatic nature. A quantitative theory of the voltage amplification in a triode has been developed[5] and has been checked experimentally.[6] In brief we may argue that the emission from the cathode will be a unique function of the off-cathode potential gradient which would be established by the electrode potentials in the absence of space charge. The voltage amplification factor as ordinarily defined will then measure the relative effectiveness of the grid and plate in establishing electric field at the cathode, and it may be computed from electrostatics as the ratio of the cathode-grid partial capacitance to the cathode-plate partial capacitance.

In ordinary practice the voltage amplification is determined as the negative of the ratio of the plate potential increment to the grid potential increment required to maintain constant plate current. Here the method is reversed. Assuming that the amplification factor is a known constant and that changes in the potential of the plate surface can be obtained directly from potentiometer readings, we use our data to determine the actual surface potential of the grid structure as a function of the current to it. The circuit used for this purpose is shown in Fig. 2. The constancy of the cathode emission is determined with great

[5] Max Abraham, Archiv f. Electrotechnik **8**, 42 (1919).
[6] B. V. Vodges and F. R. Elder, Phys. Rev. **24**, 683 (1924).

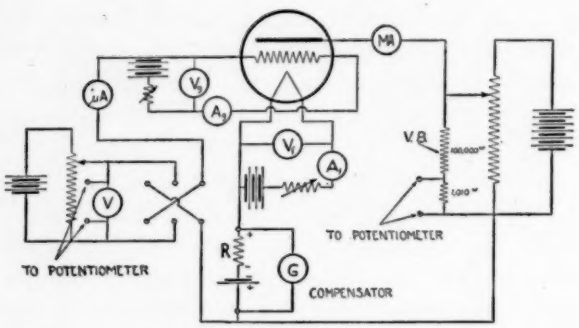

FIG. 2. Diagram of electrical circuit.

accuracy by means of the compensator circuit shown. The resistance, R, is selected so that the desired cathode emission will produce a 2-volt drop in it. This drop is balanced against the electromotive force of a storage cell by means of a sensitive galvanometer. Corresponding plate and grid potentials resulting in the constant cathode emission selected are measured accurately by means of a Leeds and Northrup type K-2 potentiometer. The potential supplied by the potential divider in the grid circuit is measured directly on the potentiometer. One-tenth of the potential difference between the plate and the cathode is taken from a volt box and measured on the potentiometer.

Data obtained in these studies are illustrated in Fig. 3. Here the potentials of the grid relative to the cathode are plotted as abscissas. Along the vertical axis we have plotted both the potential in volts of the plate relative to the negative end of the cathode and also the electron current to the grid in microamperes. In Fig. 3 two sets of data (taken at approximately the same grid temperature) are shown. Experimental points of the one set, obtained at the lower plate potentials, are shown by open circles; experimental points of the other set are shown in solid black. The cathode emission is held constant for either set, but it differs for the two sets.

The grid potential, as indicated at the left-hand side of Fig. 3, was first made sufficiently negative so that no electrons were collected by it. Under these conditions several pairs of plate and grid potentials resulting in the same cathode emission were obtained and these are plotted as separate points in the V_p curves of Fig. 3. It will be noticed that as long as the grid was sufficiently negative so that it collected none of the electrons from the cathode, the amplification factor as determined from the ratio of the plate potential to grid potential increments (i.e., from the slope of the plots of V_p against V_g shown in Fig. 3) is a constant. Furthermore this constant compares favorably with the grid-cathode to plate-cathode capacitance ratio computed from the geometry of the tube.[5]

As the potential of the grid is increased to the point where the grid receives electrons from the cathode, the amplification factor as computed from the ratio of the increments of potential is very definitely decreased. This is shown in Fig. 3 by the fact that the points fall off the straight line determined from the zero grid current region. Because of the accurate constancy of the electron emission of the cathode, we assume that the field produced at the cathode is the same as previously. If we also assume that this field can be computed from the potentials of the electrode surfaces by classical electrostatics,[7] we must then admit that the supplied potentials do not give the

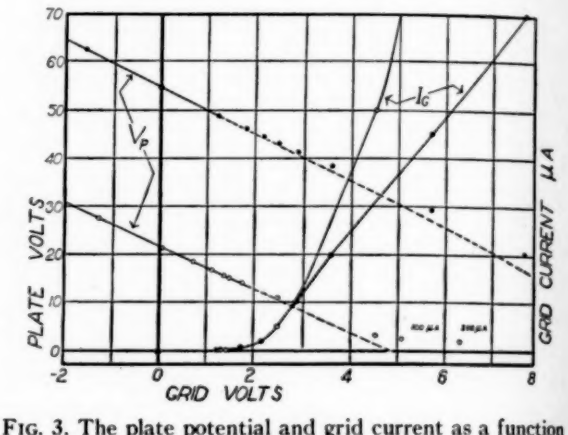

FIG. 3. The plate potential and grid current as a function of grid potential.

[7] Space charge in the neighborhood of the grid wires might alter the results measurably under some circumstances. It is unlikely that this is a major factor in general here. First it should be noticed that the reduction of the potential in the neighborhood of the cathode by the electrons (including those which do not escape through the space charge field) is only a fraction of a volt. The lowering of the potential by space charge in the neighborhood of the grid wires should be only a fraction of this amount unless electrons oscillate about the grid wires for unbelievable times. The influence of space charge in certain doubtful cases, where as a consequence of the supplied potentials, electrons should be expected to oscillate, is a subject deserving further study. The validity of the interpretation presented here is supported on the experimental side by two facts. The first is the similarity of the results obtained at various electrode potentials, and the second is the long continuation of the drifts after the grid has ceased to collect electrons and oscillation about the grid wires is impossible.

surface potentials of the electrodes directly. The surface layers of the electrodes are evidently charged by amounts depending upon the density of the collected currents. For the analysis of the results obtained in this part of the work, we shall make the further tacit assumption that the charging is limited to the grid surface. This is not exactly correct, but because (*a*) the area of the plate is great and the current densities relatively small, (*b*) the variations in plate current are relatively small, (*c*) the plate operates at a potential sufficiently high to make capture of electrons relatively improbable, and (*d*) the voltage amplification factor is fairly large so that small changes in plate potential have relatively small effect on the field in the neighborhood of the cathode, the assumption may be expected to yield fairly accurate information concerning the potential to which the grid surface becomes charged as a result of the current collected by it.

The data represented in Fig. 3 suggests that within the limits of experimental error the shift of contact potential at the grid surface is the same function of the grid current in the two cases. The computed shifts V are listed side by side in Table I for comparison.

Representative data for the contact potential shift as a function of electron current at various temperatures are shown in Fig. 4. Along the axis of abscissas the electron currents to the grid are laid off logarithmically for convenience. The ordinates represent the contact potential shifts, V, of the grid as observed. If the grid is maintained at a temperature as high as 675°K by the passage of a current through it, no contact potential shifts are detected. This checks the result obtained with the diode. With the grid maintained at 600°K, the shifts are detected only for the higher current densities, and the evidence indicates that the shifts are limited to a value only slightly in excess of 0.1 volt. With the grid

TABLE I. *Computed shifts of contact potential.*

Low Plate Potential		High Plate Potential	
Grid Current	V Volts	Grid Current	V Volts
1	0.02	2	0.03
5	0.07	5	0.05
		20	0.15
50	0.43	45	0.37
100	0.84	70	0.60

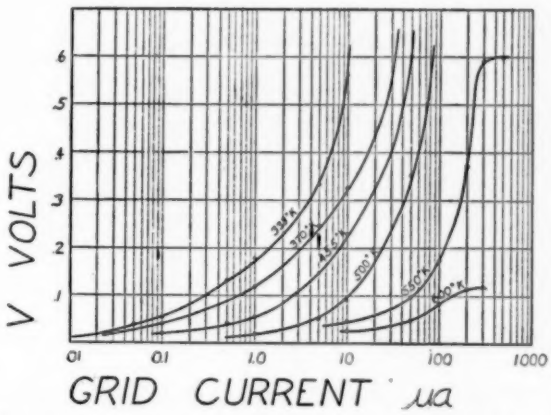

FIG. 4. Representative data for contact potential shift as a function of electron current at various temperatures.

maintained at 550°K, shifts are detected at lower current densities and the shifts observed at high electron current density to the grid are very much larger. With the grid maintained at this temperature, the analysis of the data indicates that shifts larger than 0.6 volt do not occur. For the lower grid temperatures, the evidence indicates that surprisingly large shifts occur. These shifts were followed as high as one or two volts. In general the limit did not appear to have been reached; in order to attain the low grid temperatures, the cathode in the experimental tube had to be operated at temperatures too low to supply the high electron currents required for this purpose.

2. Decay of the contact potential shift with time

When the decay of the contact potential shift was examined after the current to the grid had been cut off, the facts obtained were similar in essential features to those reported by Nottingham.[1] The shifts observed, although high, are not surprising in the light of the results just presented. The temperature dependence of the decay curves is quite informative.

Briefly the procedure used in the experiments was to establish the galvanometer at an electrical zero by an adjustment of the grid potential. The grid potential was then raised to about 10 volts positive for one minute, and during this time a relatively large current flowed to the grid. The grid setting was then returned to its initial value. Change in the contact potential of the grid, due to electrons captured during the period of high

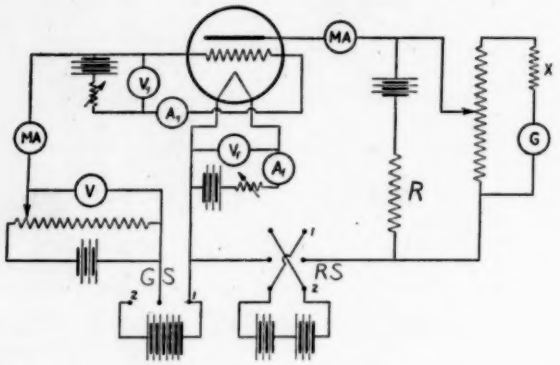

FIG. 5. Electrical circuit used in observations on decay of contact potential shift with time.

current flow to the grid, caused a reduction of the plate current which was read on the sensitive galvanometer. The deflection of the galvanometer decreased with time; at first the change was quite rapid, but as time progressed the galvanometer shifted more and more slowly. The data taken gave the galvanometer deflection as a function of the time.

The circuit used in making the observations is shown in Fig. 5. The experimental tube, in the circle, has been described in detail previously. The batteries shown are all new storage batteries maintained in the best of condition. The voltmeters and ammeters shown are all Weston model 45 instruments of suitable range. The system for the measurement of the plate current changes, used as a measure of the contact potential shifts of the grid, contains a "compensator" which is a storage battery in series with 2 megohms of resistance. The "normal" plate current in the tube is thus of the order of one, two, or three microamperes depending on whether one, two or three cells of the storage battery are used. The indicating instrument is a Leeds and Northrup type R galvanometer having a period of approximately 5 seconds, a sensitivity of about 0.5 microvolt per mm, and a critical damping resistance of about 10,000 ohms. The Aryton shunt, by means of which the galvanometer was connected to the circuit, has a resistance of only 1000 ohms, and the resistance X used to secure critical damping, reduced the effective sensitivity, but the resulting sensitivity was all that could be used conveniently. A type K-2 potentiometer circuit on a portable table was available for the more accurate determination of the heating currents and potential differences whenever this was desired.

A set of observations was started with the grid at its normal contact potential. First the temperature of the grid was brought to the desired value. Then the galvanometer was calibrated as a voltmeter for the measurement of the grid potential through determining the deflection of the galvanometer for several carefully measured grid potentials. This was done by throwing the grid control switch, G. S., to position 1, and determining the galvanometer deflection as a function of the reading of voltmeter, V. The galvanometer was then brought to the "electrical zero" by careful adjustment of the grid bias. Following this the galvanometer was removed from the circuit by turning the Ayrton shunt to the zero position. Next the plate battery reversing switch, R. S., was thrown to position 2. Finally the grid control switch was thrown to position 2. A large electron current was then collected by the grid, but the plate was protected by its negative bias, and the anode effect was thus confined to the grid wires. When the large current had been flowing to the grid for one minute, the grid control switch was returned to position 1, thus stopping the current to it. The decay time was measured from this as zero. On the first second the plate potential reversing switch was thrown back to position 1. On the next second the Ayrton shunt was turned back to full sensitivity. It was usually possible to get a reading of the

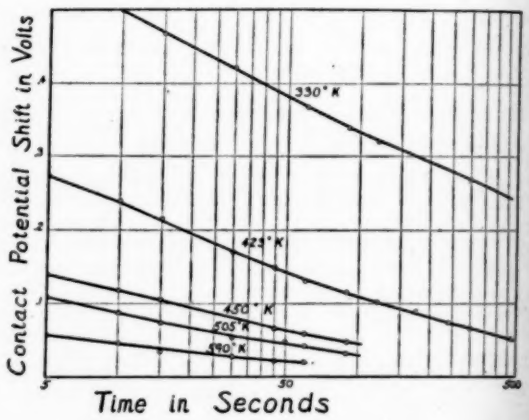

FIG. 6. Variation with time of the contact potential shift for differing grid temperatures.

galvanometer deflection on the fifth second.[8] Readings of galvanometer deflection were then ordinarily taken at 10, 15, 30, 45, 60, 120 seconds, and thereafter as often as the rate of drift appeared to justify.

Representative data obtained in thus following the history of the drifts are shown graphically in Figs. 6, 7, 8, 9 and 10. The initial rate of drift was always quite large and yet the drifts could be followed over long time intervals. It was decided

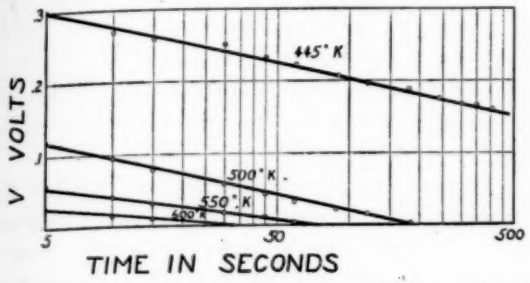

FIG. 7. Contact potential shift as a function of time for differing grid temperatures.

therefore to plot the time as abscissas on a logarithmic scale with 5 seconds as the unit of reference. The ordinates represent contact potential shift, V, in volts relative to the normal. The graphs of the contact potential shift against the logarithm of the time are very nearly linear, although some are curved slightly with the concave side upward. The different curves of Fig. 6 were obtained by changing the temperatures at which the grid was maintained, and these temperatures are shown in the figure beside the corresponding curves. For example, the grid was first maintained at 590°K. Starting with the grid in its normal state (represented by zero on the graph), a current of approximately 0.15 ma was passed to the grid for one minute. Five seconds after this current had been stopped, the surface of the grid was 0.06 volt more negative than it had been in the normal state. After one minute had elapsed, the grid surface was still 0.02 volt negative. When the grid was maintained at 505°K,

[8] The normal period of the shunted galvanometer was 6 seconds. The galvanometer had been in the circuit only half of this time on the fifth second. The device used to make readings possible was simply to set the "electrical zero" so that the "mechanical zero" of the galvanometer corresponded to the expected deflection at the instant the galvanometer was thrown into the circuit. Thus since the galvanometer was at or near its proper deflection when thrown into the circuit, it was only required to follow the drift, and this it did with some reliability.

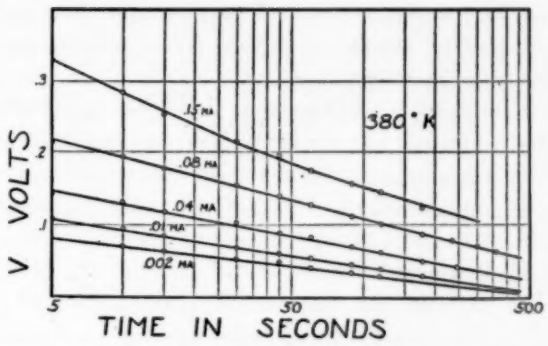

FIG. 8. Variation in contact potential shift with time at a grid temperature of 380°K for varying charging current.

the same treatment resulted in a shift of 0.108 volt as measured at the end of five seconds. For 450°K the result was a 0.14-volt shift, and for 423°K the result was a 0.273-volt shift. In order to lower the temperature of the grid to 333°K, it was found necessary to cut the cathode power from 3.2 watts to 1.47 watts. This resulted in a drop to approximately 0.02 ma for the current used in charging the grid, so that the upper curve of Fig. 6 is not directly comparable with the others, but it is included because it does represent the history of a grid drift at this temperature.

The data plotted in Fig. 7 were similarly obtained, but here the charging current was approximately 0.12 ma in each case.

Figures 8, 9 and 10 represent data taken and plotted similarly. All of the data shown in Fig. 8 were obtained with the grid maintained at 380°K. The different decay curves correspond to the various electron currents used in charging the grid, and these currents are indicated along the

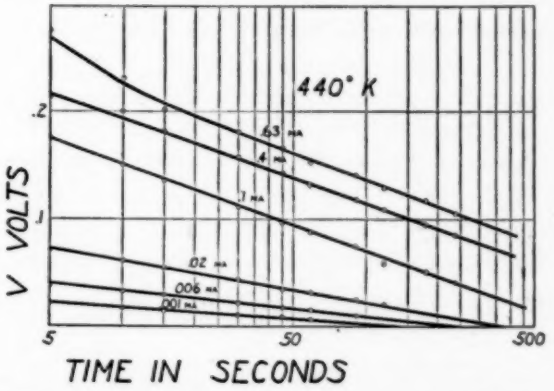

FIG. 9. Variation in contact potential shift with time at a grid temperature of 440°K for varying charging current.

curves. Fig. 9 is a similar set of data obtained with the grid at 440°K, and Fig. 10 represents data obtained at 600°K.

From the data shown, it will be noticed that the potential to which the grid is charged rises very rapidly as a function of the current to it. The charge which the grid retains for a given time decreases rapidly as the temperature of the grid is raised. A comparison of the data shows that we can get substantially the same decay curves at two different temperatures by making the electron current used in charging the grid enough different to compensate for the change in grid temperature. Fig. 11 shows curves selected from Figs. 8, 9, and 10 brought together for comparison. The data obtained with the grid maintained at 440°K and charged by a current of 0.4 ma are almost identical with those obtained with the grid maintained at 380°K and charged by a current of 0.08 ma. Similarly the decay curve obtained by maintaining the grid at 600°K and using 0.3 ma charging current does not differ much from that obtained with the grid at 440°K when only 0.02 ma of charging current is used in the excitation process. Even here there is a suggestion that an increase in temperature causes the decay curves to become slightly steeper, and this is supported by other data not presented here.

Although all of the data presented here were obtained with the single triode whose construction was discussed in detail above, the experiments included work with two diodes, and three triodes. The first triode with a nickel grid gave somewhat less definite results because variations of contact resistance in the grid circuit made precise work difficult. It should be noted, however, that the essential features concerning the dependence of the anode effect upon temperature were checked quantitatively in this tube.

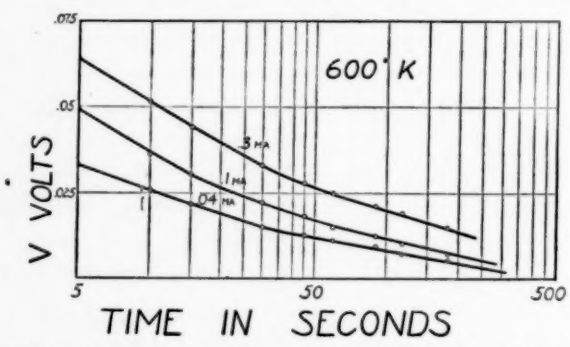

FIG. 10. Variation in contact potential shift with time at a grid temperature of 600°K for varying charging current.

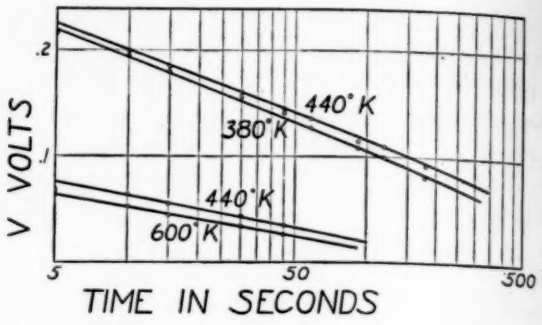

FIG. 11. Curves selected for comparison from Figs. 8, 9 and 10.

The third triode constructed for work of this type had a nickel plate and a grid consisting of eight tungsten wires each 2 mils in diameter equally spaced around supporting rings of essentially the same size and mounted similarly to those in the triode previously described. The heat treatment to which the tungsten grid could be subjected was considerably more severe than for the nickel. It consisted in part of operating the grid at a temperature of 2400°K for half an hour. After the tube had been sealed from the pumps and the thoriated tungsten filament had been carried through an activation cycle, experiments of the types reported above revealed drifts that were very much less pronounced than for the nickel grids. For example with the grid at 350°K a current of 0.35 ma to the grid for one minute produced a decay curve starting at 0.038 volt and drifting to 0.035 volt in four minutes. The semi-logarithmic plots were not so nearly linear, and the curves were generally *concave downward;* the curvature was thus in the opposite sense to that observed for nickel. These data were in general not quantitatively reproducible, and they are not considered as final. Somewhat more definite information was obtained in an effort to determine the temperature at which the films responsible for the anode effect evaporated. When the grid was heated to 1000°K and again cooled, there was no marked change in the phenomena observed in the regular cycles of operation. When, however, the grid was heated to 2400°K and again cooled, no anode effect was observed. No drifts occured even when the cur-

rent was changed very suddenly. Measurements also showed that the amplification factor at high current densities to the grid was the same as at zero grid current. In brief there was no evidence that the surface of a tungsten wire cleaned in this way and not again contaminated, could be charged.

Discussion of the Results

As a consequence of his experience Nottingham[1] proposed an explanation for the shifts of contact potential which he had observed. Originally he visualized a monatomic layer of thorium on the surface of the nickel plate. This resulted in a double potential hump through which electrons had to pass in entering or leaving the metal, and between these two humps was the valley which constituted the trap. Electrons were assumed to escape from the trap by thermionic emission over the potential barrier. Such a picture appears to account for the observed facts fairly well, although the potential barriers originally visualized by Nottingham would hardly be sufficient to justify the magnitude of the potential to which surfaces appear to be charged. Probably a layer of oxygen separates the thorium from the nickel.

It is not possible to outgas nickel as thoroughly as some of the more refractory metals, and the heat treatment of the grid structure in the experimental tube described was not as vigorous as that to which nickel electrodes are often subjected. The reason for this was that the grid wires were under tension, and they parted when raised to temperatures 100°C or so above those used in the outgassing process. All of the grids used, however, were maintained for an hour or so at a cherry red heat. This treatment would be sufficient to eliminate the films of organic matter that form layers with insulating properties which have so often given rise to anomalous results. It is quite likely, however, that the incomplete outgassing of the nickel has much to do with the magnitude of the observed effect. These considerations and the experimental evidence concerning the temperatures at which the films evaporate would tend to confirm the view that the surfaces giving rise to these effects are made up of thorium on oxygen on nickel. The "ionization" of these thorium atoms then accounts for the contact potential shifts. A mechanism such as this would account without difficulty for the order of the shifts observed. Assuming that the separation of the thorium atoms from the metallic base is of the order of 10^{-7} cm and assuming that the surface of the nickel might contain about 10^{15} thorium atoms per sq. cm, the ionization of a few percent of these would be adequate to account for a 1-volt shift.

The temperature dependence of the anode effect as revealed in these studies is very marked. The most noticeable result of increasing the temperature of a surface showing this effect is to reduce the potential to which it is charged by a given current. The variation in the magnitude of the charging is sufficiently rapid to suggest an exponential dependence on temperature, as for example through the thermionic emission of the trapped electrons. In view of the pronounced dependence of the magnitude of the shifts upon temperature, the similarity of the slopes at different temperatures as shown in Fig. 11 is quite striking.

One of the very interesting features of the data obtained with the nickel grids is the approximate linearity of the plots of contact potential shift against the logarithm of the time. Some rather definite conclusions can be drawn from this evidence. In the equilibrium condition, a certain number of the thorium atoms exist as ions. In the excitation process electrons are trapped by these ions and in effect neutralize their charge. The linearity cited must mean that as time progresses, the electrons remaining escape with progressively greater difficulty. If states of various binding energy exist, the approximate linearity of the observed curves can be accounted for on the basis of very simple assumptions concerning the distribution of electrons in these levels. The essential feature of the argument is that if the electrons occupy states of various binding energy, the states of lowest binding energy would be expected to have the most rapid decay. They would become exhausted most rapidly, and then the states of higher binding energy would dominate the situation to give a much lower rate of drift at later times as indicated by the experimental evidence.

The experimental evidence calls unmistakably for some such assumptions. The interpretation which we have suggested indicates that the time

after excitation is in itself one of the important factors in determining the rate of drift. The experimental evidence shown in Figs. 8, 9 and 10 indicates that the surfaces are not always in the same physical state (even at the same temperature) when the contact potential is shifted a certain amount V'. As shown in these figures we may arrive at a certain shift V' in any one of a number of ways—each resulting in a physically distinguishable state. We may, for example, arrive at the contact potential shift V' by exciting the surface with a high current and allowing the drift to continue a long time. In this case, by the time V' is reached, the drift will be very slow. On the other hand, by using a smaller current we may charge the surface to a potential only slightly in excess of V'. In this case V' is soon reached, and the drift is quite rapid in the neighborhood of V'.

The writer has made calculations assuming the existence of several discrete energy levels for the bound electrons in the surface separated by equal energy increments which may be as large as $\frac{1}{2}kT_0$, where k is Boltzmann's constant and T_0 is the temperature of the room on the Kelvin scale. It is then assumed that the rate of escape of the electrons from any level is governed by an exponential relationship of the form which would be expected if the electrons escaped from the given level by thermionic emission. Then if it be assumed that the equally spaced levels contain equal numbers of electrons, the computed decay curves very closely resemble those obtained experimentally.

The computations reveal these features which correspond to the results of experiment.

1. The charge remaining is a linear function of the logarithm of the time after the establishment of the initial condition from the earliest observations at five seconds until the equilibrium condition of the surface is approached.

2. With a fixed charging current, the magnitude of the charge remaining at a definite time after the charging current is shut off decreases rapidly as the temperature is increased.

3. The negative slope of the semi-logarithmic plots increases as the temperature is increased, but the variation of the slope with temperature is not rapid.

Thus while some of the assumptions underlying the computations are somewhat arbitrary in the absence of definite information concerning the surface, the picture probably contains elements of truth.

Conclusion

The nickel surfaces studied showed a large anode effect. The magnitude of the trapped charge decreased rapidly as the temperature of the surface was increased. The evidence indicates that the stability of the trapped electrons varies widely.

The writer has had the privilege of discussing this material with Dr. W. B. Nottingham, Mr. B. J. Thompson, Dr. J. S. Thompson, and Dr. J. A. Eldridge to each of whom he is deeply indebted for his interest and constructive criticism.

High Frequency Behavior of a Space Charge Rotating in a Magnetic Field

JOHN P. BLEWETT AND SIMON RAMO
Research Laboratory and General Engineering Laboratory, General Electric Company, Schenectady, New York
(Received January 17, 1940)

A theoretical discussion is given of the propagation of electromagnetic waves in a space charge which is rotating under the influence of a uniform magnetic field. Equations are derived for the relations between the amplitudes of the electric and magnetic fields, charge density, electron velocities, the applied magnetic field, the frequency, the phase velocities, and the effective dielectric constant of the space charge region. In particular, the natural frequencies are computed for such a space charge rotating about an infinitesimal conductor and enclosed by a coaxial conducting cylinder. The predicted resonant frequencies agree well with experimentally observed values for magnetron oscillators. The theory here developed is also applicable to other devices in which a rotating space charge is utilized.

1. INTRODUCTION

MANY studies have been made of the electromagnetic waves which can propagate through a stationary space charge region. This theory has been extremely useful in studying Heaviside layer characteristics as well as plasma oscillations. More recently there has been occasion to investigate the high frequency behavior of a moving space charge, as, for example, an electron beam.[1,2] The problem has become important because devices utilizing space charge waves have been built to generate and amplify high frequency signals of the order of 1000 megacycles per second.

In this paper a study is made of the high frequency properties of a space charge which is rotating under the influence of an applied uniform magnetic field and a radial electric field. Only the theory will be given here, but applications will be kept in mind in choosing boundary conditions for the determination of natural frequencies of the system. An experimental investigation of several new devices suggested by this theoretical treatment will be reported elsewhere.

A d.c. space charge condition which is theoretically possible and easily obtainable in practice will be selected. High frequency waves of infinitesimal amplitude will then be superimposed upon these d.c. conditions, and the relations between the various components of the waves will be derived. It will be shown that the waves may be considered in general to be of two types, which are characterized by the presence or absence of an axial component of the magnetic field in the wave. The effective dielectric constant of such a space charge to the propagation of electromagnetic waves is given in terms of the applied magnetic field and the frequency.

The natural frequencies of a space charge rotating about an infinitesimal axial conductor and enclosed by a perfectly conducting cylinder are computed and are seen to agree well with experimental data for magnetron oscillators. Large signals are discussed, and a solution to the large signal equations is given for a special case which is believed to be of importance.

2. D.C. SOLUTIONS

It will be shown in this section that the application of an electric field normal to an axis of cylindrical symmetry, together with a uniform magnetic field parallel to that axis, makes possible the existence of a space charge of almost uniform density, which rotates with uniform angular velocity around the axis. Since the system is an accelerated one, an exact solution would involve the equations of general relativity. A very good approximation will be given by the special theory, however, if it is assumed that at any time the electron motion is approximately linear.[3]

The magnetic field experienced by the electrons will be composed of two parts, the uniform applied field, H_0, and the magnetic field, H_1, generated by the motion of the charges. H_1 will vary with radius. The behavior of the space charge will be completely described (in cylindrical

[1] W. C. Hahn, Gen. Elec. Rev. **42**, 258 (1939).
[2] S. Ramo, Phys. Rev. **56**, 276 (1939).
[3] Cf. Page, *Introduction to Theoretical Physics*, Second Edition (Van Nostrand, 1935), p. 526.

coordinates) by the field equations:

$$(\text{curl } H)_\theta = -\frac{\partial H_1}{\partial r} = \frac{r\dot{\theta}}{c}\rho_0, \tag{1}$$

$$\text{div } E = \frac{1}{r}\frac{\partial}{\partial r}(rE_0) = \rho_0 \tag{2}$$

and the force equations:

$$\frac{m_0}{\beta}(\ddot{r} - r\dot{\theta}^2) = eE_0 + \frac{er\dot{\theta}}{c}(H_0 + H_1), \tag{3}$$

$$\frac{1}{r}\frac{d}{dt}\left(\frac{m_0}{\beta}r^2\dot{\theta}\right) = -e\dot{r}(H_0 + H_1), \tag{4}$$

where E_0 is the radial electric field, ρ_0 is the charge density, e is the charge on the electron, m_0 is the rest mass of the electron and $\beta^2 = 1 - v^2/c^2$. (Rational units will be used throughout this paper.) These equations are satisfied by the solution:[4] (if we neglect terms of the order of $r^4\Omega_0^4/c^4$ compared with unity)

$$\dot{r} = 0; \quad \dot{\theta} = \frac{-eH_0}{2m_0c} = \Omega_0, \text{ say}; \quad \rho_0 = \frac{2m_0\Omega_0^2}{e\beta^2}; \qquad E_0 = \frac{eH_0^2 r}{4m_0c^2\beta}; \quad \beta^2 = 1 - \frac{r^2\Omega_0^2}{c^2}. \tag{5}$$

It is worthy of note that the action of the field due to the charges, and the relativistic increase in mass with velocity, have equal and opposite effects on the angular velocity, whose final value is independent of radius.

A more general solution exists in which $\dot{r} \neq 0$. In this paper, however, we shall concern ourselves only with a space charge whose behavior is described by Eqs. (5). Devices may obviously be constructed to maintain such a space charge. A common example may be the magnetron operated at or above cut-off. The authors have had the privilege of reading an unpublished discussion by L. Brillouin, which lends support to this viewpoint.

3. A.C. Solutions

Let a space charge exist having infinite extent in the z direction and subject to the conditions given in Eqs. (5). It will now be our purpose to investigate the possible oscillations in this space charge and the associated fields.

[4] This solution was obtained for the nonrelativistic case by A. W. Hull, Phys. Rev. **23**, 112 (1924).

From this point on we shall give a nonrelativistic treatment, since relativistic corrections add considerably to the complexity of the equations. Hence, in substituting from the d.c. solutions, we shall set $\beta =$ unity.

The a.c. velocities, charge density, and fields must satisfy the field equations:

$$\text{curl } H = \frac{1}{c}\frac{\partial E}{\partial t} + \frac{\rho v}{c}, \tag{6}$$

$$\text{curl } E = -\frac{1}{c}\frac{\partial H}{\partial t}, \tag{7}$$

$$\text{div } E = \rho \tag{8}$$

and the force equations:

$$\frac{d}{dt}(mv) = eE + \frac{e(v \times H)}{c}. \tag{9}$$

In this section we shall deal with a small signal only, assuming that the alternating parts of fields, velocities, and charge density are small compared with the steady parts where these exist. It is thus possible to neglect products of two or more a.c. terms, and the equations become linear. The a.c. part of the expression for field, velocity, or charge density will be assumed to have the form

$$X(r)e^{i(\omega t + n\theta + \gamma z)},$$

where ω represents 2π times the frequency of oscillation, n is the order of the wave, i.e., the number of complete waves around the circumference of a circle whose axis is the axis of symmetry; and γ is the propagation constant in the z direction. Such a wave travels with phase velocities $-\omega/n$ in the azimuthal direction and $-\omega/\gamma$ in the z direction.

Equations (9) for the a.c. velocities reduce to the form:

$$\rho_0 v_r = -\frac{2i\Omega_0^2}{\alpha}\left(E_r + \frac{r\Omega_0}{c}H_z\right), \tag{10}$$

$$\rho_0 v_\theta = -\frac{2i\Omega_0^2}{\alpha}E_\theta, \tag{11}$$

$$\rho_0 v_z = -\frac{2i\Omega_0^2}{\alpha}\left(E_z - \frac{r\Omega_0}{c}H_r\right), \tag{12}$$

where

$$\alpha = \frac{d}{dt} = \frac{\partial}{\partial t} + \dot{\theta}\frac{\partial}{\partial \theta} = \omega + n\Omega_0.$$

Thus α represents n times the difference between

the azimuthal phase velocity of the wave, and the angular velocity of the electrons.

Substituting the values of a.c. charge density and velocity given by Eqs. (8), (10), (11), and (12) in Eqs. (6) and (7), we are left with the following six equations.

$$crE_r(\omega\alpha-2\Omega_0^2)+\alpha c^2\gamma rH_\theta-H_z(n\alpha c^2+[2r^2\Omega_0^3])=0, \tag{13}$$

$$\alpha\Omega_0\frac{\partial}{\partial r}(rE_r)+iE_\theta(\alpha^2-2\Omega_0^2)+i\gamma\alpha r\Omega_0E_z-i\gamma\alpha cH_r+\alpha c\frac{\partial H_z}{\partial r}=0, \tag{14}$$

$$icrE_z(\omega\alpha-2\Omega_0^2)+iH_r(n\alpha c^2+[2r^2\Omega_0^3])-\alpha c^2\frac{\partial}{\partial r}(rH_\theta)=0, \tag{15}$$

$$i\gamma E_\theta-\frac{in}{r}E_z-\frac{i\omega}{c}H_r=0, \tag{16}$$

$$\gamma E_r+i\frac{\partial E_z}{\partial r}+\frac{\omega}{c}H_\theta=0, \tag{17}$$

$$\frac{n}{r}E_r+\frac{i}{r}\frac{\partial}{\partial r}(rE_\theta)-\frac{\omega}{c}H_z=0, \tag{18}$$

where $E_re^{i(\omega t+n\theta+\gamma z)}$, etc., are the a.c. field components.

These equations can easily be reduced to two second-order partial differential equations in two of the variables. For instance, we may choose E_θ and H_θ. Eqs. (13) and (18) give E_r and H_z, and Eqs. (15) and (16) give H_r and E_z in terms of these variables. Substituting in Eqs. (14) and (17), we obtain two second-order partial differential equations, both involving E_θ and H_θ. Mathematically, four solutions should exist for these two equations. We shall find, however, that the solutions are Bessel functions of either the first or second kind, or their derivatives. Physically, this means that there are only two solutions, which differ from each other in form. Each of these two solutions will include either the term $AJ+BN$ or $A(\partial J/\partial r)+B(\partial N/\partial r)$, where J and N represent the Bessel functions of the first and second kind, and A and B are arbitrary multipliers. One of the solutions is easily seen from the form of the final second-order differential equations to be:

$$\begin{aligned}
E_r&=-\frac{\alpha\gamma c^2}{\omega}\left\{A_1\frac{\partial}{\partial r}[J_n(Dr)]+B_1\frac{\partial}{\partial r}[N_n(Dr)]\right\},\\
iE_\theta&=\frac{\alpha\gamma nc^2}{\omega r}[A_1J_n(Dr)+B_1N_n(Dr)],\\
iE_z&=-\left(\omega\alpha-2\Omega_0^2-\frac{\alpha c^2\gamma^2}{\omega}\right)[A_1J_n(Dr)+B_1N_n(Dr)],\\
iH_r&=\frac{nc}{r\omega}(\omega\alpha-2\Omega_0^2)[A_1J_n(Dr)+B_1N_n(Dr)],\\
H_\theta&=\frac{c}{\omega}(\omega\alpha-2\Omega_0^2)\left\{A_1\frac{\partial}{\partial r}[J_n(Dr)]+B_1\frac{\partial}{\partial r}[N_n(Dr)]\right\},\\
H_z&=0,
\end{aligned} \tag{19}$$

where $D^2=\omega^2/c^2-2\Omega_0^2/c^2-\gamma^2$; A_1 and B_1 are arbitrary constants; J_n and N_n represent the Bessel functions of the first and second kind and of the nth order. The a.c. charge density and velocity components follow from Eqs. (8)–(12).

This solution will be referred to as solution I and evidently corresponds to the "E wave" of the wave guide[5] since $H_z=0$.

[5] Cf. J. R. Carson, S. P. Mead and S. A. Schelkunoff, Bell Sys. Tech. J. **15**, 310 (1936).

Comparison of Carson, Mead and Schelkunoff's[5] solution for the "E type" wave in a medium of dielectric constant, ϵ, with our solution I reveals the fact that for $n=0$ the rotating space charge behaves as though it were a dielectric of dielectric constant

$$\epsilon=1-2\Omega_0^2/\omega^2=1-e\rho_0/m$$

from Eqs. (5). This is the same expression as is obtained for the effective dielectric constant of a plasma in which the electron density is ρ_0.[6] Evidently, as far as the propagation of symmetrical ($n=0$) "E type" waves is concerned, it is immaterial whether the uniform concentration of electrons is maintained by the agency of a positive ion space charge, or by crossed electric and magnetic fields.

The other solution is less easily obtained since its form depends on whether or not $\alpha^2=2\Omega_0^2$.

Suppose first that $\alpha^2\neq 2\Omega_0^2$ so that the term $2r^2\Omega_0^4/c^2$ is small compared with $\alpha^2-2\Omega_0^2$. The simplest procedure for obtaining solution II is to assume that those terms of solution I which involved $J_n(Dr)$ now involve $(\partial/\partial r)[J_n(Dr)]$ and vice versa, and then to evaluate the coefficients. This gives for solution II:

$$E_r=\frac{(n\alpha c^2+2r^2\Omega_0^3)(\omega\alpha-2\Omega_0^2)-2r^2\Omega_0^3c^2\gamma^2}{rc(\alpha^2-2\Omega_0^2+2r^2\Omega_0^4/c^2)}[A_2J_n(Dr)+B_2N_n(Dr)],$$

$$iE_\theta=-\frac{\alpha c(\omega\alpha-2\Omega_0^2)}{\alpha^2-2\Omega_0^2}\left\{A_2\frac{\partial}{\partial r}[J_n(Dr)]+B_2\frac{\partial}{\partial r}[N_n(Dr)]\right\},$$

$$iE_z=\frac{2\gamma\Omega_0^3cr}{\alpha^2-2\Omega_0^2}\left\{A_2\frac{\partial}{\partial r}[J_n(Dr)]+B_2\frac{\partial}{\partial r}[N_n(Dr)]\right\},$$

$$iH_r=-\gamma c^2\left\{A_2\frac{\partial}{\partial r}[J_n(Dr)]+B_2\frac{\partial}{\partial r}[N_n(Dr)]\right\}, \tag{20}$$

$$H_\theta=-\frac{\gamma nc^2}{r}[A_2J_n(Dr)+B_2N_n(Dr)],$$

$$H_z=\frac{(\omega\alpha-2\Omega_0^2)^2-c^2\gamma^2(\alpha^2-2\Omega_0^2)}{\alpha^2-2\Omega_0^2+2r^2\Omega_0^4/c^2}\left[A_2J_n(Dr)+B_2N_n(Dr)\right],$$

where D^2 is defined as in Eqs. (19) and A_2 and B_2 are arbitrary constants.

This is the analog of the "H wave" in the wave guide although in the presence of the rotating space charge E_z does not disappear. Under most conditions it is small, however, compared with the other field components. Had we neglected the terms in square brackets in Eqs. (13) and (15), a procedure which is justifiable under some conditions, we should have obtained a form of solution II in which E_z is actually zero.

If $\alpha^2=2\Omega_0^2$ the problem becomes complicated and the general form of solution II has not yet been deduced. Solution II is easily obtained for a two-dimensional wave ($\gamma=0$) however. It is as follows:

$$E_r=A_3(nc^2+r^2\alpha\Omega_0)/n\Omega_0cr^3,$$
$$iE_\theta=A_3nc/2r^3\Omega_0[1-(2r^2\Omega_0^2/c^2)\ln r]+B_3/r, \tag{21}$$
$$H_z=A_3/r^2;\quad E_z=H_r=H_\theta=0,$$

where A_3 and B_3 are arbitrary constants. The case of $\alpha=0$ is of particular interest since it represents a wave which travels with the same angular velocity as do the electrons. When $\alpha=0$, the Eqs. (13)–(18) reduce to four equations:

$$E_\theta=0, \tag{22}$$

$$E_r=-r\Omega_0H_z/c, \tag{23}$$

$$E_z=r\Omega_0H_r/c, \tag{24}$$

$$\text{div } H=0. \tag{25}$$

The problem is indeterminate since three equations, (23), (24) and (25) describe five

[6] L. Tonks, Phys. Rev. **37**, 1458 (1931).

variables, E_r, E_z, H_r, H_θ, and H_z. The a.c. components of electron velocity are also indeterminate, having the form 0/0. Although solutions I and II are still correct they are no longer unique. As will be shown in the next section, the condition $\alpha=0$ is one under which oscillation is generally possible.

4. Application of Boundary Conditions

It will be assumed that the rotating space charge is maintained between two perfectly conducting coaxial cylinders. A region of free space may, if it is desired, intervene between the space charge and either or both cylinders. It is then necessary to discover the conditions under which the electric fields E_θ and E_z are zero at the surface of the boundaries. If a relation between frequency and electron velocity exists which satisfies these conditions, oscillations of the type which has been postulated are possible.

The simplest case is that for which the inner boundary is infinitesimal in radius compared with the outer boundary. This corresponds in geometry to tubes of the magnetron type, except that end effects have been avoided by assuming the tube to be infinitely long. Since the N functions become infinite at the origin, their coefficients B_1 and B_2 in the two solutions must both be zero, and the solution includes only Bessel functions of the first kind. Suppose first that the space charge fills the whole region inside the outer conductor. Let the radius of the outer conductor be R. For $r=R$, E_θ and E_z are given (if $\alpha^2\neq 2\Omega_0^2$) by combining Eqs. (19) and (20):

$$iE_\theta=A_1\frac{\alpha\gamma nc^2}{\omega R}J_n(DR)-A_2\frac{\alpha c(\omega\alpha-2\Omega_0^2)}{\alpha^2-2\Omega_0^2}\frac{\partial}{\partial r}[J_n(DR)], \tag{26}$$

$$iE_z=-A_1\left(\omega\alpha-2\Omega_0^2-\frac{\alpha c^2\gamma^2}{\omega}\right)J_n(DR)+A_2\frac{2\gamma\Omega_0^3 cr}{\alpha^2-2\Omega_0^2}\frac{\partial}{\partial r}[J_n(DR)]. \tag{27}$$

The condition $E_\theta=E_z=0$ can be satisfied in several ways, three of which are not trivial. Two of these solutions are:

$$\begin{aligned} A_2&=0 \quad \text{and} \quad DR=T_n \\ A_1&=0 \quad \text{and} \quad DR=T_n', \end{aligned} \tag{28}$$

where T_n and T_n' represent roots of J_n and J_n' respectively. These conditions limit the range of oscillation to very high frequencies. The first condition requires that DR be not less than 2.4, the first root of J_0, since for $n>0$, T_n is >2.4. The only positive term in D^2 is ω^2/c^2. Hence we must have $\omega R/c>2.4$. If we assume a radius R of 1 cm, the frequency must be greater than 11,000 megacycles. The second condition requires that DR be not less than 1.8, the first root of J', since for $n\neq 1$, T_n' is >1.8. Hence $\omega R/c>1.8$ and if $R=1$ cm, the frequency must be greater than 8500 megacycles. This type of solution will not be discussed further.

The third condition which makes $E_\theta=E_z=0$ from Eqs. (26) and (27) is $\alpha=0$, A_1 and A_2 being such that the right-hand side of Eq. (27) vanishes. Since A_1 and A_2 are arbitrary, it is evident that for any value of R an oscillation can always take place whose frequency is given by

$$\omega=-n\Omega_0=neH_0/2mc. \tag{29}$$

This relation is more familiar in the form

$$\lambda H_0=21{,}400/n, \tag{30}$$

where λ = wave-length in cm and H_0 = applied magnetic field in gauss.

If $\alpha^2=2\Omega_0^2$, $\gamma=0$, E_θ and E_z are obtained by combining Eqs. (19) and (21). For $r=R$,

$$\begin{aligned} iE_\theta&=\frac{A_3nc}{2R^2\Omega_0}\left(1-\frac{2R^2\Omega_0^2}{c^2}\ln R\right)+\frac{B_3}{R}, \\ iE_z&=-A_1(\omega\alpha-2\Omega_0^2)J_n(DR). \end{aligned} \tag{31}$$

Since A_1, A_3 and B_3 are arbitrary, E_θ and E_z can be made zero for any value of R by setting $A_1=0$ and choosing values of A_3 and B_3 such that the expression for E_θ vanishes. Thus $\alpha^2=2\Omega_0^2$ is also a possible condition for oscillation. In terms of wave-length and magnetic field this expression becomes:

$$\begin{aligned} \lambda H_0&=51{,}700 \ (n=+1) \\ &\quad\ 15{,}100 \ (n=0) \\ &\quad\ 8880 \ (n=-1) \\ &\quad\ 6280 \text{ or } 36{,}500 \ (n=-2) \\ &\quad\ 4850 \text{ or } 13{,}500 \ (n=-3), \text{ etc.} \end{aligned} \tag{32}$$

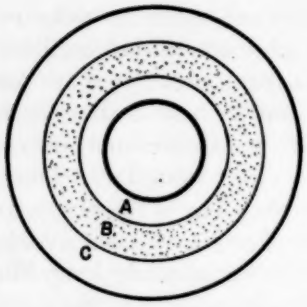

FIG. 1.

It is of interest to note that observed oscillation frequencies of the magnetron operating with space charge limited current in the so-called "electronic oscillation" mode in general satisfy relations of the form $\lambda H = \text{constant}$. A particularly common value of this constant is about 15,000,[7] which would correspond to the $n=0$ wave (Eq. (32)). Other values of the constant which satisfy Eqs. (30) and (32) for low values of n have also been observed.

If, instead of filling the whole space inside the outer conductor, the space charge is confined within a cylinder of radius $R_2 < R_1$, a solution must be obtained for the region of free space between the space charge and the outer conductor of radius R_1. The field equations which must be solved are, of course, Maxwell's equations for free space:

$$\text{curl}\, H = i\omega E/c$$
$$\text{curl}\, E = -i\omega H/c.$$

The solutions of the equations in cylindrical coordinates are well known and can be applied directly. Since the region under consideration does not include the origin, the solution will involve Bessel functions of both the first and second kind. The free space solution must then satisfy $E_\theta = E_z = 0$ for $r = R_1$ and must match the space charge solution at $r = R_2$. A difficulty arises because R_1 is actually a function of θ and t during oscillation. A method for handling such a boundary condition will be found in a paper by W. C. Hahn.[1]

The case in which the inner conductor has a finite radius requires a still more complex treatment, since the N functions can no longer be rejected in any solution. Fig. 1 represents the most general case. Solutions for free space must be set up for the regions A and C and must satisfy the conditions $E_\theta = E_z = 0$ at both the inner and the outer conductors, and must in addition be fitted to the space charge solutions at the boundaries between A and B and between B and C.

[7] E. C. S. Megaw, J. I.E.E. **72**, 330 (1933); C. W. Rice, Gen. Elec. Rev. **39**, 363 (1936).

5. Oscillations of Large Amplitude; a Special Case

The general solution for an oscillation whose amplitude can no longer be considered small compared with the d.c. quantities will be extremely complex, since it involves cross products which make contribution to the d.c. terms. A particular solution whose amplitude is not limited is obtainable, however. Eqs. (6) and (9) which are the only equations in which cross products of a.c. terms appear, can be restored to linear forms if all three a.c. components of velocity are always zero. The d.c. parts of the equations are then the same as before, and the d.c. solution can be carried over from the small signal case. A necessary condition for the disappearance of the velocities is found to be $\alpha = 0$. The situation is not the same as in the $\alpha = 0$ case described in the previous section, since the velocities are no longer indeterminate. Hence it is possible in this case to obtain a solution for the fields. It is:

$$\begin{aligned}
E_r &= \frac{r\omega\gamma}{c}[A_4 J_n(Dr) + B_4 N_n(Dr)], \\
E_\theta &= 0, \\
iE_z &= -\frac{r\omega}{c}\left\{A_4 \frac{\partial}{\partial r}[J_n(Dr)] + B_4 \frac{\partial}{\partial r}[N_n(Dr)]\right\}, \\
iH_r &= n\left\{A_4 \frac{\partial}{\partial r}[J_n(Dr)] + B_4 \frac{\partial}{\partial r}[N_n(Dr)]\right\}, \\
H_\theta &= \frac{n^2}{r}[A_4 J_n(Dr) + B_4 N_n(Dr)], \\
H_z &= n\gamma[A_4 J_n(Dr) + B_4 N_n(Dr)],
\end{aligned} \tag{33}$$

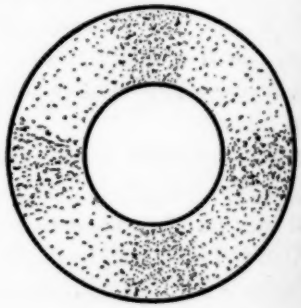

FIG. 2.

where D^2 is defined as in Eq. (19) and A_4 and B_4 are arbitrary constants.

This solution represents a state of the rotating space charge in which "spokes" of increased density maintain a fixed position relative to a coordinate system rotating with angular velocity Ω_0. Fig. 2 is intended to represent this state of affairs. The a.c. at any point is then due only to changes in charge density and not at all to changes in electron velocity.

6. Discussion

We have assumed throughout that the boundaries are perfectly conducting and that electrons travel in circles around the axis so that no current flows from the inner to the outer conductor. Thus no d.c. power is being fed into the system, and we cannot expect to make any estimates of a.c. power output. This is also evident from the fact that currents and voltages calculated from our solutions are always $\pi/2$ out of phase. For the same reason it is impossible to estimate the resistance which a tube will present to an a.c. signal. This situation could be remedied by introducing a small d.c. radial velocity, but this increases the complexity of the a.c. equations so that they are quite unmanageable by our present technique.

It is a pleasure to acknowledge our indebtedness to Mr. W. C. Hahn for many stimulating discussions and suggestions.

APRIL 1, 1940 PHYSICAL REVIEW VOLUME 57

On the Problem of Degeneracy in Quantum Mechanics

J. M. Jauch and E. L. Hill
Department of Physics, University of Minnesota, Minneapolis, Minnesota
(Received January 25, 1940)

The problem of degeneracy in quantum mechanics is related to the existence of groups of contact transformations under which the Hamiltonian is invariant. The correspondence between transformations in classical and quantum theories is developed. The Fock-Bargmann treatment of the symmetry group of the hydrogenic atom comes under this theory. The symmetry group of the 2-dimensional Kepler problem is found to be the 3-dimensional rotation group; that of the n-dimensional isotropic oscillator is isomorphic to the unimodular unitary group in n dimensions. The 2-dimensional anisotropic oscillator has the same symmetry as the isotropic oscillator in classical mechanics, but the quantum-mechanical problem presents complications which leave its symmetry group in doubt.

Introduction

In the study of quantum-mechanical problems the question of the degeneracy of the energy levels plays an important role. It is often the case that this degeneracy is associated with simple symmetry properties of the Schrödinger equation, and considerable attention has been paid to the symmetry conditions associated with the rotation-reflection group and the group of permutations of identical particles.[1]

On the other hand, certain problems possess symmetry properties of more subtle types. It was shown by Fock[2] some years ago that the Schrödinger equation for the hydrogen atom actually has the symmetry of the 4-dimensional rotation group for the bound states, and the symmetry of the Lorentz group for the positive energy states. The degeneracy of the system with respect to the quantum number l is due to the invariance under these wider groups, of which the 3-dimensional rotations form a sub-group. This interpretation was verified and extended by Bargmann,[3] who showed the formal relationship of the Lenz-Pauli integrals with these groups. In spite of the satisfactory way in which these considerations clarified the hydrogen atom problem, they seem peculiar to this case, and it is not clear at once whether they can be extended to other examples.

[1] E. g., E. Wigner, *Gruppentheorie und ihre Anwendung auf die Quantenmechanik der Atomspektren* (Vieweg & Sohn, 1931).
[2] V. Fock, Zeits. f. Physik **98**, 145 (1935).
[3] V. Bargmann, Zeits. f. Physik **99**, 578 (1936).

In this paper we wish to develop further the relation between general contact-transformation theory and the problem of degeneracy. We shall show that in certain cases at least, including the hydrogen atom, the degeneracy arises from the invariance of the Hamiltonian under a group of contact-transformations. These more general *dynamical* groups, involving simultaneous transformations on the coordinates and momenta, contain as sub-groups the usual *geometrical* groups based on point transformations of the coordinates. It remains unclear whether all cases of degeneracy can be explained in this way, and we shall discuss one case (2-dimensional anisotropic oscillator) which presents complications, and is unsolved as yet from this point of view.

It should be remarked that degeneracies can arise from finite groups of discrete transformations as well as from continuous groups. Such is the case, for example, with the permutations on identical particles, the Kramers spin-doubling,[4] the doubling of the energy levels in the Dirac theory of the hydrogen atom, etc. These are characterized by the constant number of degenerate components for the various levels. We shall restrict ourselves here to continuous groups possessing infinitesimal elements.

Continuous Groups of Contact-Transformations in Classical Mechanics

We shall base our discussion of the quantum-mechanical theory on the corresponding classical problem. As a preliminary we give a brief statement of the classical theory.[5]

In the transformation theory of classical dynamics attention is focused on the existence of integrals of the equations of motion of the form

$$F(q_1, \cdots, q_n; \quad p_1, \cdots, p_n) = \text{const.}, \quad (1)$$

where the q's and p's are the coordinates and conjugate momenta of the system. We restrict ourselves to problems in which the integrals are not explicit functions of the time t.

Having such an integral we define an infinitesimal contact-transformation

$$Q_k = q_k + \delta q_k; \qquad P_k = p_k + \delta p_k, \quad (2)$$

where

$$\delta q_k = \epsilon(F, q_k); \qquad \delta p_k = \epsilon(F, p_k). \quad (3)$$

The symbol (A, B) designates the Poisson-bracket

$$(A, B) = \sum\left(\frac{\partial A}{\partial q_k}\frac{\partial B}{\partial p_k} - \frac{\partial A}{\partial p_k}\frac{\partial B}{\partial q_k}\right)$$

and ϵ is the parameter of the transformation. Such a transformation takes one orbit in phase space (coordinates q, p) into an infinitely near orbit lying on the same energy surface.[6]

Suppose now that we have found a set of independent integrals $F_1, F_2, \cdots, F_r$. Each of these integrals can be used to generate a one-parameter group of contact-transformations by the above procedure. It follows from the Lie theory of continuous transformation groups that these transformations will form a group if the set of integrals satisfy conditions of the form[7]

$$(F_k, F_m) = \sum C_{km}{}^{g} F_g, \quad (4)$$

where the coefficients $C_{km}{}^{g}$ are constants, or are at most functions of the total energy. The problem of finding the continuous groups of symmetry transformations of a given dynamical problem is thus reduced to the search for integrals by means of which one can specify the infinitesimal elements of the group. For our purpose it is not necessary to find the finite transformations of the group.

Continuous Groups of Contact-Transformations in Quantum Mechanics

The general procedure for adapting these considerations to quantum-mechanical theory is known, but certain necessary alterations must be made.[8] The integrals must be represented by

[4] H. A. Kramers, Proc. Amsterdam Acad. **33**, 959 (1930). E. Wigner, *Göttingen Nachrichten, Mathematisch-Physikalische Klasse* (1932), p. 546.

[5] Cf., E. T. Whittaker, *Analytical Dynamics* (Cambridge Press, third edition), Chapters 10, 11, 12.

[6] Reference 5, Section 144.

[7] S. Lie and F. Engel, *Theorie der Transformationsgruppen* (Teubner). G. Vivanti, *Leçons élémentaires sur la Theorie des Groupes de Transformations* (Gauthier-Villars, Paris, 1904). L. P. Eisenhart, *Continuous Groups of Transformations* (Princeton University Press, 1933).

[8] For the quantum-mechanical transformation theory see P. A. M. Dirac, *Quantum Mechanics* (Oxford Press, second edition, 1935), or E. C. Kemble, *Fundamental Principles of Quantum Mechanics* (McGraw-Hill, New York, 1937).

Hermitian operators, so that it may be necessary to symmetrize them in the p's and q's. In our actual examples we use the Cartesian coordinates and momenta as usual, but we suppose here merely that they obey the ordinary commutation rules. The integral property of the F's is expressed by their commutation with the Hamiltonian.

The transition to quantum mechanics is based on the correspondence

$$\text{Poisson-bracket} \rightarrow (1/i\hbar)\ \text{commutator}.$$

For our purposes we require this correspondence to be an algebraic equivalence such that the commutators of the F operators satisfy the operator relations

$$[F_k, F_m] = i\hbar \sum C_{km}{}^{g} F_g. \tag{5}$$

Here the C's must be constants, or at most operators depending on the Hamiltonian alone. Although in principle they need not be the coefficients appearing in Eq. (4), it is to be anticipated that they will be the same.

The formal proof that the operators satisfying Eq. (5) define a group of transformations (in Hilbert space) is easily supplied, and will not be given here. From a formal point of view the finite transformations of the group can be considered to be generated by the unitary operators

$$U(\lambda_1, \cdots, \lambda_r) = e^{i(\lambda_1 F_1 + \cdots + \lambda_r F_r)}, \tag{6}$$

the λ's being the finite parameters of the group.

The further statement of our problem is now identical with that employed in the study of the geometrical groups. The matrices for the operators of Eq. (6) form a unitary representation of the group with the eigenfunctions of each energy level as basis. We shall suppose each of these representations irreducible. In our examples the irreducibility has been proved by direct computation of the matrices. The degree of each representation is the degree of degeneracy of the energy level in question. Naturally all possible unitary representations of the group in question may not occur in a given problem, due primarily to secondary restrictions which are placed on the allowable eigenfunctions; i.e., single-valuedness, quadratic integrability, etc.

Before passing to the discussion of the examples, a few further remarks on the preceding theory seem called for. As we have developed it, the procedure is frankly exploratory, and arises directly out of the well-known similarities between classical and quantum dynamics. The essential point is to find suitable integral operators satisfying Eq. (5), and it is here that the classical theory furnishes valuable guidance. When the classical integrals fail to go over properly into quantum operators the method fails (e.g., 2-dimensional anisotropic oscillator).

In the search for classical integrals we are guided by the knowledge that for our type of problem there exist $(2n-1)$ time-independent integrals. However, these integrals exist in principle only *im kleinen;* i.e., over small and suitably restricted ranges of the variables. For our purposes it is apparently necessary that they exist over a whole energy surface.[9] On the other hand, the classical problems which lend themselves to the quantization procedure are very limited in number. It appears quite possible that the problem of quantization in quantum mechanics and the existence of transformation groups on the orbits in the corresponding classical problem are intimately related.

Another point concerns the number of parameters in the group. When we have found $(2n-1)$ suitable classical integrals, their Poisson-brackets may still not satisfy Eq. (4). In this case we can continue to form new integrals using Poisson's theorem.[10] In this manner we proceed until we have completed a set satisfying Eq. (5), if possible. We are confronted with two questions: (1) Under what conditions will the process terminate so that we obtain a group, and (2) if it does terminate shall we stop there, or shall we seek further integrals to generate a still larger group of transformations? Possibly questions of this sort can be answered in terms of the general theory of transformation groups. Our present view is that we have found everything requisite if $r \geqq (2n-1)$ so that the classical group is transitive with respect to transformations on an energy surface in phase space. The analogous criterion in quantum mechanics seems to be the *irreducibility* of the representations.

Examples

A. The hydrogenic atom (3-dimensional)

As this problem has been discussed in detail by Fock[2] and Bargmann,[3] we shall confine ourselves to a statement of the results. The symmetry group is built up on the integrals

$$\mathbf{L} = \mathbf{r} \times \mathbf{p}; \qquad \mathbf{A} = (1/2mZe^2)(\mathbf{L} \times \mathbf{p} - \mathbf{p} \times \mathbf{L}) + \mathbf{r}/r.$$

$\mathbf{L}$ is the ordinary angular momentum operator, and $\mathbf{A}$ is the Lenz-Pauli vector integral. The commutation rules of these six integrals and their explicit reduction to the 4-dimensional rotation group are given in detail by Bargmann. The

[9] We are indebted to Dr. W. Kaplan for discussion and correspondence on this point.

[10] Reference 5, Section 145.

results can be readily verified by considering the solutions in the momentum space where corresponding operators can be found.[11] This second procedure is equivalent to that of Fock.

B. The Kepler problem in two dimensions

The Hamiltonian is

$$H=(1/2m)(p_1^2+p_2^2)-Ze^2/(q_1^2+q_2^2)^{\frac{1}{2}}.$$

We find the three integrals

$$L_3=q_1p_2-q_2p_1,$$

$$A_1=-(1/2mZe^2)(L_3p_2+p_2L_3)+q_1/r,$$

$$A_2=+(1/2mZe^2)(L_3p_1+p_1L_3)+q_2/r,$$

having the commutation relations

$$[L_3, A_1]=i\hbar A_2; \quad [L_3, A_2]=-i\hbar A_1,$$

$$[A_1, A_2]=(i\hbar/mZ^2e^4)(-2H)L_3.$$

If we define

$$A_1=(i\hbar/m^{\frac{1}{2}}Ze^2)(2|E|)^{\frac{1}{2}}F_1,$$

$$A_2=(i\hbar/m^{\frac{1}{2}}Ze^2)(2|E|)^{\frac{1}{2}}F_2,$$

$$L_3=i\hbar F_3,$$

where E is the total energy eigenvalue, we find for $E<0$;

$$[F_1, F_2]=F_3; \quad [F_3, F_1]=F_2; \quad [F_2, F_3]=F_1,$$

which are the commutation rules for the 3-dimensional rotation group. For $E>0$:

$$[F_1, F_2]=-F_3; \quad [F_3, F_1]=F_2; \quad [F_2, F_3]=F_1,$$

which are the commutation rules for the group of linear transformations on three real variables with the invariant form $(x_1^2+x_2^2-x_3^2)$, which we may call the 3-dimensional Lorentz group.

For the bound energy states the energy values are

$$E_{\lambda,\nu}=-(mZ^2e^4/2\hbar^2)/(\lambda+\nu+\tfrac{1}{2})^2.$$

$$(\lambda, \nu=0, 1, 2, \cdots).$$

Using plane polar coordinates the wave functions have the form

$$\psi^{\pm}{}_{\lambda,\nu}=f_{\lambda\nu}(r)e^{\pm i\lambda\varphi}.$$

For $\lambda>0$ there exists a doubling due to the subgroup of rotations associated with F_3, while all states for which $\lambda+\nu=N=$const. form a degenerate set. The matrix of F_3 is diagonal, and the direct computation of the matrices for F_1 and F_2 leads to the customary representations D_N, the degree of degeneracy being $g(N)=2N+1$, N integral.

C. The 2-dimensional isotropic harmonic oscillator

The Hamiltonian is

$$H=(p_1^2+p_2^2)/2m+k(q_1^2+q_2^2)/2,$$

for which the following are integrals

$$F_1=(1/i2\hbar)(q_1p_2-q_2p_1),$$

$$F_2=(1/i4\hbar)\{(1/m^{\frac{1}{2}}k^{\frac{1}{2}})(p_1^2-p_2^2)+m^{\frac{1}{2}}k^{\frac{1}{2}}(q_1^2-q_2^2)\},$$

$$F_3=(1/i2\hbar)\{(1/m^{\frac{1}{2}}k^{\frac{1}{2}})p_1p_2+m^{\frac{1}{2}}k^{\frac{1}{2}}q_1q_2\}.$$

The first arises from the angular momentum, and the second from the energy difference of the two separate oscillators, while the third has no obvious physical significance. The commutation rules are

$$[F_i, F_k]=F_l,$$

the indices forming a cyclic permutation on (1, 2, 3). If we build the representation on the usual oscillator functions obtained by separation of the variables, the matrix of F_2 will be diagonal, with the matrix elements

$$(N_1, N_2|F_2|N_1, N_2)=i(\tfrac{1}{2}N-N_1),$$

where N_1 and N_2 are the quantum numbers of the two oscillators, and $N=N_1+N_2=$const.

The abstract group is therefore the same as that of the 2-dimensional Kepler problem, with the degree of degeneracy $g(N)=N+1$. However, since N can assume all positive integral values, the representations include the half-integral as well as the integral cases. To our knowledge this is the first instance in which the half-integral representations of the rotation group have been known to appear in physical problems other than those connected with relativistic or spin theory.

However, for the purposes of generalization to higher dimensions we prefer to interpret the

[11] E. Hylleraas, Zeits. f. Physik **74**, 216 (1932). B. Podolsky and L. Pauling, Phys. Rev. **34**, 109 (1929). In line 6 of page 115 of this reference one should put $\zeta=nP/Zp_0$.

group which appears here as the unitary unimodular group on two complex variables, which is doubly-isomorphic to the 3-dimensional rotation group.

D. The n-dimensional isotropic oscillator

The treatment of the preceding example can be generalized readily to any number of dimensions. We give only the result of the calculation.

Considering the problem as a collection of n one-dimensional oscillators it is always possible to find (n^2-1) linearly independent integrals, namely, the $\binom{n}{2}$ angular momenta, the $(n-1)$ differences of the energy of the separate oscillators, and the $\binom{n}{2}$ combinations of the form $q_1q_2+p_1p_2$. It has been verified that the group generated by these infinitesimal transformations is isomorphic to the unimodular unitary group in n dimensions, which has (n^2-1) parameters.

Under the transformations of this group the eigenspaces of the Hamiltonian transform according to the representations by symmetric tensors. The dimensions of the representations are

$$g(N)=\binom{N+n-1}{n-1},$$

where $N=\Sigma N_i$, the N_i's being the quantum numbers of the individual oscillators. This is then the degree of degeneracy of the energy levels, as can be checked directly.

It may be noted that there exist further representations of this group built on tensors which are not wholly symmetric,[12] but they do not occur in this physical application.

E. The 2-dimensional anisotropic oscillator

As remarked in the introduction, this problem presents certain peculiarities. The Hamiltonian can be written as

$$H=(p_1^2/2M_1+M_1\omega_1^2q_1^2/2)+(p_2^2/2M_2+M_2\omega_2^2q_2^2/2).$$

If the ratio of the two frequencies ω_1/ω_2 is rational, the energy levels are degenerate. Let us write

$$n\omega_1=m\omega_2=\tau; \qquad \alpha=M\omega,$$

where n and m are positive integers, and introduce the new variables

$$b=(p-i\alpha q)/(2\alpha)^{\frac{1}{2}}; \qquad b^*=(p+i\alpha q)/(2\alpha)^{\frac{1}{2}}.$$

It is easily verified that in both classical and quantum mechanics the following expressions are integrals

$$F_1=\tfrac{1}{2}(b_1^{\,n}b_2^{*m}+b_1^{*n}b_2^{\,m}),$$

$$F_2=-(i/2)(b_1^{\,n}b_2^{*m}-b_1^{*n}b_2^{\,m}).$$

For the classical mechanics we can define the integrals

$$B_1=\frac{(\omega_1\omega_2)^{\frac{1}{2}}}{\tau}\cdot F_1\cdot(b_1b_1^*)^{-\frac{1}{2}(n-1)}\cdot(b_2b_2^*)^{-\frac{1}{2}(m-1)},$$

$$B_2=\frac{(\omega_1\omega_2)^{\frac{1}{2}}}{\tau}\cdot F_2\cdot(b_1b_1^*)^{-\frac{1}{2}(n-1)}\cdot(b_2b_2^*)^{-\frac{1}{2}(m-1)},$$

$$B_3=(1/2\tau)(b_2b_2^*-b_1b_1^*),$$

which have the Poisson-bracket relations

$$(B_1, B_2)=B_3\cdots$$

with cyclic permutations of the indices. We can thus conclude that there exists a group of contact-transformations in phase space which leaves the system of orbits of given energy invariant. This group is isomorphic to the 3-dimensional rotation group.

We have tried various expedients for carrying these results over to the quantum-mechanical problem, but so far have not found it possible to do so. In view of the negative results, it would scarcely be profitable to elaborate on them here. We feel, however, that the difficulties encountered in this relatively simple problem throw question on the true interpretation of classical multiply-periodic motions in quantum mechanics.

We are very much indebted to Professors Fock and Podolsky for correspondence relative to their work on the hydrogen atom.

[12] H. Weyl, *The Classical Groups* (Princeton University Press, 1939), p. 201.

On the Connection Between the Spin and Statistics of Elementary Particles*

J. S. DE WET†
Princeton University and Institute for Advanced Study, Princeton, New Jersey
(Received January 25, 1940)

It is shown that Fermi-Dirac quantization by the procedure of Heisenberg and Pauli cannot be carried out for tensor wave equations. Since the general wave equations for particles with integral spin are tensor equations, it follows that for these integral spin equations Fermi-Dirac quantization cannot be carried out. During the course of the discussion it appears that for equations derived from Lagrangians which are nonlinear in the derivatives of the functions, Fermi-Dirac quantization cannot be carried out. Since the Heisenberg-Pauli theory applies only to nonlinear Lagrangians, a special discussion of linear Lagrangians (linear in the derivatives of the functions) is given. It is shown how equations derived from such Lagrangians can be put into Hamiltonian form. Lagrangians of this type occur for the equations for half-odd spin.

INTRODUCTION

THE problem of the connection between the spin and statistics of particles was first tackled by Pauli.[1] He attempted to show that Fermi-Dirac quantization was not admissible for the scalar wave equation. His work was not correct but subsequently Sokolow and Iwanenko[2] showed that the Einstein-Bose quantization of the scalar wave equation that had been given by Pauli and Weisskopf[3] could not be extended to the Fermi-Dirac case. Since then Fierz[4] has considered the general wave equations of Dirac[5] and has given Einstein-Bose quantizations of these equations. He showed that the corresponding Fermi-Dirac quantizations could be carried out for the equations for half-odd spin, but that the integral spin case led to difficulties. Here we will prove a very general result. We will show that, on the basis of the Heisenberg-Pauli[6] theory of the quantization of wave fields it is not possible to carry out the Fermi-Dirac quantization of tensor equations. Since the equations for integral spin are all tensor equations it follows immediately that these equations cannot be quantized by plus commutation brackets. As mentioned before, Fierz has shown that it is possible to carry out Fermi-Dirac quantization as well as Einstein-Bose for the equations for half-odd spin. However Sokolow and Iwanenko[2] have shown that for a particle with spin $\frac{1}{2}$ the Einstein-Bose quantization leads to serious difficulties with the negative energy values, while the Fermi-Dirac quantization allows these difficulties to be overcome to some extent by enabling the use of a subtraction device. The Sokolow and Iwanenko discussion holds for the general half-odd spin equations, but since the general case is so closely analogous to the spin halfcase, the work is not given in detail. However, a statement of the essential points of the argument is given for completeness. The position then is as follows: For the integral spin equations Fermi-Dirac quantization by the Heisenberg-Pauli procedure is not possible. The half-odd spin equations do admit both Fermi-Dirac and Einstein-Bose quantizations, but the Einstein-Bose leads to serious difficulties, while the Fermi-Dirac leads to somewhat lesser difficulties.

In the course of the discussion of the Fermi-Dirac commutation relations, it appears as an elementary result that Fermi-Dirac quantization is not possible for Hamiltonian forms of equations derived from Lagrangians which are nonlinear in the derivatives of the functions. Since the theory as given by Heisenberg and Pauli applies only to such Lagrangians, a discussion is given of Lagrangians linear in the derivatives of the functions. It is shown how equations derived from certain such Lagrangians can be put into Hamiltonian form. Such linear Lagrangians

* Abstract of a Ph.D. thesis submitted to Princeton University.
† Commonwealth Fund Fellow.
[1] W. Pauli, Ann. d. Inst. Henri Poincare **6**, 137 (1936).
[2] A. Sokolow and D. Iwanenko, Physik. Zeits. Sowjetunion **11**, 590 (1937).
[3] W. Pauli and V. F. Weisskopf, Helv. Phys. Acta **7**, 709 (1936).
[4] M. Fierz, Helv. Phys. Acta **12**, 3 (1939).
[5] P. A. M. Dirac, Proc. Roy. Soc. London **A155**, 47 (1936).
[6] W. Heisenberg and W. Pauli, Zeits. f. Physik **56**, 1 (1929).

appear in the case of the equations for half-odd spin, and the discussion is of use in carrying out the quantization of these equations.

1. Summary of the Classical Hamilton Jacobi Theory for Continua

The Heisenberg-Pauli procedure for the quantization of wave fields can be divided into two parts. The first part consists in considering the equations classically and putting them into Hamiltonian form, analogous to the Hamiltonian form of equations of motion in point dynamics. When this has been done, the functions involved are replaced by operators and commutation relations are introduced between these in such a way that the Heisenberg equations of motion for the operators agree with the wave equations. Here we give a short account of the essential results of the first part, i.e., finding the Hamiltonian form of given equations. For a full discussion see the Heisenberg-Pauli paper referred to earlier.

We consider a system with dependent variables ψ^α $(\alpha=1, 2, 3, \cdots n)$ and independent variables x^σ. The $\psi^\alpha(x)$ may be vector or spinor fields and the x^σ $(\sigma=1, 2, 3, 4)$ will be the space time coordinates of the system. Let

$$I=\int L[\psi^\alpha(x), \psi^\alpha{}_{;\sigma}(x)]d\mathbf{x}. \tag{1.1}$$

$\psi^\alpha{}_{;\sigma}$ is to mean $\partial\psi^\alpha/\partial x^\sigma$ and $d\mathbf{x}$ is the four-dimensional volume element $dx^1dx^2dx^3dx^4$. We restrict ourselves to special relativity. Then I is an invariant if L is invariant. The Euler equations of (1.1) are

$$0=\frac{\partial}{\partial x^\sigma}\left(\frac{\partial L}{\partial\psi^\alpha{}_{;\sigma}}\right)-\frac{\partial L}{\partial\psi^\alpha} \quad (\alpha=1, 2, 3, \cdots n). \tag{1.2}$$

The summation convention is used throughout. The tensor $T^\sigma{}_\tau$ given by

$$T^\sigma{}_\tau=L\delta^\sigma{}_\tau-(\partial L/\partial\psi^\alpha{}_{;\sigma})\psi^\alpha{}_{;\tau} \tag{1.3}$$

satisfies

$$\partial T^\sigma{}_\tau/\partial x^\sigma=0 \tag{1.4}$$

in virtue of (1.2) as is easily verified. Let

$$\begin{aligned}\mathfrak{H}&=T^4{}_4\\&=L(\psi^\alpha, \psi^\alpha{}_{;\tau}, \psi^\alpha{}_{;4})-(\partial L/\partial\psi^\alpha{}_{;4})\psi^\alpha{}_{;4}\\&\qquad(\tau=1, 2, 3).\end{aligned} \tag{1.5}$$

Define π_α by

$$\pi_\alpha=\partial L/\partial\psi^\alpha{}_{;4}. \tag{1.6}$$

π_α and ψ^α are then called conjugate variables. If we solve (1.6) for $\psi^\alpha{}_{;4}$ in terms of π_α, (which is possible provided L is not linear in $\psi^\alpha{}_{;4}$) and substitute for $\psi^\alpha{}_{;4}$ in $\mathfrak{H}$, $\mathfrak{H}$ becomes a function of π_α, ψ^α, $\psi^\alpha{}_{;\tau}$

Then it can be shown that the Eqs. (1.2) can be written in the form

$$\frac{\partial\psi^\alpha}{\partial x^4}=-\frac{\partial\mathfrak{H}}{\partial\pi_\alpha}, \quad \frac{\partial\pi_\alpha}{\partial x^4}=\frac{\partial\mathfrak{H}}{\partial\psi^\alpha}-\frac{\partial}{\partial x^\tau}\left(\frac{\partial\mathfrak{H}}{\partial\psi^\alpha{}_{;\tau}}\right) \tag{1.7}$$

or if we define H by

$$H=\int_S\mathfrak{H}(\pi_\alpha, \psi^\alpha, \psi^\alpha{}_{;\tau})dS, \tag{1.8}$$

where $dS=dx^1dx^2dx^3$ these equations become

$$\frac{\partial\psi^\alpha}{\partial x^4}=-\frac{\delta H}{\delta\pi_\alpha(x)}, \quad \frac{\partial\pi_\alpha}{\partial x^4}=\frac{\delta H}{\delta\psi^\alpha(x)}, \tag{1.9}$$

where $\delta H/\delta\pi_\alpha(x)$, $\delta H/\delta\psi^\alpha(x)$ are the functional derivatives of H with respect to $\pi_\alpha(x)$ and $\psi^\alpha(x)$. Eqs. (1.9) we call the Hamiltonian form of the Eqs. (1.2). We see how the formalism enables one to put given equations into Hamiltonian form provided the Lagrangian L is nonlinear in the derivatives of the functions. We will discuss later the case where the Lagrangian is linear in the derivatives of the functions. The preceding work can be generalized by having L a function of $\bar\psi^\alpha$ and its derivatives, as well as of ψ^α and its derivatives.

In going over to the quantum theory, we replace the functions $\psi^\alpha(x)$ by operators $\psi^\alpha(x)$ and functions $\bar\psi^\alpha(x)$ by the operators $\psi^{*\alpha}(x)$, where $\psi^{*\alpha}$ is the Hermitian adjoint of ψ^α. Since these operators do not necessarily commute, the order of the terms becomes important. In all the applications the Eqs. (1.2) are linear and can be written unambiguously in terms of the operators. Similarly the Eqs. (1.9) are the same as (1.2) no matter what the order of the terms in H. However, the order of the terms in $T^\sigma{}_\tau$ and hence in H is not arbitrary. The order must be chosen in such a way that (1.4) is satisfied taking note of the noncommutativity of the terms. In addition $T^\sigma{}_\tau$ must be self-adjoint.

The problem then is to choose commutation

relations between the operators in such a way that

$$[\pi_\alpha(x), H]=i\hbar\frac{\delta H}{\delta\psi^\alpha(x)},$$
$$[\psi^\alpha(x), H]=-i\hbar\frac{\delta H}{\delta\pi_\alpha(x)},$$
$$[\pi_\alpha{}^*(x), H]=i\hbar\frac{\delta H}{\delta\psi^{*\alpha}(x)}, \tag{1.10}$$
$$[\psi^{*\alpha}(x), H]=-i\hbar\frac{\delta H}{\delta\pi_\alpha{}^*(x)},$$

where $[A, B]=AB-BA$.

The choice of commutation relations such that (1.10) is satisfied is discussed in the next Section. Two cases are discussed, the Einstein-Bose and the Fermi-Dirac commutation relations. It will be found that, for the Fermi-Dirac commutation relations, there is a further restriction on the order of terms in H and hence in $T^\sigma{}_\tau$. When the relations (1.10) are satisfied, the Eqs. (1.9) can be written in the form

$$i\hbar\frac{\partial A}{\partial x^4}=[A, H]. \tag{1.11}$$

where $A=\psi^\alpha, \psi^{*\alpha}, \pi_\alpha, \pi_\alpha{}^*$.

These are the Heisenberg equations of motion. Thus if we choose commutation relations such that (1.10) are satisfied the Heisenberg equations of motion agree with the Eqs. (1.2).

2. The Commutation Relations

We consider in this section the commutation relations to be introduced between the operators π, π^*, ψ, ψ^* which are such that the relations (1.10) hold. We will see that the Fermi-Dirac commutation relations lead to difficulties unless certain conditions are satisfied. It will follow that these commutation relations are not admissible when the equations to be quantized are tensor equations.

a. The Einstein-Bose commutation relations

We state the following result. The proof is given by Heisenberg and Pauli. Given the following commutation relations

$$[\pi_\alpha(x), \psi^\beta(x')]=i\hbar\delta_\alpha{}^\beta\delta(\mathbf{x}-\mathbf{x}'),$$
$$[\pi_\alpha{}^*(x), \psi^{*\beta}(x')]=i\hbar\delta_\alpha{}^\beta\delta(\mathbf{x}-\mathbf{x}'), \tag{2.1}$$

all other pairs of operators chosen from $\pi_\alpha, \pi_\alpha{}^*, \psi^\alpha, \psi^{*\alpha}$ commuting; e.g.,

$$[\pi_\alpha(x), \psi^{*\beta}(x')]=0,$$

where

$$\delta(\mathbf{x}-\mathbf{x}')=\delta(x^1-x^{1\prime})\delta(x^2-x^{2\prime})\delta(x^3-x^{3\prime})$$

is Dirac's δ function. *Then*

$$[\pi_\alpha(x), H]=i\hbar\frac{\delta H}{\delta\psi^\alpha(x)},$$
$$[\psi^\alpha(x), H]=-i\hbar\frac{\delta H}{\delta\pi_\alpha(x)},$$
$$[\pi_\alpha{}^*(x), H]=i\hbar\frac{\delta H}{\delta\psi^{*\alpha}(x)}, \tag{2.2}$$
$$[\psi^{*\alpha}(x), H]=-i\hbar\frac{\delta H}{\delta\pi_\alpha{}^*(x)},$$

where $H\{\psi^\alpha, \psi^{*\alpha}, \pi_\alpha, \pi^*{}_\alpha\}$

$$=\int_S \mathfrak{H}(\psi^\alpha, \psi^\alpha{}_{;\tau}, \pi_\alpha, \pi_{\alpha;\tau}, \psi^{*\alpha}, \cdots\pi^*{}_{\alpha;\tau})dS \tag{2.3}$$

and $\mathfrak{H}$ is quadratic in the operators $\psi^\alpha, \psi^\alpha{}_{;\tau}, \pi_\alpha, \pi_{\alpha;\tau}$ and their Hermitian adjoints.

The result is not dependent on the order of the terms in $\mathfrak{H}$. We mention this as in the case of the Fermi-Dirac commutation relations the order of the terms is important.

b. The Fermi-Dirac commutation relations

We establish a similar result with the so-called Fermi-Dirac commutation relations. We define plus commutation brackets as follows:

$$[A,B]_+=AB+BA.$$

The result we prove is the following: Given the following commutation relations:

$$[\pi_\alpha(x), \psi^\beta(x')]_+=i\hbar\delta_\alpha{}^\beta\delta(\mathbf{x}-\mathbf{x}'),$$
$$[\pi_\alpha{}^*(x), \psi^{*\beta}(x')]_+=-i\hbar\delta_\alpha{}^\beta\delta(\mathbf{x}-\mathbf{x}'), \tag{2.4}$$

all other pairs of operators chosen from $\pi_\alpha, \pi^*{}_\alpha, \psi^\alpha, \psi^{*\alpha}$ anticommuting; e.g.,

$$[\pi_\alpha(x), \psi^{*\beta}(x')]_+=0$$

and

$$H\{\pi_\alpha, \psi^\alpha, \pi^*{}_\alpha, \psi^{*\alpha}\} = \int_S \mathfrak{H}(\pi_\alpha, \psi^\alpha, \pi_{\alpha;\tau}, \psi^\alpha{}_{;\tau}, \pi^*{}_\alpha \cdots \psi^{*\alpha}{}_{;\tau}) dS, \quad (2.5)$$

where $\mathfrak{H}$ is a bilinear form of the type

$$\mathfrak{H} = A_{\sigma\mu\alpha\beta} F^\sigma{}_\alpha G^\mu{}_\beta, \quad (2.6)$$

$A_{\sigma\mu\alpha\beta}$ being constants and $F^\sigma{}_\alpha$, $G^\mu{}_\beta$ given by

$$F^\sigma{}_\alpha \equiv (\pi_\alpha{}^*, \psi^\alpha, \psi^\alpha{}_{;\tau}, \pi^*{}_{\alpha;\tau}),$$
$$G^\mu{}_\beta \equiv (\pi_\beta, \psi^*{}_\beta, \psi^*{}_{\beta;\tau}, \pi_{\beta;\tau}). \quad (2.7)$$

Then

$$[\psi^\alpha(x), H] = -i\hbar \frac{\delta H}{\delta \pi_\alpha(x)},$$
$$[\pi_\alpha(x), H] = i\hbar \frac{\delta H}{\delta \psi^\alpha(x)},$$
$$[\psi^{*\alpha}(x), H] = -i\hbar \frac{\delta H}{\delta \pi_\alpha{}^*(x)}, \quad (2.8)$$
$$[\pi_\alpha{}^*(x), H] = i\hbar \frac{\delta H}{\delta \psi^{*\alpha}(x)}.$$

Proof:

We establish the result by straightforward verification. From (2.4) we get by differentiation

$$[\pi_\alpha(x), \psi^\beta{}_{;\tau}(x')]_+ = i\hbar \delta^\beta{}_\alpha \frac{\partial}{\partial x'^\tau} \{\delta(\mathbf{x}-\mathbf{x}')\} \quad (2.9)$$

and corresponding results. Using the result

$$[A, BC] = [A, B]_+ C - B[A, C]_+,$$

we easily see that the only terms which contribute to $[\pi_\alpha(x), \mathfrak{H}(x')]$ are terms of the following form

(a) $$\mathfrak{H}_a = \psi^\alpha(x') G^\mu{}_\beta(x'),$$

(b) $$\mathfrak{H}_b = \psi^\alpha{}_{;\tau}(x') G^\mu{}_\beta(x')$$

and all terms of $G^\mu{}_\beta(x')$ anticommute with $\pi_\alpha(x)$.

The contribution to $[\pi_\alpha(x), \mathfrak{H}(x')]$ of $\mathfrak{H}_a$, $\mathfrak{H}_b$, respectively, is

(a) $$i\hbar \delta(\mathbf{x}-\mathbf{x}') G^\mu{}_\beta(x'),$$

(b) $$i\hbar \frac{\partial}{\partial x'^\tau} \{\delta(\mathbf{x}-\mathbf{x}')\} G^\mu{}_\beta(x')$$

and the contribution of H_a and H_b to $[\pi_\alpha(x), H]$

$$\left(\text{where } H_a = \int_{S'} \mathfrak{H}_a(x') dS'\right)$$

is

(a) $$i\hbar G^\mu{}_\beta(x) = i\hbar \frac{\delta H_a}{\delta \psi^\alpha(x)},$$

(b) $$-i\hbar \frac{\partial}{\partial x^\tau} G^\mu{}_\beta(x) = i\hbar \frac{\delta H_b}{\delta \psi^\alpha(x)}.$$

Since the part of H which contributes to $[\pi_\alpha(x), H]$ is composed of sums of terms like H_a, H_b, the second of the results (2.8) follows. The other results can be verified in a similar manner.

We note that the order of the terms in $\mathfrak{H}$ as given by (2.6) is important. If $\mathfrak{H}$ were given by $A_{\sigma\mu\alpha\beta} G^\mu{}_\beta F^\sigma{}_\alpha$ instead, it would be necessary to change the signs on the right-hand side of (2.4) in order that (2.8) might hold. This imposes another restriction on the order of the terms in H and hence in $T^\sigma{}_\tau$.

We note that the commutation relations (2.6) include the following:

$$[\psi^\alpha(x), \psi^{*\alpha}(x')]_+ = 0. \quad (2.10)$$

Thus

$$\psi^\alpha(x)\psi^{*\alpha}(x) + \psi^{*\alpha}(x)\psi^\alpha(x) = 0.$$

But $\psi^\alpha(x)\psi^{*\alpha}(x)$ and $\psi^{*\alpha}(x)\psi^\alpha(x)$ are essentially positive. Thus (2.10) leads to

$$\psi^\alpha(x)\psi^{*\alpha}(x) = \psi^{*\alpha}(x)\psi^\alpha(x) = 0, \quad (2.11)$$

where the 0 on the right-hand side is the null operator. It is obvious that the relations (2.11), while formally admissible, will lead to vacuous results in our theory.

The only case in which the difficulty *does not* arise is when

$$\pi_\alpha = A_{\alpha\beta}\psi^{*\beta}, \quad \psi^{*\beta} = a^{\beta\alpha}\pi_\alpha, \quad (2.12)$$

where

$$A_{\alpha\beta} a^{\beta i} = \delta^i{}_\alpha. \quad (2.13)$$

We are restricted to a linear relation between π_α and $\psi^{*\alpha}$ since our equations are linear. The $A_{\alpha\beta}$ or $a^{\alpha\beta}$ will not be perfectly general but will be subject to certain restrictions, which we will discuss as they arise. It is easily seen that the work of this section still applies, where $\mathfrak{H}$ is now a function of ψ^α, π_α, $\psi^\alpha{}_{;\tau}$, $\pi_{\alpha;\tau}$ only, and of the

form

$$\mathfrak{H}=A_{\sigma\mu\alpha\beta}F^{\sigma}{}_{\alpha}G^{\mu}{}_{\beta} \tag{2.14}$$

with

$$F^{\sigma}{}_{\alpha}\equiv(\psi^{\alpha},\psi^{\alpha}{}_{;\tau}),\quad G^{\mu}{}_{\beta}\equiv(\pi_{\beta},\pi_{\beta;\tau}) \tag{2.15}$$

and the commutation relations

$$[\pi_{\alpha}(x),\psi^{\beta}(x')]_{+}=i\hbar\delta^{\beta}{}_{\alpha}\delta(\mathbf{x}-\mathbf{x}'). \tag{2.16}$$

Only the first two results of (2.8) now arise. The commutation relations (2.16) written in terms of ψ^{α}, $\psi^{*\alpha}$ become

$$[\psi^{*\alpha}(x),\psi^{\beta}(x')]_{+}=i\hbar a^{\alpha\beta}\delta(\mathbf{x}-\mathbf{x}'). \tag{2.17}$$

By taking the Hermitian adjoint of (2.17) it is clear that $ia^{\alpha\beta}$ must be Hermitian.

The additional condition on $ia^{\alpha\beta}$ is that it be positive definite; i.e., when the $\psi^{*\alpha}$, ψ^{β} undergo linear transformations which reduce $ia^{\alpha\beta}$ to a diagonal matrix, the diagonal elements must be positive. The *positive* definiteness is not essential. All that is essential is that $ia^{\alpha\beta}$ is definite. For if it is negative definite, all we need do is change the sign of the right-hand side of the commutation relations (2.16) and at the same time interchange all the terms in $\mathfrak{H}$. The interchange of the terms in $\mathfrak{H}$ will not affect results like (1.4).

Our general method has been to put the equations to be quantized into a classical Hamiltonian form. Then we replace the functions by operators and introduce commutation relations. We see that this can be carried out for the Fermi-Dirac case, if, and only if, the given equations can be put into a classical Hamiltonian form with ψ^{α} and $A_{\alpha\beta}\bar{\psi}^{\beta}$ as conjugate variables (with $ia^{\alpha\beta}$ a definite Hermitian matrix). Our problem therefore reduces to the question of the existence of such classical Hamiltonian forms for given equations.

At this stage we can note that whenever the Lagrangian from which the equations are derived is nonlinear in the derivatives of the functions the conjugate variables which the formalism given in Section 1 provides are not related to each other in the way necessary for the possibility of Fermi-Dirac quantization. This enables us to say at a glance that the Pauli-Weisskopf[3] Einstein-Bose quantization of the scalar wave equation and the Kemmer[7] Einstein-Bose quantization of Proca's equations cannot be extended to the Fermi-Dirac case simply by replacing the minus commutation brackets by plus commutation brackets, since the Lagrangians they start from are nonlinear in the derivatives of the functions. Since there is in general not a unique Hamiltonian form for given equations, further discussion is necessary. We will find however that for tensor equations a classical Hamiltonian form, suitable for Fermi-Dirac quantization by the commutation relations of this section, does not exist.

We have not yet said anything about relativistic invariance. The ψ^{α} which occur in the equations will be the components of either a tensor or a spinor. When the ψ^{α} are the components of a tensor, they will undergo the tensor transformation indicated by the indices when we apply a Lorentz transformation of coordinates. Similarly, when the ψ^{α} are components of a spinor they will undergo an associated linear transformation when we apply a Lorentz transformation of coordinates. It is by no means obvious that the commutation relations (2.1) and (2.16) are relativistically invariant. Heisenberg and Pauli have considered this in detail and have shown this to be the case if

(a) π_{α} transforms contragrediently to ψ^{α} and is in addition the 4th contravariant component of a vector.

(b) $$\frac{\partial}{\partial x^{\tau}}\left(\frac{\partial^{2}\mathfrak{H}}{\partial\psi^{\alpha}{}_{;\tau}\partial\psi^{\alpha}{}_{;s}}\right)=0.$$

The second requirement is satisfied in all cases that arise since the equations we are dealing with are linear and hence the L's that occur are quadratic at most. The first is satisfied in the cases where the conjugate variables are obtained from an invariant L by (1.6).

As far as our present considerations are concerned (a) requires that $A_{\alpha\beta}$ have the transformation character $A^{4}{}_{\alpha\beta}$ as indicated by the indices, the 4 being a tensor index, and the α, β tensor or spinor indices as the case may be. A further requirement of the relativistic invariance is that $A^{4}{}_{\alpha\beta}$ shall be numerically invariant under Lorentz transformations (and the associated spin transformations if the α, β are spinor indices). This is necessary since we require that the form of the equations shall be the same in all Galilean frames.

[7] N. Kemmer, Proc. Roy. Soc. London **A166**, 127 (1938).

When the α, β are tensor indices $A^{\sigma}{}_{\alpha\beta}$ must be a tensor of odd rank and must be numerically invariant under Lorentz transformations. The only numerically invariant tensors under Lorentz transformations are $g_{\sigma\tau}$, $\delta^{\sigma}{}_{\tau}$, $\epsilon_{\sigma\mu\tau\nu}$ and combinations of these.[8] It is not possible with these to construct a numerically invariant tensor $A^{\sigma}{}_{\alpha\beta}$ of odd rank. From this follows that it is not possible to find a Hamiltonian form for tensor equations, which will be suitable for Fermi-Dirac quantization and will satisfy the requirements of relativistic invariance.

Now the general wave equations for integral spin are tensor equations. For our present purposes the explicit form of the equations is not important and they are not given here. The tensor form of the equations is given in Fierz's paper. Since they are tensor equations it follows that their Fermi-Dirac quantization by the above procedure cannot be carried out.

3. Lagrangians Linear in the Derivatives of the Functions and the Quantization of the Half-Odd Spin Equations

We have seen in the preceding paragraph that Lagrangians to which the Heisenberg-Pauli theory of Section 1 applies, i.e., Lagrangians nonlinear in the derivatives of the functions, cannot yield Hamiltonian forms for which Fermi-Dirac quantization can be carried out. It is clear that we need some means of putting equations derived from linear Lagrangians into Hamiltonian form. Accordingly we show how this can be done for a certain type of Lagrangian linear in the derivatives. Then we will point out briefly how this is applied to the quantization of the equations for half-odd spin (which are not tensor equations, or equivalent to tensor equations). This will show that these equations admit Fermi-Dirac quantization, as well as Einstein-Bose, as has been shown by Fierz. For completeness we give a brief account of the Sokolow and Iwanenko discussion of the relative merits of Einstein-Bose and Fermi-Dirac quantizations, which shows the latter to lead to lesser difficulties.

Consider a Lagrangian of the form

$$L=\chi^{\alpha}A^{\sigma}{}_{\alpha\beta}\psi^{\beta}{}_{;\sigma}+F(\psi,\chi), \tag{3.1}$$

where the $A^{\sigma}{}_{\alpha\beta}$ are constant matrices. The Euler equations are

$$A^{\sigma}{}_{\alpha\beta}\psi^{\beta}{}_{;\sigma}+\frac{\partial F}{\partial\chi^{\alpha}}=0, \quad -A^{\sigma}{}_{\alpha\beta}\chi^{\alpha}{}_{;\sigma}+\frac{\partial F}{\partial\psi^{\beta}}=0. \tag{3.2}$$

We will find that, proceeding in the same way as in Section 1 by forming a tensor $T^{\sigma}{}_{\tau}$ according to (1.3) and defining the conjugate variables as before according to (1.6) the equations can be put into Hamiltonian form, with $\mathfrak{H}$ (and H) defined as before. The simplest way of showing this is by verification.

We form the tensor $T^{\sigma}{}_{\tau}$ from L by (1.3)

$$\begin{aligned}T^{\sigma}{}_{\tau}&=L\delta^{\sigma}{}_{\tau}-(\partial L/\partial\psi^{\beta}{}_{;\sigma})\psi^{\beta}{}_{;\tau}\\&=\{A^{\rho}{}_{\alpha\beta}\chi^{\alpha}\psi^{\beta}{}_{;\rho}+F(\psi,\chi)\}\delta^{\sigma}{}_{\tau}-A^{\sigma}{}_{\alpha\beta}\chi^{\alpha}\psi^{\beta}{}_{;\tau}\end{aligned} \tag{3.3}$$

and $\partial T^{\sigma}{}_{\tau}/\partial x^{\sigma}=0$ in virtue of (3.2). As before $\mathfrak{H}$ is given by

$$\mathfrak{H}=T^{4}{}_{4}=A^{\tau}{}_{\alpha\beta}\chi^{\alpha}\psi^{\beta}{}_{;\tau}+F(\psi,\chi) \quad (\tau=1,2,3). \tag{3.4}$$

The conjugate variables are given as in (1.6) by

$$\pi_{\beta}=\partial L/\partial\psi^{\beta}{}_{;4}=A^{4}{}_{\alpha\beta}\chi^{\alpha} \tag{3.5}$$

or

$$\chi^{\alpha}=a^{\alpha\beta}\pi_{\beta}, \tag{3.6}$$

where

$$A^{4}{}_{\alpha\beta}a^{\alpha\epsilon}=\delta^{\epsilon}{}_{\beta}. \tag{3.7}$$

Substituting for χ^{α} in (3.4) in terms of π_{α} we have

$$\mathfrak{H}=A^{\tau}{}_{\alpha\beta}a^{\alpha\epsilon}\pi_{\epsilon}\psi^{\beta}{}_{;\tau}+F(\psi,\chi(\pi)). \tag{3.8}$$

Regarding π_{β} and ψ^{β} as conjugate variables and $\mathfrak{H}$ as the energy density, the Hamiltonian equations are

$$\begin{aligned}\frac{\partial\pi_{\beta}}{\partial x^{4}}&=\frac{\partial\mathfrak{H}}{\partial\psi^{\beta}}-\frac{\partial}{\partial x^{\tau}}\left(\frac{\partial\mathfrak{H}}{\partial\psi^{\beta}{}_{;\tau}}\right)\\&=\partial F/\partial\psi^{\beta}-A^{\tau}{}_{\alpha\beta}a^{\alpha\epsilon}\pi_{\epsilon;\tau}\end{aligned} \tag{3.9}$$

and

$$\begin{aligned}\partial\psi^{\epsilon}/\partial x^{4}&=-\partial\mathfrak{H}/\partial\pi_{\epsilon}\\&=-a^{\alpha\epsilon}(A^{\tau}{}_{\alpha\beta}\psi^{\beta}{}_{;\tau}+\partial F/\partial\chi^{\alpha}).\end{aligned} \tag{3.10}$$

Multiplying (3.10) by $A^{4}{}_{\delta\epsilon}$ we get

$$A^{\tau}{}_{\delta\beta}\psi^{\beta}{}_{;\tau}+\partial F/\partial\chi^{\delta}=-A^{4}{}_{\delta\epsilon}\partial\psi^{\epsilon}/\partial x^{4} \tag{3.11}$$

equivalent to the first of (3.2). Eq. (3.9) is

[8] $g_{\sigma\tau}$ is the tensor which has the following components in all Galilean frames:

$$g_{11}=g_{22}=g_{33}=-g_{44}=1 \quad g_{\sigma\tau}=0 \ (\sigma\neq\tau).$$

the same as the second of (3.2) noting (3.5) and (3.6).

We have thus shown that the Hamiltonian equations with π_β and ψ^β as conjugate variables and $\mathfrak{H}$ given by (3.8) are the same as the Euler equations (3.2) of the Lagrangian (3.1). This therefore provides a means of putting equations derived from such Lagrangians into Hamiltonian form. It is easily seen that the above work holds also for Lagrangians

$$L=\bar{\psi}^\alpha A^\sigma{}_{\alpha\beta}\psi^\beta{}_{;\sigma}+F(\psi,\bar{\psi}) \tag{3.12}$$

and

$$L=\chi^\alpha A^\sigma{}_{\alpha\beta}\psi^\beta{}_{;\sigma}+\bar{\chi}^\alpha B^\sigma{}_{\alpha\beta}\bar{\psi}^\beta{}_{;\sigma}+F(\chi,\bar{\chi},\psi,\bar{\psi}). \tag{3.13}$$

We see that the Hamiltonian form of the equations derived from a Lagrangian of the type (3.12) would be suitable for Fermi-Dirac quantization, provided $ia^{\alpha\beta}$ satisfied the conditions specified in Section 2.

The general equations for particles with half-odd spin can be derived from a Lagrangian of the form (3.12) and can be put into Hamiltonian form by the use of the theory of this section. The possibility of both Einstein-Bose and Fermi-Dirac quantization then follows very simply since the L is of the form (3.12). A complete discussion is given in my thesis[9] to which the interested reader may refer.

At this stage the position is that the integral spin equations do not admit Fermi-Dirac quantization, while the half-odd equations admit both E-B and F-D quantization. For the sake of completeness we give a short account of Sokolow and Iwanenko's discussion of this. They considered the case of the electron only, but the general half odd spin case is completely analogous to the spin-half case.

If we expand the operators in terms of a complete orthogonal set of functions we get for the total energy

$$H=\sum_{\kappa_r,\,s}E(\kappa)\{a_+(\kappa_r,s)a_+{}^*(\kappa_r,s) -a_-(\kappa_r,s)a_-{}^*(\kappa_r,s)\}, \tag{3.14}$$

where s is summed over the values $1, 2, \cdots 2r+1$ (where the spin is r) and κ_r over the values $2\pi n_r/L$ where the n_r are positive or negative integers and L the side of the box in which the system is contained. $E(\kappa)$ is given by $E(\kappa)=+\{m^2c^4+\hbar^2c^2(\kappa^2{}_1+\kappa^2{}_2+\kappa^2{}_3)\}^{\frac{1}{2}}$ and the a_+, $a^*{}_+$, a_-, $a^*{}_-$ are operators. In the case of the E-B commutation relations the commutation relations between the a's are

$$\begin{aligned}[a^*{}_+(\kappa_r,s),\,a_+(\kappa_r',s')]&=\delta_{\kappa_r,\kappa_r'}\delta_{ss'},\\ [a^*{}_-(\kappa_r,s),\,a_-(\kappa_r',s')]&=\delta_{\kappa_r,\kappa_r'}\delta_{ss'},\end{aligned} \tag{3.15}$$

all other pairs chosen from a_+, $a^*{}_+$, a_-, $a^*{}_-$ commuting. These commutation relations can be satisfied by putting

$$\begin{aligned}a^*{}_+(\kappa_r,s)a_+(\kappa_r,s)&=N_+(\kappa_r,s)+1,\\ a_+(\kappa_r,s)a^*{}_+(\kappa_r,s)&=N_+(\kappa_r,s)\end{aligned} \tag{3.16}$$

and similarly for the a_-'s, where N_+, N_- are self-adjoint operators with eigenvalues 0, 1, 2, 3, $\cdots$. The total energy then becomes

$$H=\sum_{\kappa_r,\,s}E(\kappa)\{N_+(\kappa_r,s)-N_-(\kappa_r,s)\} \tag{3.17}$$

and it is obvious that the total energy may have large negative values.

In the case of the Fermi-Dirac commutation relations, (3.15) is replaced by the same relations with plus commutation brackets. These relations can be satisfied by

$$\begin{aligned}a^*{}_+a_+&=1-N_+, & a^*{}_-a_-&=N_-,\\ a_+a^*{}_+&=N_+, & a_-a^*{}_-&=1-N_-,\end{aligned} \tag{3.18}$$

where the N_+, N_- have eigenvalues 0, 1. The total energy then becomes

$$H=\sum_{\kappa_r,\,s}E(\kappa)\{N_+(\kappa_r,s)+N_-(\kappa_r,s)-1\}. \tag{3.19}$$

If we neglect the constant term in (3.19) the energy now becomes positive.

We thus see that the F-D commutation relations has some advantage over the E-B as it enables the use of this device to make the total energy positive.

This completes the discussion of the connection between the spin and statistics of elementary particles. The integral spin equations do not admit F-D quantization by the Heisenberg-Pauli procedure, while the F-D quantization is possible for the half-odd spin equations and leads to lesser difficulties than the Einstein-Bose.

The author wishes to thank Professors E. P. Wigner and H. P. Robertson for helpful criticism.

[9] A copy is available at the Princeton University Library for inter-library loan.

The Photoelectric and Optical Properties of Sodium and Barium*

ROBERT J. MAURER†
University of Rochester, Rochester, New York

(Received January 22, 1940)

Experimental spectral distribution curves have been obtained for sodium and barium using polarized and unpolarized radiation. The work function of sodium was determined as 2.28 ev and that of barium as 2.48 ev. The experimental data are compared with the theory of Mitchell. The theory fails satisfactorily to account for the absolute photoelectric yields and for the ratio of the photoelectric yields obtained with radiation polarized parallel and perpendicular to the plane of incidence.

THEORY

A GENERAL theory of the photoelectric effect in metals has been given by Mitchell.[1,2,3] This theory rests upon an observation by Tamm and Schubin[4] that the interaction of a light wave with a metal can be divided into two parts. Plausible reasoning leads to the conclusion that, within the range of wave-lengths ordinarily investigated, the interaction of a light wave with an electron moving in the periodic field of the lattice can make a negligible contribution to the photoelectric current. Upon this interaction does depend the reflection, refraction, and damping of the light wave. The photoelectric current results from an interaction between light wave and electron which is due to the surface field of the metal.

If the periodic field of the lattice is neglected, the reflection and refraction of the light wave may be introduced into the theory by means of Maxwell's equations and the experimental optical constants of the metal. Unfortunately, the calculations which are required for a complete comparison of this form of the theory with a set of experimental data are quite laborious. In this paper the experimental data will be compared with two forms of the theory which will be designated as approximations *A* and *B*.

Approximation *A* consists in neglecting the reflection and refraction of the light wave. A discontinuous potential jump at the surface of the metal is assumed. Myers[5] and Hill[6] have shown that the difference between calculations made with a square and an image field is chiefly due to the high reflection coefficient of the square barrier for slow electrons. By neglecting the reflection coefficient of the square barrier the calculations are not only greatly simplified but the agreement with experiment should be improved. The photoelectric yield is then proportional to the integral

$$\iiint \frac{1}{\nu^4}\frac{K_z^2}{[K_z^2+\mu\nu]^{\frac{1}{2}}}\frac{2}{8\pi^3} \times \frac{dK_x dK_y dK_z}{1+\exp\left\{\dfrac{h^2(K_x^2+K_y^2+K_z^2-\mu\bar{\nu})}{8\pi^2 mKT}\right\}}, \quad (1)$$

where the nomenclature is Mitchell's and the integral is taken over all electrons which, after absorption of a quantum, will have sufficient energy to escape. Except near the threshold the exponential is negligible compared with unity.

Near the threshold the variation of the Fermi distribution function cannot be neglected. If in this region the excitation probability is assumed independent of ν and proportional to K_z, then Eq. (1) goes over into DuBridge's[7] modification of Fowler's equation,

$$I=\alpha A T^2 \varphi(x). \quad (2)$$

By means of the usual "Fowler plot" the thresh-

* Part of a dissertation presented to the Faculty of the Graduate School of the University of Rochester in candidacy for the Degree of Doctor of Philosophy.

† Now at the Massachusetts Institute of Technology, Cambridge, Massachusetts.

[1] K. Mitchell, Proc. Roy. Soc. **A146**, 442 (1934).
[2] K. Mitchell, Proc. Camb. Phil. Soc. **31**, 416 (1935).
[3] K. Mitchell, Proc. Roy. Soc. **A153**, 513 (1936).
[4] I. Tamm and S. Schubin, Zeits. f. Physik **68**, 97 (1931).
[5] R. Myers, Phys. Rev. **49**, 938 (1936).
[6] A. G. Hill, Phys. Rev. **53**, 184 (1938).
[7] L. A. DuBridge, *New Theories of the Photoelectric Effect* (Hermann and Cie, Paris, 1935).

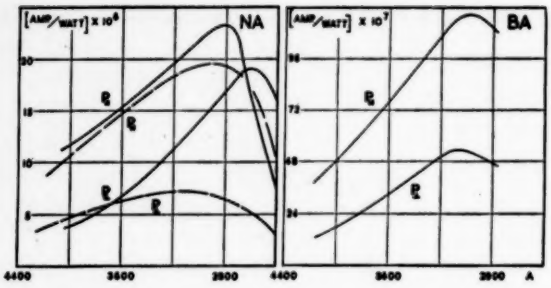

FIG. 1 (left). Calculated spectral distribution curves for sodium, electric vector parallel ($P_{\parallel}$), and perpendicular ($P_{\perp}$) to the plane of incidence. The difference between the solid and dashed curves shows the effect of neglecting the frequency variation of the optical constants.

FIG. 2 (right). Calculated spectral distribution curves for barium, electric vector parallel ($P_{\parallel}$), and perpendicular ($P_{\perp}$) to the plane of incidence.

old and the parameter α can be evaluated. DuBridge has interpreted α as the fraction of the number of electrons which come up to unit area of the surface in one second which absorb a quantum of energy when the light intensity is unity. By using the value of α so determined, the yields for frequencies far from the threshold (which have been calculated from (1) in arbitrary units) can be plotted to the same scale.

The theoretical curves shown in Figs. 4 and 8 were calculated in this manner. The constant potential inside the metal was fixed by the addition of the work function and the width of the Fermi band of electrons at 0°K. For sodium a band 3.24 ev wide and for barium one 3.28 ev wide were assumed.

The width of the Fermi band was determined by the number of "free" electrons per unit volume.

$$\xi_0=\hbar^2[3\pi^2n]^{\frac{1}{3}}/2m. \qquad (3)$$

It was assumed that sodium possesses 1 "free" electron per atom and that barium possess 1.8 "free" electrons per atom.

This adjustment of theoretical and experimental curves to coincidence at the threshold where experiment and theory agree appears more logical than previous methods of comparison by adjustment of the yields at the maxima of the spectral distribution curves.

Approximation B is the form of the theory given by Mitchell in 1936.[3] The reflection and refraction of the light wave is taken account of by means of Maxwell's equations. This form of the theory allows the absolute photoelectric yield and its dependence upon the angle of incidence and state of polarization of the incident beam to be discussed.

To account for the photoelectric current excited by radiation whose electric vector vibrates in a plane parallel to the surface, Mitchell assumed that the surface is built up of small elements whose normals make an average angle ω with the normal to the geometrically plane surface. The elements are assumed small compared with the wave-length of the incident radiation but large compared with the wave-length of the photoelectrons. The angle ω must be evaluated from the ratio of the photoelectric yields for radiation polarized parallel and perpendicular to the plane of incidence.

Figure 1 presents the theoretical photoelectric yield curves for sodium for polarized radiation with the electric vector vibrating parallel and perpendicular to the plane of incidence. These curves were calculated from Eqs. 16 and 19 of Mitchell's 1936 paper.[3] The angle of incidence is taken as 60° and $\omega=70°$. The positions of the maxima in these curves are necessarily wrong because of Mitchell's assumption that the width of the Fermi band is equal to the work function.

The solid curves were calculated by making use of the optical constants of sodium which have been published by Ives and Briggs.[8] The dashed curves were calculated by using the values of n_0 and K_0 for $\lambda=5461$A and neglecting the variation of the optical constants with wave-length. The importance of a complete knowledge of the optical constants is obvious. It is to be noted that the frequency dependence of $P_{\parallel}$ is different from that of $P_{\perp}$. This is a possible explanation of the fact that no maxima occur in many of the $P_{\perp}$ curves which have been reported.

Similar curves for barium are shown in Fig. 2. The optical constants which were used were those reported in this paper.

EXPERIMENTAL

Photo-currents were measured with FP-54 tubes used in DuBridge-Brown circuits. The grid leaks were S.S. White and platinum-in-glass resistors. For the determination of the yields of sodium, using unpolarized radiation, the radia-

[8] H. Ives and H. Briggs, J. Opt. Soc. Am. **27**, 181 (1937).

tion intensities were measured with a thermopile-galvanometer system having a sensitivity of 4×10^{-8} watt per cm deflection. For measurements with polarized light a small calibrated photo-cell was used to determine intensities. The surface in this cell was a thick matte layer of sodium on nickel. This cell was checked for linearity of response and independence of yield on azimuth of polarization.

The light sources were a 500-watt tungsten lamp and a low pressure d.c. mercury arc. The radiation was resolved with a Bausch and Lomb single quartz monochromator. Tests with filters established that the amount of scattered light was negligible.

Because of the small dispersion of quartz in the visible, an appreciable band of wave-lengths was transmitted by the monochromator. Thus, with the slits set at 0.05 mm a wave-length band almost 200A wide was passed at 5500A. The effect of this upon the precision of the threshold determinations was calculated as follows. With an assumed surface whose true yield was given by Fowler's theory the apparent yield was calculated by graphical integration. A wave-length band of 200A was taken. At the assumed threshold (5400A) the apparent yield was 17 percent too high and 200A from the threshold was 5 percent too high. The resulting error in the work function, determined by Fowler's method, was less than 0.01 ev.

The monochromator was mounted upon a heavy iron base which turned upon ball bearings to allow successive readings to be taken upon photo-cell and thermopile.

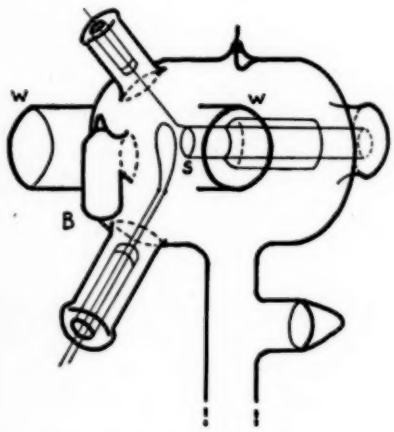

FIG. 3. Sodium photo-cell.

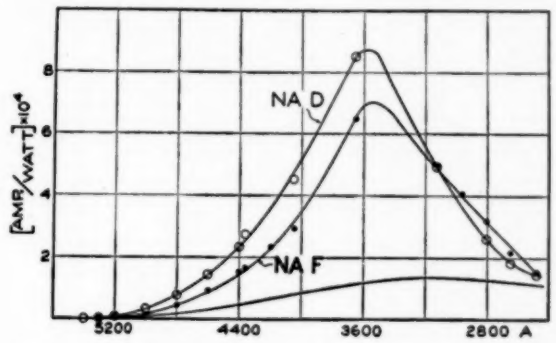

FIG. 4. Extreme variation in the shape of the spectral distribution curve for sodium, unpolarized radiation. The lower solid curve is calculated.

SODIUM

Figure 3 illustrates the photo-cell used for the measurements upon sodium surfaces with unpolarized radiation. The sodium was deposited upon the polished plane glass surface *S* by slow distillation from the reservoir *B*. Before the tube was sealed off from the pumps a heavy layer of sodium was deposited upon the inner walls of the tube. The skirt upon the re-entrant tube carrying *S* effectually insulated *S* from the rest of the tube. The quartz windows *W* fixed the angle of incidence at 60°.

The sodium was Baker's analyzed grade and was predistilled five times in glass. The pressure in the tube was measured with an ionization gauge and was about 2×10^{-8} mm Hg after sealing off from the pumps.

Five surfaces were formed with *S* held at temperatures between 25°C and 97°C during the distillation. None of the surfaces was sufficiently specular to allow the measurement of optical properties. Fowler curves, plotted for these surfaces, yielded thresholds between 2.28 ev and 2.29 ev. The values of α ranged between 3.3×10^{-32} and 5.0×10^{-32} cm²-sec. per quantum. In plotting the Fowler curves the photoelectric yields were expressed in terms of electrons per quantum. The extreme variation in the shape of the spectral distribution curves is shown in Fig. 4. The Fowler curves for these surfaces are shown in Fig. 5.

These surfaces were fairly stable. A threshold shift to the red of about 20A was detectable 60 hours after the formation of one surface. The rest of the spectral distribution curve showed no change.

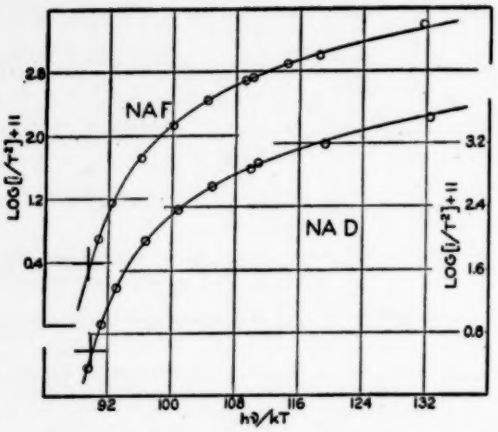

FIG. 5. Fowler plots for sodium surfaces for which the distribution curves are given in Fig. 4. For NaF $\varphi = 2.29$ ev; $\alpha = 3.3 \times 10^{-32}$ cm²-sec./quantum; $T = 298°$K. For NaD $\varphi = 2.28$ ev; $\alpha = 5.0 \times 10^{-32}$ cm²-sec./quantum; $T = 296°$K.

An attempt was made to prepare specular sodium surfaces by distilling the metal upon a polished glass plate which was cooled with liquid air during the distillation and kept cooled during the measurements. The tube used was similar to that illustrated in Fig. 6. The surfaces deposited in this way however were contaminated with gas and did not give a good fit to the Fowler curve. A typical spectral distribution curve for such a specular surface, taken with polarized radiation, is shown in Fig. 7. Table I gives the ratio of the photoelectric yields and of the energy absorbed, as calculated from the measured reflectivity of the surface.

BARIUM

The tube illustrated in Fig. 6 was used for the investigation of barium. The quartz windows fixed the angle of incidence at 60°. The barium was suspended above the tantalum ribbon *D* until the preliminary outgassing of this assembly had been completed. The barium was then lowered upon the ribbon which had a shallow *V* cross section. The shield *C* protected the polished, plane surface *S* during the melting and outgassing of the barium. The thick layer of barium, which deposited upon the inner walls of the tube during this operation, was used as anode. The pressure in the tube, after sealing off from the pumps, was 2×10^{-8} mm Hg.

TABLE I. *Sodium 7. Ratio of photoelectric yields and of energy absorbed.*

λ(A)	$P_{II}/P_{\perp}$ $\omega = 70°$ (CALC.)	$P_{II}/P_{\perp}$ (EXP.)	$A_{II}/A_{\perp}$
5200		2.2	1.5
4800		1.8	1.3
4400		1.7	1.3
4000	3.0	1.5	1.2
3600	2.3	1.5	1.1
3200	1.7	1.4	1.1
2800	1.4		
2400	0.5		

The data obtained from two surfaces in separate tubes are shown in Fig. 8. For the measurements upon Surface 2 a Glan-Thompson prism of 12 mm cross section was used to obtain polarized radiation.

Fowler plots, with the yields expressed in terms of electrons per quantum, indicated a threshold of 2.48 ev for each surface. The value of α for surface 1 was 2.3×10^{-32} cm²-sec. per quantum. Surface 2 gave values of $\alpha_{II} = 2.0 \times 10^{-32}$ cm²-sec. per quantum and $\alpha_{\perp} = 1.0 \times 10^{-32}$ cm²-sec. per quantum. Fig. 9 is a Fowler plot for barium 1.

Cashman and Bassoe[9] recently reported a threshold of 2.49 ev for barium but their spectral distribution curve did not pass through a maximum. Dr. Cashman has informed the author, however, that barium surfaces more recently investigated by him have shown a maximum in the spectral distribution curve.

Table II compares the ratios of the photoelectric yields and of the energies absorbed by the surface. The energies absorbed were calculated from the measured optical constants of barium.

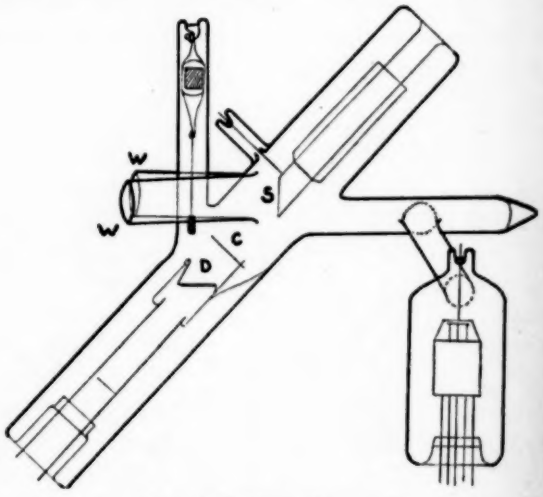

FIG. 6. Barium photo-cell.

[9] R. Cashman and E. Bassoe, Phys. Rev. **55**, 63 (1939).

TABLE II. *Barium 2. Ratio of photoelectric yields and of energy absorbed.*

λ(A)	$P_{\parallel}/P_{\perp}$ $\omega=70^{\circ}$ (CALC.)	$P_{\parallel}/P_{\perp}$ (EXP.)	$A_{\parallel}/A_{\perp}$
5780			1.93
5460			1.87
4916		1.7	1.82
4358		2.1	1.74
4047	2.7	1.9	1.65
3650	2.3	2.0	
3341	2.2	2.0	
3130	2.1	2.0	

OPTICAL CONSTANTS OF BARIUM

The optical constants of barium were measured by the method of Drude.[10] A high pressure capillary mercury arc and the Bausch and Lomb monochromator, provided with Wratten filters, served as a light source. At 4916A, the arc was used to adjust the monochromator and then a tungsten lamp was substituted. The exit slit of the monochromator served as the source slit for a spectrometer having quartz optics. The polarizer and analyzer were Glan-Thompson prisms of 12 mm cross section cemented so as to transmit to 3000A. A Babinet-Soleil compensator was mounted before the analyzer.

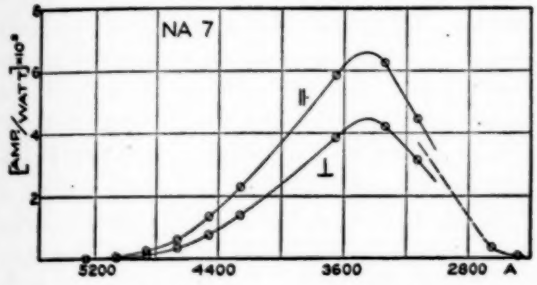

FIG. 7. Spectral distribution curves for sodium, electric vector parallel and perpendicular to the plane of incidence.

In the visible region of the spectrum, extinction was determined with the eye. In the ultraviolet, a sodium photo-cell was placed to intercept the beam emerging from the analyzer. Approximate settings of analyzer and compensator for minimum photo-current were first found. A curve of photo-current *versus* compensator setting was next taken. This accurately symmetrical curve could be folded upon itself to determine a better compensator setting for minimum photo-current.

[10] P. Drude, Wied. Ann. **64**, 159, (1898).

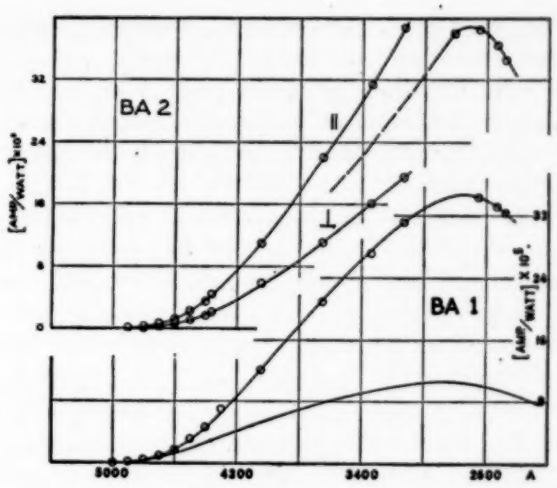

FIG. 8. Spectral distribution curves for two barium surfaces in separate tubes. The curves marked ⊥ and ∥ are for the radiation polarized with the electric vector ⊥ and ∥, respectively, to the plane of incidence. The distribution curve for Ba1 is for unpolarized radiation. The lower solid curve is calculated.

An improved analyzer setting was then determined in the same manner. One repetition of the procedure usually fixed compensator and analyzer positions satisfactorily. This method was rapid and more precise than the use of a fluorescent screen. The precision obtainable in the ultraviolet was as good as that obtained in the visible with the eye.

The most serious source of constant error was the residual strain in the quartz windows. A check showed that no rotation of the plane of polarization was caused by the windows. The net phase shift due to the windows was determined by measuring the phase shift produced by an aluminum mirror both inside and outside the tube. At 5461A the net phase shift of the

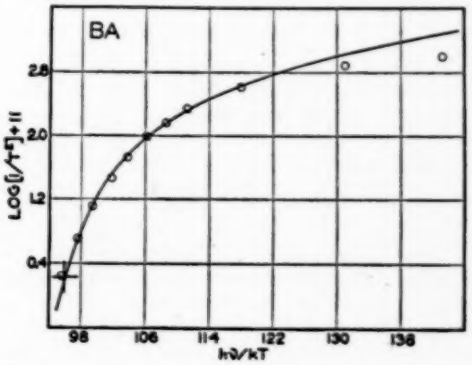

FIG. 9. Fowler plot for barium, electrons/quantum; $\varphi=2.48$ ev; $\alpha=2.3\times10^{-32}$ cm²-sec./quantum; $T=300°$K.

windows was 1°. The measured phase shifts have been corrected by using this result and the assumption that the phase shift due to the windows was inversely proportional to the wavelength. The dispersion of the birefringence can be safely neglected.

The results of the measurements upon barium 1 are shown in Fig. 10. Barium 2 was not a good optical surface but exhibited some "bloom." For the sake of comparison, however, the data from both surfaces are summarized in Table III. The nomenclature is that of König[11] and all calculations were made with his exact formulae. These results are in fair agreement with those of O'Bryan.[12] It is particularly interesting to note that two surfaces with very similar photoelectric properties show dissimilar optical properties.

Conclusion

It can be seen from the comparison of the theoretical and experimental curves of Figs. 4 and 8 that when the parameters, in the form of Mitchell's theory which we have called approximation *A*, are determined so as to fit the data near the threshold with a Fowler plot, the theory fails by a factor of about 4 to predict the correct yields at the maximum of the curve.

As Fig. 1 indicates, the optical constants of a metal can be of great importance in determining the form of the spectral distribution curve and the theory cannot neglect them.

The concept of surface roughness as an explanation of the photo-currents obtained when the electric vector vibrates in a plane parallel to the surface of the metal seems untenable. The large value of ω, which must be assumed in order to obtain small ratios, $P_{11}/P_{\perp}$, is physically implausible. Furthermore, the frequency dependence of the calculated ratio $P_{11}/P_{\perp}$ is completely wrong in the case of sodium. The calculated absolute yields of barium are about 50 times smaller than the experimental yields.

Table III. *Optical constants of barium.*

	Barium 1				Barium 2		
λ(A)	n_0	k_0	$n_0^2k_0\nu \times 10^{-14}$	R_0(%)	n_0	k_0	R_0(%)
5780	0.90	2.32	9.77	54.8	0.81	1.74	38.3
5461	.90	2.19	9.71	52.0	.79	1.65	35.6
4916	.81	2.19	8.77	47.1	.74	1.59	32.8
4358	.72	2.12	7.55	45.4	.69	1.47	30.6
4047	.69	2.01	7.12	42.5	.73	1.25	23.6
3650	.72	1.66	7.10	34.7			
3130	.76	1.41	7.84	28.8			

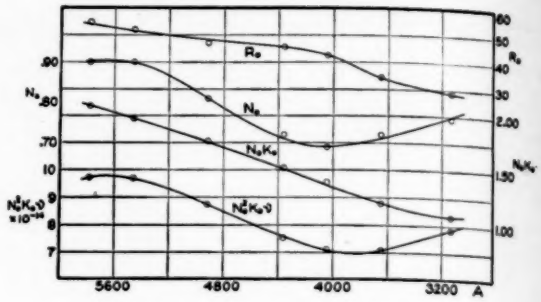

Fig. 10. Optical constants of barium.

A simple explanation of the difference between the yields, P_{11} and $P_{\perp}$, would be that it is caused by the change in reflectivity of the surface with the variation of the azimuth of polarization. If this is so the ratio of the energies absorbed at a given frequency should be the same as the ratio $P_{11}/P_{\perp}$. The data presented in Tables I and II do not justify this explanation.

Shiff and Thomas[13] have criticized Mitchell's method of taking account of the reflection and refraction of the light wave. Makinson[14] has applied to potassium the method of Shiff and Thomas, which does not assume a discontinuous change in the optical constants at the surface of the metal. The absolute yields which are obtained are larger than those given by Mitchell's theory and similar calculations for sodium would probably give better agreement with experiment. However, the difficulties faced by Mitchell's theory in explaining polarization phenomena are not removed.

The author is greatly indebted to Dr. L. A. DuBridge for advice and assistance; and to the Charles A. Coffin Foundation for the grant of a fellowship.

[11] W. König, *Handbuch der Physik*, Vol. 20 (1928).
[12] H. O'Bryan, J. Opt. Soc. Am. **26**, 122 (1936).
[13] L. Shiff and L. Thomas, Phys. Rev. **47**, 860 (1935).
[14] R. Makinson, Proc. Roy. Soc. **A162**, 367 (1937).

LETTERS TO THE EDITOR

Prompt publication of brief reports of important discoveries in physics may be secured by addressing them to this department. Closing dates for this department are, for the first issue of the month, the eighteenth of the preceding month, for the second issue, the third of the month. Because of the late closing dates for the section no proof can be shown to authors. The Board of Editors does not hold itself responsible for the opinions expressed by the correspondents.

Communications should not in general exceed 600 words in length.

Search for a Neutron-Deuteron Reaction

Attempts have been made to obtain a reaction of neutrons with deuterons but without success. The only quantitative estimate of the limit of the transmutation cross section, made on the basis of gamma-ray measurements,[1] is 3×10^{-26} cm². Schiff[2] has estimated the cross section of the reaction to be 3×10^{-27} cm².

Since the discovery that H^3 is radioactive, it seemed advisable to check the existence of the reaction by radioactive methods. An attempt was therefore made to prepare H^3 by the bombardment of heavy water with neutrons slowed in paraffin. In order to obtain experience in the detection of radioactive H^3 this isotope was prepared by the method of Alvarez.[3] It was found that the radioactive hydrogen thus produced was easily detected by the G-M counter used for the later work. In the experiment designed to produce this substance by the neutron-deuteron reaction a sample of heavy water (99.6 percent) was placed within a few inches of the beryllium target which served as the source of the neutrons. This was bombarded with deuterons in the amount of 130μ amp. hr. of deuterons accelerated to 8 Mev in a cyclotron. The water was then electrolyzed and the hydrogen passed through a palladium valve, through a liquid-air trap, and into an all-glass G-M counter arrangement. Two counter tubes had been connected and filled with equal pressures of purified hydrogen. Their backgrounds were measured and found to be comparable. The hydrogen of one was replaced by the irradiated gas, and the counting rates obtained. A tip between the counters was broken, the contents were thoroughly mixed and the counting rates were again taken. The ratios of the counting rates in the two tubes before and after mixing the gases were compared and found to agree within a small fraction of the probable error.

Measurements were also made, under identical bombarding conditions, of the activities in aluminum and silver. The Al^{28} activity indicated a capture cross section of Al^{27} for slow neutrons 300 times that of D^2. The ratio of the capture cross section of Ag^{109} to D^2 was found to be 10,000.

Calculations were then made to limit the cross section of the reaction

$$D^2+n^1=H^3.$$

Calculation of the absolute cross section from the geometry of the experiment, assuming reasonable values for such data as were not known accurately, indicated a value of 2×10^{-28} cm². A more direct evaluation may be made from the comparison with aluminum. Goldhaber[4] considers that the capture cross section of Al^{27} for slow neutrons, derived from scattering data, is close to 10^{-25} cm². This gives a maximum value for the formation of H^3 of 3×10^{-28} cm², in excellent agreement with the other value.

The authors wish to express their gratitude to Dr. L. Skaggs and Mrs. E. Graves for the use of scaling and counting circuits, and to the American Philosophical Society, the Research Corporation, and the Chemical Foundation for aid in the construction of the cyclotron used in obtaining the beam of deuterons.

L. B. BORST
WILLIAM D. HARKINS

Jones Chemical Laboratories,
University of Chicago,
Chicago, Illinois,
March 14, 1940.

[1] Kikuchi, Aoki, and Takeda, Tokyo Institute of Phys. and Chem. Research **31**, 195 (1937).
[2] L. I. Schiff, Phys. Rev. **52**, 242 (1937).
[3] L. W. Alvarez and R. Cornog, Phys. Rev. **56**, 613 (1939).
[4] Private communication.

Photophoresis of Small Particles in a Magnetic Field

At the New York Meeting of the Physical Society on February 24 I presented some important matter which did not appear in the abstract.[1]

In a vertical magnetic field which is homogeneous, commutable and free of residual magnetism, particles move when irradiated by intense light in the direction of the magnetic lines of force as if they were single magnetic north or south poles (magneto-photophoresis). Thus intense light apparently produces single magnetic poles on every particle and between these "magnetrodes" a real visible magnetic current flows. The hypothesis of single poles gives a natural and better explanation than the old ones for the behavior of these particles and for the puzzling form of the corona of the sun (pointed out by G. E. Hale) whose lines follow exactly the magnetic lines of force and for other phenomena.

References: *Regarding the determination of the charge:* Physik. Zeits. **39**, 673 (1938) and the "Micro-Coulomb Experiment" appearing in Proc. Roy. Soc. London. *Regarding photophoresis etc.:* Physik. Zeits. **31**, 478 (1930) and **33**, 201 (1932) and Ann. de physique, Paris, April, 1940.

FELIX EHRENHAFT

Formerly, University of Vienna,
March 16, 1940.

[1] See abstract 38, Proceedings of the New York Meeting, Phys. Rev. **57**, 562 (1940).

System of Units for Nuclear and Cosmic-Ray Phenomena

It has become customary, in dealing with nuclear or cosmic-ray phenomena, to measure some quantities in terms of units which are different from those used in macroscopic physics. Thus, the energy of a particle is generally measured in electron volts; the charge of a nucleus is expressed by its atomic number, i.e., in terms of the electronic charge, etc. No attempt, however, has been made so far to bring the new units into a consistent system. Such a lack of systematization has been the source of many incongruities and misunderstandings, as illustrated by the following example. The so-called energy measurements on cosmic-ray particles are usually performed by measuring the radius of curvature ρ in a magnetic field H. If we call p the momentum of the particle, e its electric charge, c the velocity of light and we measure H in gauss, e in electrostatic units, ρ, c and p in c.g.s. units, it is $H\rho=(pc)/e$. The quantity $(pc)/e$ is a potential in electrostatic units and its measure in volts is $V_p=300(pc)/e=300H\rho$. The results of magnetic deflection experiments are generally described by the quantity V_p. This quantity is often called energy, which is misleading since V_p is actually proportional to the momentum of the particle and not to its energy, although its numerical value approaches that of the energy in electron volts when the velocity of the particle approaches the velocity of light. Other authors describe a particle as having a momentum equal to V_p "electron volts." The quotation marks acknowledge the contradiction in terms, since electron volts are a measure of energy rather than momentum.

The increasing importance of the study of sub-atomic phenomena makes it very desirable to remove the above incongruities by adopting a consistent system of units. The writer wishes to point out that this can be done retaining almost all of the units already used. The suggested system is summarized in Table I.

In this system, the charge of a nucleus is measured by its atomic number, the velocity of a particle becomes identical with the quantity usually designed by β, the energy is expressed in electron volts, the momentum is the quantity V_p defined above, the mass is measured by the same number which measures the rest energy in electron volts. The units of length, of potential difference and of electric field strength are the conventional ones. The units of time, of force and of magnetic induction (deflecting field) are more unusual. They have, however, a simple meaning and could be conveniently adopted. The system has four independent units, as any consistent system describing electromagnetic as well as mechanical quantities.[1] Like in all four-units systems, both the dielectric constant and the magnetic permeability have physical dimensions. Their numerical values in vacuum are $e_0=7.0\times10^6$ e/v cm and $\mu_0=1/7.0\times10^6=1.43\times10^{-7}$ v cm/e c².

TABLE I. *Suggested system of units for nuclear and cosmic-ray phenomena.*

QUANTITY	SYMBOL	DEFINITION
		Fundamental Units
electric charge	e	charge of the positive electron
potential	v	usual definition of volt
velocity	c	velocity of light
length	cm	usual definition of centimeter
		Some Derived Units
time	cm/c	time required by the light to travel 1 centimeter
energy	ev	energy of an electron accelerated by the potential difference of 1 volt
mass	ev/c²	mass of a particle having a rest energy of 1 electron volt
momentum	ev/c	momentum of a particle for which (total energy)² − (rest energy)² = 1
electric field strength (E)	v/cm	usual definition of volt per centimeter
force	ev/cm	force acting on an electron in a field of 1 volt per centimeter
magnetic induction (B)	v/c cm	magnetic induction of a field in which a particle with unit momentum and unit charge has a radius of curvature of 1 centimeter when traveling perpendicularly to the field (1 v/c cm = 1/300 gauss).

As a name for the unit of velocity, the word *römer* has been suggested to the writer by Professor W. H. Zachariasen. Should this name be accepted, the symbol of the unit might be changed from c to r. The system, as a whole, could be conveniently designed as system of *electron-relativistic units*, considering the two universal constants which have been chosen as units for the electric charge and for the velocity.

Professors A. H. Compton, C. Eckart and W. H. Zachariasen were kind enough to discuss with the writer the content of this note.

BRUNO ROSSI

Ryerson Physical Laboratory,
The University of Chicago,
Chicago, Illinois,
March 11, 1940.

[1] See, for instance, A. Sommerfeld, Ann. d. Physik 36, 335 (1939).

Isomeric Silver and the Weizsäcker Theory

A detailed study of the 6.7-hour radioactive cadmium,[1] formed in the reaction Ag $(d,2n)$ Cd, has resulted in several new observations. This body is known to emit K- and L-conversion electrons of a 93.5 kev γ-ray; K x-rays of silver, indicating K-electron capture as well as internal conversion; and a very weak gamma-ray with an absorption coefficient in lead about equal to that of annihilation radiation. The anomalously high ratio of L- to K-conversion electrons[2] suggested that the excited state responsible for them might have an appreciable life. We have found that the electrons do come from an excited state of stable silver, which decays with a half-life of 40 ± 2 sec. This period has been followed for 12 half-lives after chemical separation from radioactive cadmium, and its growth in the Cd solution has also been observed. The hard gamma-ray does not separate with the Ag, but about half of the x-rays do, as would be expected. We have also observed a very weak γ-ray of about 90 kev, which accompanies the 40-sec. Ag and is almost certainly the unconverted fraction of the 93.5 kev γ-ray. Bjerge and Westcott[3] have reported a 40-sec. period in Ag bombarded by Rn-Be neutrons, which has been assigned[4] to the 44-sec. rhodium period formed in a n,α reaction. Since no well-established (n,α) reactions are known for such high values of Z, and such low energy neutrons, this observation may now be interpreted by assuming an (n,n) excitation. The excited state of Ag should also be formed in (p,p), (α,α) and (x,γ) reactions.

We compared the absorption of the hard γ-rays with that of annihilation radiation from the 3.5-hr. Cu^{63}, under enough lead to reduce the ionization to less than eight percent. The Cd γ-ray is more penetrating. An experiment with coincidence counters also showed it to be for the most part a nuclear γ-ray. We found evidence for the expected Auger electrons from a sample of pure radioactive Cd, distilled in vacuum, from bombarded silver. This distillation technique should find many uses in the field of artificial radioactivity.

From the ratio of the numbers of K and L conversions, a theory proposed by one of us[5] requires a multipole order of 4 ± 0.1 for the transition between the two silver states. The measured internal conversion coefficient of 98 percent demands a similar, but not quite so precise value of this multipole order, from the theory of Dancoff and Morrison.[6] If we assume the value 4 to be correct, and calculate the lifetime of a 93.5 kev level in Ag by means of Weizsäcker's formulae corrected by Hebb and Uhlenbeck[7] to include decay by internal conversion, we obtain an expected value of 30 sec. On this theory, multipole orders of 3 and 5 would give lifetimes of about 10^{-3} and 10^{6} sec., respectively. The agreement between these three methods of computing the order indicates further that the transition is an electric rather than a magnetic 2^4 pole, so that the spin difference between the two states in silver is 4 units. In view of the approximations made in the theory, the agreement with respect to lifetime is a most encouraging check.

We wish to thank Professor E. O. Lawrence for his interest in this work, and the Research Corporation for financial assistance.

Luis W. Alvarez
A. C. Helmholz
Eldred Nelson

Radiation Laboratory,
Department of Physics,
University of California,
Berkeley, California,
March 11, 1940.

[1] L. A. Delsasso, L. N. Ridenour, R. Sherr and M. G. White, Phys. Rev. **55**, 113 (1939).
[2] G. E. Valley and R. L. McCreary, Phys. Rev. **55**, 322 (1939).
[3] T. Bjerge and C. H. Westcott, Nature **134**, 177 (1934).
[4] G. Guében, Nature **138**, 1095 (1936).
[5] E. Nelson, Phys. Rev. **57**, 252 (1940); E. Nelson and M. H. Hebb, Phys. Rev., in press.
[6] S. M. Dancoff and P. Morrison, Phys. Rev. **55**, 122 (1939).
[7] M. H. Hebb and G. E. Uhlenbeck, Physica **5**, 605 (1938).

Elementary Derivation of Thermal Diffusion

Thermal diffusion is usually thought not amenable to elementary derivation.[1] It may, then, be of value to point out a method of showing its existence and sign from elementary considerations. Thermal diffusion shows itself if a mixture of two gases is kept at a non-uniform temperature. It causes a gradient of the partial pressure of either gas which is observed as a partial separation of the gases. To support this partial pressure gradient the "partial gas" must experience a constant force due to collisions with molecules of the other gas. Hence there must be a continual net transfer of momentum from one gas to the other. To evaluate this one can find the momentum change suffered by a molecule of type "1" in a collision with a "2" molecule and sum over all collisions.

The result of this may be most easily understood by the following very rough treatment. Consider the heavier molecules as stationary, the light gas as composed of two streams of uniform velocities moving toward the cold and hot sides, respectively. The velocity of the stream coming from the hot side is somewhat greater than the velocity of the other stream. Each light molecule with velocity V loses its momentum to the heavy molecules at a rate $V\sigma$ where σ is the cross section for complete dissipation of momentum. Since each stream must carry the same momentum per cm³ (to make the net particle flux zero) the momentum transfer per second of the streams is proportional to $V\sigma$. The dependence of $V\sigma$ on the velocity can be found by a dimensional argument. Let the molecules interact by an inverse sth power repulsion, $F=-K/r^s$. Then σ may depend on K, on the mass of the light molecule (strictly the reduced mass), on V, and on s. From the dimensions of these quantities it is seen that σ must be proportional to $(K/mV^2)^{2/(s-1)}$ or to $V^{-4/(s-1)}$. Thus $V\sigma$ varies as $V^{(s-5)/(s-1)}$. This gives a force supporting an excess of light component at the hot side for molecules "harder" than Maxwellian molecules ($s=5$) or at the cold side for $s<5$ and no thermal diffusion for Maxwellian molecules.

A more rigorous treatment would take account of the motion of the heavy molecules and of the distribution in velocities of both types. Denote by $f_1(\mathbf{c}_1)$ and $f_2(\mathbf{c}_2)$ the velocity distributions of the light and heavy gases, respectively, normalized to their respective particle densities. Define a cross section for momentum transfer as follows: If a uniform stream of particles of mass μ, the reduced mass of the collisions, impinges on a scattering center $F=-K/r^s$, then the total momentum transferred to the scattering center is the product of the cross section, σ, and the momentum per cm² of the stream. Then as before this cross section must vary with the relative velocity as $V^{-4/(s-1)}$. The momentum gained per second by the light gas is then given by the expression

$$\int\int \tfrac{1}{2}(\mathbf{p}_2-\mathbf{p}_1)f_1(\mathbf{c}_1)f_2(\mathbf{c}_2)\sigma V d\mathbf{c}_1 d\mathbf{c}_2 = C\int\int(\mathbf{p}_2-\mathbf{p}_1)f_1(\mathbf{c}_1)f(\mathbf{c}_2)V^{(s-5)/(s-1)}d\mathbf{c}_1 d\mathbf{c}_2,$$

where $\mathbf{p}_1$ and $\mathbf{p}_2$ are the momenta of the light and heavy molecules, respectively. C is positive and does not depend on the velocities. $f_1(\mathbf{c}_1)$ and $f_2(\mathbf{c}_2)$ while not Maxwellian still must obey the relationship $\int f(\mathbf{c})\mathbf{p}d\mathbf{c}=0$ since this expression divided by m is the rate of flux of molecules. Hence for $s=5$ the term in V drops out and the integral vanishes. For harder molecules the collisions of high relative velocity are more effective. The collisions of highest relative velocity are predominantly those in which the lighter molecule is coming from the hotter region and the heavier from the colder region. Thus the resulting force is such as to support a greater partial pressure of light molecules in the hot part of the gas, and conversely as before for molecules softer than $s=5$. It may also be seen from this argument that the effect must be proportional to the product of the two fractional concentrations and to the relative mass difference.

S. Phillips Frankel

University of Rochester,
Rochester, New York,
February 14, 1940.

[1] S. Chapman, Phil. Mag. **7**, 1 (1929); Furry, Jones, and Onsager, Phys. Rev. **55**, 1083 (1939).

A New Afterglow Phenomenon

A new afterglow phenomenon, which has been observed in three separate discharge tubes at different pressures, is illustrated in the accompanying spectra (Fig. 1). These

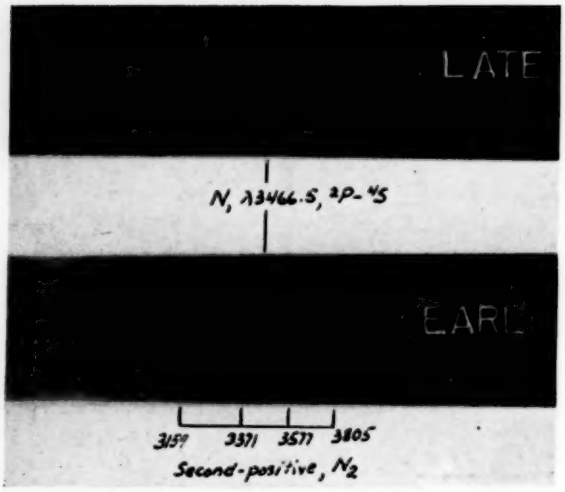

FIG. 1. Lower spectrum is of the early afterglow; the upper is that of the last part of the glow.

pictures were obtained on Eastman 33 plates in a small quartz spectrograph. They represent the early and late phases of a nitrogen afterglow at a pressure of the order of 20 mm. The bottom spectrum is that of the early and hence strong part of the afterglow, and the top one that of the last part of the glow. In order to obtain a plate strong enough to print it was necessary to expose the late part of the glow about three times as long as the early part. The contrast is striking. The forbidden nitrogen line, 3467, corresponding to the $^2P-{}^4S$ transition, is much more intense in comparison with the second positive N_2 bands late in the glow than it is in the early part. A long series of observations on the variation with pressure of this type of glow in the range thus far observed has shown that the ratio of forbidden to allowed radiation increases with pressure, a result which was quite surprising. In view of this, it is possible then to summarize the results in the present experiment by saying that the spectrum of the late phase of an afterglow corresponds to that of the early phase of a higher pressure afterglow or the effect on the spectrum of the afterglow as its lifetime increases is that of an apparent increase in pressure.

Observations on an afterglow at a lower pressure of about 10 mm shows this effect very clearly and these spectra will be published soon. It is believed that an explanation of this new afterglow effect will lead to an understanding of the puzzling afterglow phenomena which accompany discharges in nitrogen and further experiments are now in progress to study this effect under a variety of other conditions.

JOSEPH KAPLAN

Departments of Physics and Astronomy,
University of California at Los Angeles,
Los Angeles, California,
March 5, 1940.

Double Ionization by the Auger Effect: The Cause of a Satellite Intensity Anomaly for the X-Ray Diagram Line $M\alpha_1$

In a paper[1] published in 1936 the present author postulated an intensity anomaly due to the Auger effect, for the x-ray diagram line $M\alpha_1$, existing somewhere in the region immediately below atomic number 88. Some evidence in that paper was presented to show the existence of an Auger intensity anomaly.

Because of his interest Professor H. E. White reproduced in his book, *Introduction to Atomic Spectra*, some of the *M*-series plates[2] of the author's thesis (Cornell, 1931). Very recently, in looking at that book, it was of great interest to the present author to observe unmistakably the intensity anomaly which he had predicted (see p. 305).

To make this intensity anomaly more unmistakable, the plates are again reproduced. Fig. 1 shows the same $M\alpha$ lines; negatives were made, and finally a series of prints having the same maximum line density were secured. (The maximum density of the original plates was in the safe range to preserve density-intensity proportionality.) Hence it is felt that this presents a truer picture than Professor White's figure, although it was due to the original figure in Professor White's book that recognition of the Auger intensity anomaly was possible.

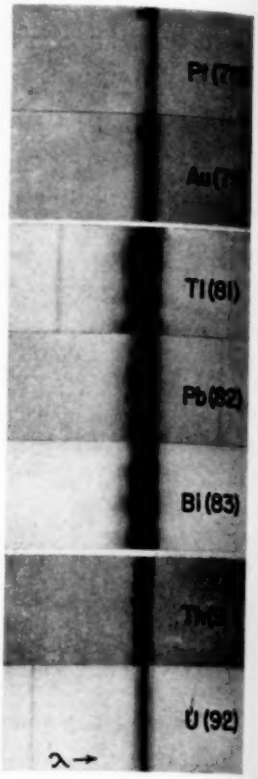

FIG. 1. $M\alpha$ lines of several elements. (The Pt and Au lines were taken with a quartz crystal; the rest by means of a calcite crystal.)

In reference 1, the writer pointed out that the radiationless transition $(M_{III} \rightarrow M_V)_z$ plotted on an energy scale against atomic number (see Fig. 2), intersects the $N_{IV, V}$ shell (for $z+1$ as an *M*-electron is already missing) in the region of $z=88$. This causes the Auger effect, acting to doubly ionize atoms for some atomic numbers below $z=88$, and preparing the respective atoms for the occurrence of the $M\alpha$ satellite group. (This work was patterned after the concepts of Coster and Kronig.[3])

Thus below $z=88$, for some atomic numbers, satellites should occur with considerable intensity: we should expect an intensity anomaly such as has already been described.[1, 4] The radiationless transition $M_{III} \rightarrow M_V$ initiated by electron ionization of the M_{III} shell, occurs with simultaneous ejection of an $N_{IV, V}$ electron. This process is especially probable when the normalized radial wave function for the

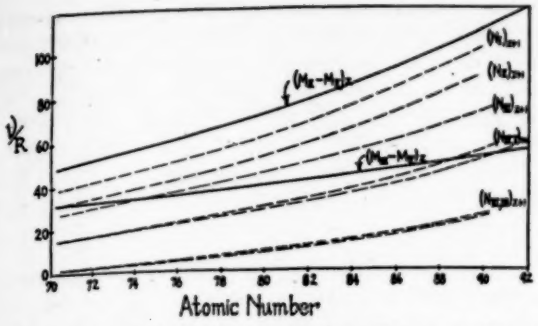

FIG. 2. The radiationless transition $M_{III} \rightarrow M_V$ on a ν/R scale plotted against atomic number, Z, and the ionization energy of the N-shells for $Z+1$.

ejected electron strongly overlaps the particular wave function for the $N_{IV,\,V}$ electron.

Now turning to Fig. 1, we see that the intensity of the satellite group on the left (short wave-length side) of each $M\alpha$ line increases from $z=78$(Pt) up to roughly $z=82$(Pb); beyond, at Th(90) and U(92), the satellite group intensity has decreased very markedly. Thus there exists an unmistakable intensity maximum due to the Auger effect, and we may say definitely that for the $M\alpha_1$ satellites the initial state is $M_V N_{IV,\,V}$; the final state $N_{VII} N_{IV,\,V}$.

F. R. HIRSH, JR.

California Institute of Technology,
Pasadena, California,
February 26, 1940.

[1] F. R. Hirsh, Jr., Phys. Rev. **50**, 191 (1936).
[2] F. R. Hirsh, Jr., Phys. Rev. **38**, 914 (1931).
[3] D. Coster and R. deL. Kronig, Physica **2**, 13 (1935).
[4] F. R. Hirsh, Jr., Phys. Rev. **48**, 722 (1935).

Cosmic-Ray Intensities and Air Masses

Blackett[1] has shown that the "temperature effect" of cosmic rays is due to the vertical shift of the layer in which mesotrons are formed and has further suggested that it may be possible to correlate cosmic-ray data with the structure of depressions. Loughridge and Gast[2] have pointed out that cosmic-ray intensities in America show a noticeable change at the fronts separating different air masses.

Our polar continental (Pc) air mass[3] originates in Manchuria and Siberia and comes to Japan proper as the Northwest monsoon in the colder half of the year. The tropical maritime (Tm) air mass flowing from the North Pacific subtropical high pressure belt comes to Japan proper as southerly tropical air mainly in the warmer half of the year. The polar maritime (Pm) air mass originates in Okhotsk sea and the sea to the east of Japan and comes to Japan proper as the mild Northeast wind in the rainy season. The Pm air mass found in Japan is shallow, but plays an important weather rôle. The mass is seldom thicker than 2000 m and is usually overrun by Tm air mass; the interaction of these two air masses results in the formation of a stationary front and is responsible for the gloomy and rainy weather of the Bai-u period of Japan. There are two other modified polar continental air masses, which lose their original coldness and dryness in the lower layers. One comes to Japan proper by the sea route from Northwest, and the air mass type transforms from the fresh one (Pc) to the modified one (NPc_1). The other arrives in north and central China by the land route and then comes to us by the sea route with the general westerly wind (NPc_2).

Cosmic-ray intensities under various typical air mass conditions prevailing in Tokyo during the year 1937 were picked up from the results obtained with a Steinke cosmic-ray meter inside 10 cm Pb and were given together with their barometer effects in Table I. The air masses were identified from the synoptic charts analyzed by the Forecasting Division of the Central Meteorological Observatory, Tokyo.

We see from the table that (1) both the correlation coefficient and the barometric coefficient are relatively high in the fresh Pc air mass and Tm air mass, and show a gradual decrease as the air mass type transforms from the fresh one to the modified one. (2) The correlation coefficient and the barometric coefficient are very low in Pm air mass, which is shallow and is overrun by Tm air mass. (3) The reduced cosmic-ray intensity is relatively low in warm air (Tm and Pm), but is high in cold air (Pc).

The explanation of these results on the basis of the instability of the mesotron will shortly be given in this column.

This work was done as a part of the program of the cosmic-ray sub-committee of the Japan Society for the Promotion of Scientific Research.

Y. NISHINA
Y. SEKIDO
H. SIMAMURA

Institute of Physical and Chemical Research,
Tokyo, Japan,

H. ARAKAWA

Central Meteorological Observatory,
Tokyo, Japan,
February 20, 1940.

[1] P. M. S. Blackett, Phys. Rev. **54**, 973 (1938).
[2] Donald H. Loughridge and Paul Gast, Phys. Rev. **56**, 1169 (1939).
[3] H. Arakawa, Bull. Am. Met. Soc. **18**, 407 (1937).

TABLE I. *Correlation of air mass conditions and cosmic-ray intensities.*

AIR-MASS TYPE	Pc	NPc_1	NPc_2	Pm	Tm
Number of observations (6 hour mean)	49	75	24	30	67
Mean observed cosmic-ray intensity (J)	1.6266	1.5933	1.5881	1.5658	1.5647
Correlation coeff. between the atmos. pressure and the cosmic-ray intensity	−0.75	−0.44	−0.50	−0.04	−0.64
Barometric coefficient (percent per cm Hg)	−1.46	−0.92	−1.08	−0.15	−1.22
Reduced intensity to normal atmos. pressure 755 mm Hg (J)	1.6269	1.5944	1.5943	1.5670	1.5672
	(+2.0%)	(0.0%)	(0.0%)	(−1.7%)	(−1.7%)
	(Annual Mean Value of $I_{755}=1.5943J$)				

The Energy Loss of Electrons in Carbon and the Decay of the Mesotron

In a recent issue of the *Physical Review* Fermi[1] suggested that the energy loss suffered by extremely fast particles in solid materials might be less than the loss in a corresponding amount of gas, because of the effect of the dielectric constant. This is of particular interest in regard to the mesotron, because direct measurements on its lifetime involve a comparison of its rate of absorption in solid and gaseous materials, especially graphite and air.[2] We have measured the energy loss in graphite for 10-Mev electrons, which are easily obtainable in the laboratory under controlled conditions. Since the magnitude of the effect of the dielectric constant depends essentially upon the ratio of the total energy of the particle to its rest energy, a 10-Mev electron should experience as great an effect as a mesotron of about 2000 Mev. Our results therefore apply to the case of the cosmic-ray measurements. Unfortunately there seems to be no feasible method of measuring energy loss in a gas, so we have simply compared our results with the values calculated by means of the Bloch formula.

A band of electrons of 8 to 12 Mev was selected out of the beta-ray spectrum of Li^8 by means of slits in a magnetic field. They then passed into a cloud chamber, across the center of which was placed a slab of graphite weighing 0.82 g/cm². A magnetic field of 3480 gauss was applied to the chamber. In this field a 10-Mev electron has a radius of curvature of only about 10 cm, and hence can be measured with great accuracy. Only those tracks making an angle of incidence less than 10 degrees with the normal to the absorber were used. The curvatures on the two sides of the absorber were measured and the changes in radius of curvature are plotted in Fig. 1. The average energy loss

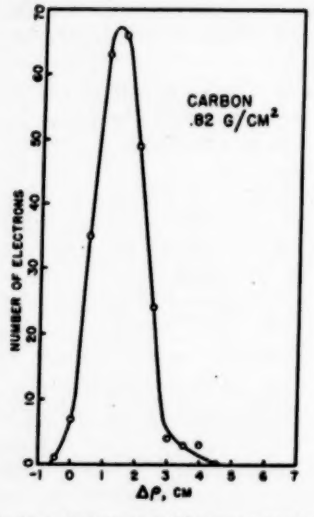

FIG. 1. Distribution of electrons with respect to change in radius of curvature.

for the 255 tracks observed is 1.86 Mev/g/cm². From the observed average angle of scattering (6 degrees in the projection) and the average angle of incidence the path length correction is estimated to be one percent. A correction of one percent should also be applied for the departure of the emergent tracks from the plane perpendicular to the magnetic field. Systematic errors (calibration of field etc.) amount to ±2 percent. If we assume that the breadth of the experimental curve is a fair indication of the magnitude of the *random* errors (such as changes in curvature due to scattering in the gas of the chamber), the probable error in the mean value from this cause is ±4 percent. Taking into account all these figures we get 1.82±0.08 Mev/g/cm² for the energy loss. From this we subtract the loss due to radiation, and have left 1.69±0.08 Mev/g/cm², which is the loss due to collisions alone. It may be mentioned here that the earlier measurements of Turin and Crane[3] give 1.8±0.2 Mev/g/cm² after corrections similar to the above are applied.

TABLE I. *Theoretical values for the collision loss for* 10-*Mev electrons.*

DIELECTRIC CONSTANT	EN. LOSS MEV/G/CM²	DIELECTRIC CONSTANT	EN. LOSS MEV/G/CM²
1.00	1.93*	1.5	1.60
1.01	1.90	2.	1.54
1.05	1.77	4.	1.46
1.1	1.71	10.	1.36
1.2	1.66		

* Bloch value.

Theoretical values for the collision loss for 10-Mev electrons, calculated by means of the Bloch formula and the Fermi formula for the dielectric constant effect are given in Table I. Our experimental value fits best with a dielectric constant of about 1.1, and, considering the probable error in our result, we may say that a dielectric constant of 1.05 to 1.5 is indicated. It may also be said, on the basis of this experiment, that the dielectric constant effect is by no means large enough to affect seriously the conclusions drawn from the experiment of Rossi, Hilberry and Hoag on the decay of the mesotron.

H. R. CRANE
N. L. OLESON
K. T. CHAO

University of Michigan,
Ann Arbor, Michigan,
March 6, 1940.

[1] E. Fermi, Phys. Rev. **56**, 1242 (1939).
[2] Bruno Rossi, H. Van Norman Hilberry and J. Barton Hoag, Phys. Rev. **56**, 837 (1939). Bruno Rossi, Cosmic-Ray Symposium, Chicago, June, 1939; Rev. Mod. Phys. **11**, 296 (1939).
[3] J. J. Turin and H. R. Crane, Phys. Rev. **52**, 63, 610 (1937).

Radioactive Zirconium and Columbium from Uranium Fission*

Radioactive zirconium and columbium have been obtained from a sample of uranium bombarded by slow neutrons from the Columbia cyclotron. In the zirconium separated from the uranium a strong 17.0-hour period was identified. From this a 75-minute period columbium has been observed to grow as a daughter product. Both of these have been shown[1] by Wilson-chamber observations to be negative electron emitters. This 75-minute columbium does not disintegrate into the 66-hour molybdenum reported by O. Hahn and F. Strassmann[2] from uranium, but our experiments do not as yet exclude a substantially longer or shorter period molybdenum daughter product from columbium.

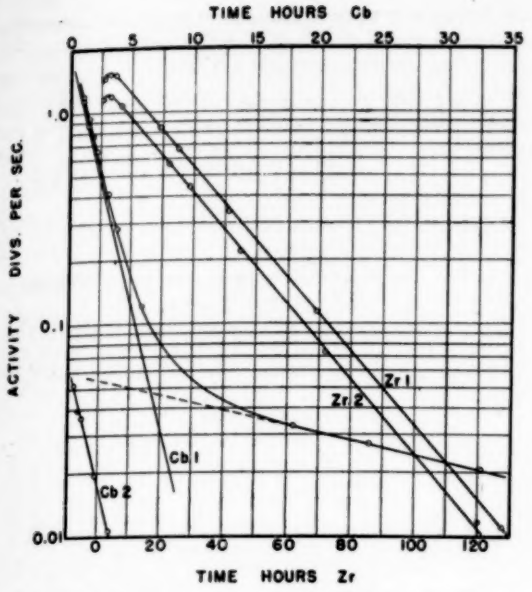

FIG. 1. Decay curves of zirconium and columbium from uranium.

An aqueous uranyl nitrate solution was irradiated for several days. The Zr was precipitated as a phosphate from a concentrated hydrochloric acid solution. To serve as carriers inactive isotopes of all previously reported fission products (i.e., Rb, Cs, Sr, Ba, Y, La, Mo, Sb, Te, Br, I) were added in quantities of a few milligrams each, previous to the precipitation. Simultaneously Th, Bi and Pb were added to carry down any natural radioactive bodies.

The zirconium phosphate precipitate was purified from traces of all other elements, except Hf and Pa, by means of the above precipitation; followed by a hydrogen fluoride and aqua regia treatment, coupled with a potassium sodium carbonate melt. (This chemical treatment will be described more fully in a chemical journal.) In order to prove that the observed activity was not associated with Pa or Hf, the Zr was fractionally crystallized as an oxychloride; it has been previously shown that by this treatment Pa[3] concentrates in the mother liquor, while Hf[4] accumulates in the front. The activities per milligram ZrO_2 after different chemical treatments were constant within experimental error. The decay curves of two typical Zr preparations are shown in Fig. 1. The average half-life was found to be 17.0 ± 0.2 hours.

A previously unknown radioactive columbium isotope was separated from the Zr. After addition of inactive Cb_2O_5, Cb was separated by (1) $KNaCO_3$-melt and precipitation from the filtrate with (*a*) HCl and (*b*) with NH_3 from an HCl solution, and (2) by a $NaHSO_4$-melt and precipitation from an acetic acid solution by hydrolysis. Two decay curves of this columbium are also shown in Fig. 1.[5] The period averaged from a number of such curves equals 75 ± 3 minutes.

The existence of mother-daughter relationship between the Zr and Cb was indicated by the build-up of the Zr activity after a Cb separation (see Fig. 1). Conclusive evidence was obtained by successive separations of Cb from the Zr. The data are given in Table I; while the Zr decayed by a factor of 7.7 the Cb yield decreased by a factor of 7.

TABLE I. *Evidence of mother-daughter relationship between* Zr *and* Cb.

SEPARATION	1	2
Age of Zr at moment of Cb separation (hr.)	23	74
Activity of Zr+Cb per 1 g ZrO_2 just before Cb separation (div./sec.)	68	8.8
Activity of Cb just after separation (div./sec.)	28	4.1

Absorption measurements indicate that the β-rays of both Zr and Cb have a maximum energy of about 1 Mev.

Evidence has also been obtained of a longer-life zirconium isotope, emitting electrons of low energy (about 0.25 Mev, with a period of more than 20 days.

The discovery of the above-mentioned products fills the gap in the light weight group of the previously known fission fragments. At least one radioactive isotope of every element between bromine (35) and ekamanganese (43) and antimony (51) and lanthanum (57) has now been reported. The large gap of seven elements between these two groups still remains unfilled.

We are indebted to Dr. J. R. Dunning for helpful discussions and active interest in the work. The aid of the Research Corporation is gratefully acknowledged.

A. V. GROSSE
E. T. BOOTH

Department of Physics,
Columbia University,
New York, New York,
March 5, 1940.

* Publication assisted by the Ernest Kempton Adams Fund for Physical Research of Columbia University.

[1] We are indebted to Mr. G. Weil for making the cloud-chamber experiments.
[2] O. Hahn and F. Strassmann, Naturwiss. **27**, 451, 544 (1939).
[3] A. v. Grosse, Berichte d. Deutsch. Chem. Ges. **61**, 238 (1928).
[4] G. v. Hevesy, *Das Element Hafnium* (1927), p. 6.
[5] The long period tail on Cb 1 is due to a trace (3 percent) of 17-hour zirconium as an impurity.

Compton Line Profiles Applied to Chemical Binding

The purpose of this letter is to describe a method which may be used in obtaining new information regarding the physical state of the electrons forming bonds in gaseous molecules and in solids. The method depends upon the experimental determination of the Compton line shape by the inelastic scattering of x-rays[1] or electrons[2] for the system whose electronic structure is being studied.

In order to apply such experimental information we shall make the fundamental assumption that all of the electrons in a molecule may, as far as their effect upon the line shape is concerned, be divided into classes each characterized by the rôle played in the molecule by the electrons of that class. In methane for example there are but two classes, the first consisting of the two equivalent K-shell electrons and the second of the eight equivalent electrons forming the four C—H electron-pair bonds. We shall then attribute to each class κ a line shape function, $y_\kappa(\beta)$, $(\beta = v/c)$, and the over-all line shape for the whole molecule will consist of the sum of the component line shapes, $y_\kappa(\beta)$, weighted

according to the number of electrons in that class. A second important condition is that

$$\left\{\tfrac{1}{2}mc^2\int_0^\infty \beta^2 y_\kappa(\beta)d\beta\right\}\Big/\left\{\int_0^\infty y_\kappa(\beta)d\beta\right\}=\epsilon_\kappa,$$

where ϵ_κ is the correct kinetic energy for an electron in the class κ.

Application of this method to the hydrocarbons is interesting because it might be expected to throw light on the nature of multiple and of resonating bonds. Also, profiles determined for relatively few electron classes should suffice to describe all molecules in the homologous series. Simplified theoretical calculations have already been made for many hydrocarbons,[3] and from these it may be concluded that any appreciable difference in the momentum distribution between two classes of electrons, for example those in the C−C and the C=C bonds, should manifest itself unmistakably in variation between the corresponding Compton line profiles for those classes as derived from experiment.

BRUCE L. HICKS

Physics Department,
University of Wyoming,
Laramie, Wyoming,
March 4, 1940.

[1] Jesse W. M. DuMond, Rev. Mod. Phys. **5**, 1 (1933); Jesse W. M. DuMond and H. A. Kirkpatrick, Phys. Rev. **52**, 419 (1937); H. A. Kirkpatrick and Jesse W. M. DuMond, Phys. Rev. **54**, 802 (1938).
[2] A. L. Hughes and Marvin M. Mann, Jr., Phys. Rev. **53**, 50 (1938); A. L. Hughes and M. A. Starr, Phys. Rev. **54**, 189 (1938); **55**, 343 (1939).
[3] Paper presented by the author at the October, 1939, meeting of the Colorado-Wyoming Academy of Science.